Mathematical Modeling of Frazil Ice Formation and Evolution

By Shuang Ming Wang

A thesis submitted to the Faculty of Graduate Studies in partial fulfillment of the requirements for the degree of

Doctor of Philosophy

Department of Civil Engineering
University of Manitoba
Winnipeg, Manitoba, Canada

December, 2006

THE UNIVERSITY OF MANITOBA

FACULTY OF GRADUATE STUDIES

*****

COPYRIGHT PERMISSION

Mathematical Modeling of Frazil Ice Formation and Evolution

By

Shuang Ming Wang

A Thesis/Practicum submitted to the Faculty of Graduate Studies of The University of Manitoba in partial fulfillment of the requirement of the degree

Of

Doctor of Philosophy

Abstract

In cold regions the production of frazil ice in supercooled turbulent water has a profound impact on the design, operation and maintenance of water resources infrastructure. Studies on frazil ice formation are therefore important and imperative for ice engineering. This study mainly focuses on the development of mathematical models for frazil ice formation and evolution, which is an important part of modeling ice formation in a river.

A general mathematical model is formulated that includes the modeling of flow and turbulence, heat transfer, and frazil ice transport in open channel flow. In addition the methodologies to model the physical processes of ice formation are described. Three mathematical models to simulate the supercooling process and frazil ice evolution were developed based on the general mathematical model and frazil ice dynamics. A zero-dimensional mathematical model was able to simulate water temperature history, frazil ice number evolution in the well-mixed water and the varied size distribution of frazil ice during the supercooling process. A vertical one-dimensional mathematical model was able to simulate water temperature variation with time at the different water depths, velocity and turbulent intensity distribution over the water depth, and the vertical distribution of frazil ice number concentration. The variation of mean size of frazil ice particle is also simulated. An extended one-dimensional mathematical model was developed from the vertical one-dimensional model by including the size distribution of frazil ice and the complicated physical processes. The three mathematical models developed are calibrated and verified using experimental data.

Acknowledgements

The assistance and support of many people over the past four years allowed me to complete this thesis; the names of a few follow,

First of all I would like to thank Dr. Jay Doering, my advisor, who has provided endless support, guidance, and encouragement throughout my graduate studies. It has been a great pleasure to have been one of Dr. Doering's graduate students and it is a time that I will always be proud of. Thanks also go to my examining committee members, Dr. P. Rasmussen, Dr. Tachie and Mr. Carson for their questions and contribution to this thesis.

I would like to thank all the graduate students in Hydraulics Research and Testing Facility (HRTF) who have provided me with assistances and valuable discussions on my study. I enjoyed the time with all these excellent people. My friends both in Winnipeg and in China have also provided me with an encouragement during my study; I would like to also take this opportunity to express my deep appreciation to them. Special thank also goes to University of Manitoba for selecting me as the recipient of the prestigious Edward Toporeck Graduate Fellowship in Engineering and to Manitoba Hydro for funding my research.

Last but not least, I would like to give thanks to my family for their continuous support and encouragement throughout my studies and life.

TABLE OF CONTENTS

List of Figures

List of Tables

List of symbols

Symbol	Units	Definitions
A_s	m^2	surface area of ice particle
A_{sw}	m^2	water surface area
B	m	width of channel
B_i		birth function for frazil ice particle
B_u		constant=5.1
B		constant
$C_E(v_i, v_j)$		rate of the collision energy transfer to crystal per unit volume of fluid
C_f	kg/m^3	mass concentration of water
C_i	kg/m^3	mass concentration of ice
C_{iv}		mean volume concentration of frazil ice
$C_{1\varepsilon}$		coefficient for $k-\varepsilon$ equation
$C_{2\varepsilon}$		coefficient for $k-\varepsilon$ equation
C_k		the volumetric concentration of frazil in k^{th} size fraction
C_n		number concentration of ice
C_p	$Jkg^{-1}\,^oC$	specific heat of water, 4.18×10^3
C_w	$Jkg^{-1}\,^oC$	heat capacity of the water
C_μ		Constant=0.09
D_i		death function for frazil ice
D_m	m	mean diameter of the frazil ice
D_{flume}	m	centerline diameter of the flume
d_{ice}	m	diameter of frazil surface
d_t	m	frazil thickness

d_1	m	diameter of the smaller frazil ice
d_2	m	diameter of the largest frazil ice
d_{50}	m	mean frazil surface diameter
E_{dr} and E_{sh}		coefficients to account for particle interference effects
E_{ti}		the rate of energy transfer
F_1		number of particles produced per unit of collision energy
F_2		number of particles surviving to become crystals
F_n		number of particles from collision per unit volume and per unit time
f		fraction factor
f_l		focal length of the camera
f_{coll}^{i}		frequency of collision between ice particles
G		growth rate of ice crystal
G_i		source term
G_c		source term for frazil concentration equation
G_n		source term for frazil ice number equation
g	m/s^2	acceleration due to gravity
g_i	m/s^2	the j^{th} gravity component
$g_n(l)$		frazil ice number density function
H	m	water depth
H_{wi}	$W/m^{2o}C$	heat exchange coefficient between water and ice
h_w	$W/m^{2o}C$	heat transfer coefficient
h_{wi}	$W/m^{2o}C$	heat exchange coefficient between water and single frazil particle
h	$W/m^{2o}C$	heat transfer coefficient
h_{wi}	$W/m^{2o}C$	heat transfer for all the particles in interval class i

H_{wi}	$W/m^{2o}C$	heat transfer for all the ice particles
$I(v_i, v_j)$		number of nuclei produced per unit time
i		i^{th} time increment
K_u		the Kurtosis of the velocity derivative
K_v		frazil volumetric factor, 0.785
k_1		the value of kinetic energy at the first point of grid
k_c		constant
κ		Karman constant
k_s	m	roughness of bed
k_w	W/m^{oC}	thermal conductivity of water, 0.5659
k_{ws}		the value of kinetic energy at water surface
K	m^2/s^2	kinetic energy of turbulence
L_i	J/kg	latent heat of fusion, 3.34×10^5
l	m	particle length scale
l_o		Prandtl's mixing length
l_l		characteristic length for the vertical frazil movement
M	%	frazil ice concentration in volume
m		number of sub-sample
m^*		variable $m^* = \bar{r}/\eta$
N		matrix
N_u		Nusselt number
N_{u_T}		turbulent Nusselt number
$\overline{N}$		matrix of intensity derivatives
n_c		population density of crystals in the region R.
n_i		number of frazil ice particles at interval i

n_m		number of frazil ice particles for mth group
n_n		number of frazil ice particles
n_{nwn}		number of particles per unit volume and unit increment of particle size
$\bar{n}_{\max}$		maximum number of frazil ice
$\bar{n}$		average frazil number
P_r		Prandtl number
P_w		water pressure
Q	m^3/s	flow discharge
Q_{aw}	W	heat exchange rate between air and water
Q_i		heat release due to freezing for radius interval i
Q_n		net heat loss per unit area at water surface
Q_{iw}	W	heat exchange rate between water and ice
q	W	heat transfer from ice to water per unit area
R_h	m	hydraulic radius
R_e		Reynolds number
r	m	radius of frazil ice
S		variance
S_b	W	source term due to heat loss at channel boundary
S_f	W	latent heat release from frazil growth
$S_{floc,k}$	W	source/sink term due to secondary nucleation and flocculation.
S_{c_k}	W	source term due to thermal growth of frazil
S_N		Product of two functions
T	^oC	water temperature
T_f	^oC	bulk temperature of fluid

T_e	^oC	equilibrium temperature of water and ice mixture
T_a	^oC	air temperature
T_i	^oC	ice surface temperature
$T_{min,}$	^oC	maximum supercooling of water
t	s	length of a time series
t_{sp}	$minutes$	length of principal supercooling
t_n	s	time of initial appearance of ice particle
t_c	s	period of initial ice formation
U	m/s	mean water velocity
U_i	m/s	water velocity of i^{th} .component
U_l	m/s	turbulence fluctuation
U_r	m/s	relative velocity
U_{rise}	cm/s	rise velocity of frazil ice
u_*	m/s	bed shear velocity
V_b	rpm	velocity of the bed
$\overrightarrow{V_f}$	m/s	convective velocity of the water
$\overrightarrow{V_e}$	m/s	velocity of the crystal through space
V_i	m^3	Ice volume produced per unit time for the interval i
v_i	m^3	volumetric size of the colliding particles for group i
v_j	m^3	volumetric size of the colliding particles for group j
v_m	m^3	volume of merged ice particles
v_{Sec}	m^3	volume contributed to the secondary nuclei production
z	m	vertical distance measured from the bed
z_*		dimensionless number= zu_*/ν
α_{floc}		a calibration factor for floculation

α_i and α_j		coefficient for secondary nucleation
α_T		turbulence intensity
α_{ws}		constant=0.18
$\alpha(x)$		number of particles per unit volume and unit increment of particle size
β_i		coefficient for flocculation/break up
$\beta(v_i, v_j)$		the collision frequency function
γ_i		coefficient for gravitational removal
γ_{wa}		the ice-water interfacial tension
θ		coefficient for differential scheme
Δt	s	time step
ε	m^2/s^2	energy dissipative rate
ε_1		The first value of energy dissipation rate at the grid
ε_s		diffusion coefficient
η	m	dissipation length
ζ		coefficient for secondary nucleation term
Φ		dissipation function
ϕ	$W/m^2°C$	Heat transfer coefficient
ϕ_i and ϕ_j		the number concentration of the i^{th} and j^{th} size particles
ν	m^2/s	kinetic viscosity
ν_t	m^2/s	kinetic eddy viscosity
ρ_w	kg/m^3	water density

ρ_i	kg/m^3	ice density
ρ_m	kg/m^3	ice-water mixture density
σ_c and σ_t		Prandtl/schmidt numbers
τ	N/m^2	bed shear stress
τ_i		coefficient for gravity removal
ω	m/s	rise velocity of frazil particles
ϖ_i		frazil rise velocity for i^{th} size fraction
ϖ_m		frazil rise velocity for m^{th} size fraction
η		kolmogorov length scale.
κ		Karman constant
Δ_i		volume of the fluid
Δ_{vi}		the difference of ice volume for the two neighboring radius intervals
ΔT		supercooling of ice-water mixture
σ_c		Prantal/Schmidt number for concentration of frazil ice
σ_t		Prantal/Schmidt number for water temperature
δ		ratio between volume of particles of two neighboring radius interval

CHAPTER 1

General Description

1.1 Introduction

The formation of ice in rivers and waterways is a natural phenomenon in cold regions, but sometimes it can create engineering challenges and affect the design, operation and maintenance of hydraulic facilities. The associated problems include floods produced by ice jams, negative effects on hydropower operation, inland navigation, water diversion, the environment, and river morphology. Accurate (theoretical) river ice forecasts could be a great asset in dealing with these problems since such forecasts would provide the necessary time to schedule procedures to mitigate the adverse effects on the operations of the various river structures. With adequate warning, procedures could be implemented in an orderly and effective manner. Additionally, emergency measures such as an evacuation or a flood fighting effort might be instituted in a timely manner.

Ice research has drawn the attention of research engineers and scientists. Generally ice

research is divided into two areas: the study of river ice and the study of sea ice, both of which involve similar physical processes although salinity and strongly nonlinear waves are involved in the formation of sea ice. This study will be confined to the formation of river ice. River ice phenomena include the formation, evolution, transport, accumulation, and deterioration of various forms of ice (Shen, 1996).

River ice processes involve complex interactions between the hydrodynamics, mechanics, and the thermal dynamics. Several reviews of river ice processes and the state-of-research are available (e.g., Ashton, 1986; Gerard, 1990; Prowse, 1993; Beltaos, 1995; and Shen, 1996), in which it is stated that the studies of frazil ice formation and anchor ice formation are very limited, and that more attention and effort are required in these two areas.

Frazil ice is defined as a fine, small, needle-like structure or thin, flat, circular plates of ice suspended in water (USA CRREL, 1997), and it is the origin of almost all the others forms of river ice (Ettema et al., 1984). Early studies of frazil ice usually focused on the supercooling process, nucleation, frazil ice growth and evolution both from an experimental and a mathematical perspective. Mathematical modeling has been useful in predicting the ice formation and its corresponding consequences, while the experimental study often provided useful data for the development of the mathematical models and for elucidating unclear mechanisms about ice formation.

1.2 Physical Processes of Frazil Ice Formation

The process of frazil ice formation can be characterized by several physical processes including initial seeding, secondary nucleation, flocculation and break up, and buoyancy removal. All of these processes are fundamental for ice formation and their mechanisms are important for mathematical formulation of ice formation. The process of ice formation can be reflected and illustrated by the supercooling process, which shows the water temperature variation during ice formation.

1.2.1 Supercooling Process

In the presence of a low ambient air temperature, the heat loss from a water surface exceeds the heat gain. As a result, the water temperature drops to the freezing point. With the heat loss continuing at the water surface, the water becomes supercooled (i.e., $T<0\,^{0}C$), and then frazil ice starts to form. The formation of frazil ice releases latent heat to the water; the maximum point of supercooling occurs when the heat loss from the water surface just exceeds the heat produced by frazil ice formation. Subsequently, the water will warm up gradually because the heat released from frazil ice production exceeds the heat loss from the water surface. Finally, the mixture of water and ice will reach an equilibrium state T_e. A typical supercooling process is depicted in figure 1.1.

1.2.2 Initiation of Frazil Ice

The initial formation of frazil ice begins when turbulent water is supercooled and the water is seeded with ice crystals from the atmosphere (Svensson and Omstedt, 1994). This phenomenon is usually referred to as heterogeneous nucleation, which requires the presence of a foreign particle to serve as the nuclei. Heterogeneous nucleation is commonly observed in nature, while homogeneous nucleation, not requiring any foreign particles, is not realized in any natural water body since it only occurs for water temperatures less than -38 °C. Frazil ice usually starts to appear at the nucleation temperature T_N as indicated in figure 1.1.

The amount of the initial frazil ice produced most likely depends on the amount of seeding of foreign particles. Foreign particles usually come from a mass transfer process whereby seed crystals are introduced from the atmosphere into the water column. The sources of the seed crystals are the wind and the air-borne water droplets created by splashing, wind spray, and air-bubbles bursting that freeze in the air and drop back into the flow as ice particles (Osterkamp, 1978; Daly, 1984).

1.2.3 Secondary Nucleation

Secondary nucleation is responsible for the production of small crystals and is the cause of the rapid proliferation of frazil ice particles. Three mechanisms have been identified by Denk and Botsaris (1972), by which secondary nuclei could be generated by the parent crystal: (1) the growth and the detachment of surface irregularities; (2) the ordering of the solute

molecules near the surface of the parent crystal, which leads to a high local super-saturation and induces primary nucleation; and (3) the uptake of impurities by the growing parent crystal which sufficiently reduces the impurity concentration near the crystal surface such that primary nucleation becomes locally possible. The last two mechanisms are unlikely sources of secondary nuclei because of the high level of super-saturation (supercooling) required for primary nucleation and because the possible numbers of nuclei produced by these mechanisms would not be sufficient to explain observations (Mercier, 1984). In any case, at a low super-saturation the first mechanism is the main source of secondary nuclei (Ottens et al., 1972).

Evans et al. (1974a, b) demonstrated experimentally that the rate of production of the secondary nuclei in agitated crystallizers is removal-limited, that is, it depends on the rate of the detachment of surface irregularities rather than the rate of growth of the irregularities. They indicated that fluid shear and collisions of the crystals with hard surfaces (including other crystals) could cause the detachment of the surface irregularities.

It is commonly agreed that the dominant mechanism of secondary nucleation for frazil ice crystals is collision breeding. The rate of production of the nuclei depends on: the rate of the collisions between the crystals; on the energy associated with each collision; and to a lesser extent on the super-saturation and the impurity concentration (Mercier, 1984).

1.2.4 Flocculation and Break up

The mechanism of flocculation is not yet well understood although the process of sintering is usually used to explain the mechanism (Daly, 1994). Sintering apparently results from the tendency of crystals to minimize their surface free energy. Martin (1981) has determined the bonding time required for small spheres and disks in the sintering process to be on the order of 0.01 seconds. This is sufficiently fast to account for the observed flocculation of frazil ice particles in turbulent water. Mercier (1984) in his simulation assumed that turbulent shear and the differential rates of rising were the two mechanisms causing collision of crystals for sintering. Figure 1.2 shows the sintered ice block observed by Clark and Doering (2004). Break up of a larger frazil bloc may happen when it collides between or with solid boundaries, but it seems that flocculation is more significant than the break up process.

1.2.5 Buoyancy Removal

Frazil ice particles in water are subjected to a buoyancy force, drag force, and turbulent mixing action. Therefore, their movements in water are determined by a combination of these actions. For smaller frazil particles, the turbulent mixing is dominant and keeps the ice particles entrained in the water. As the crystals grow and flocculate together, they may reach a size where their buoyancy force overcomes the turbulent transport and the crystals will float to the surface. On the other hand, the surface ice may break up and be resuspended in the water. The relative time that ice floats on the water surface compared to ice being at depth in a flow is scarcely known. Buoyancy is primarily effective for the removal of larger

ice particles.

1.3 The Evolution of Frazil Ice Particles

1.3.1 Frazil Ice Morphology

Various shapes of frazil ice, such as flat disked shapes, six-pointed stars, hexagonal plates, spheres, and small pieces of dendrite ice have been observed in laboratory experiments and in field observations. These various shapes come from a complex interaction between the imposed heat transfer conditions and the intrinsic crystallography of ice (Daly, 1984). However, it is commonly agreed that the dominant shape of ice crystals during the supercooling period in a turbulent water body is a flat disk.

Hanley and Rao (1982) indicated that needle shaped frazil ice forms only when the turbulence level of the water is low. Needle-shaped particles were also observed in a natural river setting by Osterkamp and Gosink (1982). Clark and Doering (2002) observed needle shaped ice that formed in the counter-rotating flume at the Hydraulics Research and Testing Facility (figure 1.3), and reported that typically such particles form near the surface, but are quickly entrained in the flow through turbulence. Hexagonal plates have also been observed both in the laboratory (Clark and Doering, 2002) and in the field (Osterkamp and Gosink, 1982).

The different irregular shapes of ice particles observed were dependent on the degree of supercooling, the turbulence intensity and the depth of particle nucleation. Figure 1.4 shows several examples of irregular ice particles.

1.3.2 Size Range of Frazil Ice Disks

Crystal size varies considerably during ice formation (Daly, 1991). During seeding, the typical dimension of the seeding crystals is about 10^{-5} to 10^{-4} m in diameter. When frazil ice starts to form the typical size ranges from 10^{-5} to 10^{-2} m while the typical dimension of frazil flocs is 10^{-3} to 10^{-1} m (Svensson and Omstedt, 1994; Daly, 1984).

It has been observed that flat disks have a thickness to diameter ratio ranging from 1:5 to 1:100 (Arakawa, 1954). Daly and Colbeck (1986) investigated the aspect ratio of frazil crystals grown in a laboratory flume and found that the ratio of diameter to thickness was about 10, and it gradually decreased along the flow. According to Daly (1984), the diameter-to-thickness ratios range from 5 to 100. Frazil ice crystals apparently maintain their disk shape up to a diameter of 300 μm, which seems to be the maximum disc size limited by instability (Daly, 1984).

1.3.3 Frazil Ice Size Distribution

Once frazil ice is initiated in turbulent water, the ice crystals will grow in size and in number and the size distribution will vary with time. Some experiments (Bukina, 1967; Mercier,

1984; Daly and Colbeck, 1986; Ye and Doering, 2004; Clark and Doering, 2004) have been conducted to study the size distribution of frazil ice in turbulent water.

Bukina (1967) conducted an experiment in a crystallization tray with the turbulence generated by an agitator to determine the size distribution of the ice crystals, and from which an equation for the distribution was developed

$$n_b(2r) = \frac{b}{6}(2r)^3 \exp^{b(2r)}, \tag{1.1}$$

where r is the radius of the frazil ice, n_b is the number of ice particles, and b is a coefficient characterizing the position of the maximum of the crystal distribution curve. It is equal to a value of -14.1 on the average.

Mercier (1984) summarized some observations of suspended particle distributions in natural water and suggested that the particle size distribution can be described by an equation with the following form

$$g_n(l) = \frac{dC_n(l)}{dl} = al^{-b}, \tag{1.2}$$

where $g_n(l)$ is the number density distribution (number of particles per unit fluid volume, per unit particle length), $dC_n(l)$ is the number concentration (number of particles per unit fluid volume) for a particle length scale $l - dl/2$ to $l + dl/2$; a and b are constants (b =4.0). Svensson and Omstedt (1994) suggested a parameter α_{floc} representing the flocculation/break up process in their mathematical model and calibrated the parameter with a value of 0.001 based on Mercier's (1984) suggested spectrum.

A log normal distribution has been found by experiments to be a good approximation for the size distribution of individual frazil ice discs (Daly and Colbeck, 1986; Horjen, 1994; Ye and Doering, 2004; and Clark and Doering, 2004).

Daly and Colbeck (1986) carried out a series of experiments to examine the dynamic size distribution and the concentration of frazil ice crystals in a CRREL flume. They found that the measured crystal size ranged from about 35 μm to 0.5 mm. The mean of the size distributions was generally above 0.1 mm. As noted, they observed that the size distribution could be approximated by a log normal distribution. A different mean and a different standard deviation were given for each experiment, but a general formulation was not noted.

Horjen (1994) formulated the size distribution according to Daly and Colbeck (1986) results as

$$n_{num}(d_{ice}) = \exp\left(-\frac{1}{2}\frac{(\log d_{ice} - \log \mu)^2}{s^2}\right), \qquad (1.3)$$

where $n_{num}(d_{ice})$ represents the number of particles per unit volume and per unit increment of particle size (spectral size distribution), $\log \mu$ denotes the logarithmic mean (expected) value, s^2 is the logarithmic variance, i.e., the logarithm of the particle diameter is in the interval of $[\log \mu - 3s,\ \log \mu + 3s]$. (The square root s of the variance is the standard deviation). If d_1 and d_2 are the diameter of the smallest and largest particles of frazil ice, respectively, then

$$\log \mu = \left(\log d_1 + \log d_2\right)/2 \tag{1.4}$$

or

$$\mu = \sqrt{d_1/d_2}$$

$$s = \frac{1}{6}\log\left(d_2/d_1\right).$$

Ye and Doering (2004) showed that the frazil ice distribution by volume can be represented approximately by a lognormal distribution, which is concluded from their experimental data analysis. The instantaneous mean diameter of frazil ice and the standard deviation were formulated in terms of the flow Reynolds number, frazil ice concentration, etc.

Clark and Doering (2004) conducted a series of experiments in a counter-rotating flume using an improved frazil ice observation system, which was able to observe particles as small as 0.055 mm. They found that a lognormal distribution fit the experimental data quite well at different times during the supercooling process (see figure 1.5). The variation of the mean size of the frazil ice was also given as shown in figure 1.6, and it is mathematically formulated in chapter 6 of this thesis. However, a mathematical description of the standard deviation is not given.

1.4 Brief Review of Mathematical Models Development on Frazil Ice Formation

The study of frazil ice formation has become one of the most important tasks in the field of

ice engineering because frazil ice is the origin of most forms of river ice. Therefore frazil ice modeling is the most basic portion of the modeling of ice formation in rivers.

The most important factors in frazil ice formation are the seeding rate, the heat transfer rate and the turbulence level of the water. Some mathematical models (Daly, 1984; Mercier, 1984; Svensson and Omstedt, 1994; Hammar and Shen, 1995) have been developed to simulate frazil ice formation in water. These models are briefly introduced in the following sections.

1.4.1 Daly (1984)

Based on the Randolph and Larson (1971) theory of crystallization, Daly (1984) developed a descriptive and predictive crystal distribution model. The model can be described by two equations: the crystal number continuity equation and the heat balance equation. These two equations are linked by the growth and the secondary nucleation rate of the ice crystals, which are dependent on both the heat balance and the crystal size distribution. In theory, the equations can be solved if the various required boundary and initial conditions are known. However, Daly (1984) also noted that the equations are dimensionally incompatible and strongly nonlinear.

1.4.2 Mercier (1984)

Mercier (1984) extended the work of Daly (1984) and formulated a kinetic model of frazil ice growth and verified it against experimental data. In his model, the transport equation for

a one-point, joint scalar probability density function (PDF) is employed to incorporate fast, nonlinear reaction kinetics into a general transport model. In addition, a stochastic algorithm for simulating the differential sedimentation and the radial diffusion was developed. A Monte Carlo technique was applied to solve the PDF transport equation.

1.4.3 Svensson and Omstedt (1994)

In Svensson and Omstedts' model, frazil ice particles are classified into several discrete radius intervals, within which all the particles are assumed to be of an equal radius. The number of particles in each group is assumed to be a function of initial seeding, ice particle growth, secondary nucleation, flocculation/break up, and gravitational removal. Ice particle growth is determined by the heat transfer rate between the water and the ice particles. Secondary nucleation is simulated in terms of the collisions between the particles and flocculation is considered based on a sintering mechanism. Gravitational removal is assumed to have more effect on the larger particles. The number continuity equation, which describes the evolution of the particle size distribution from an initial stage, together with the overall heat transfer equation, are both solved to obtain the frazil ice numbers in the subsequent time step.

1.4.4 Hammar and Shen (1995)

Hammar and Shen's model is comprised of three differential equations: the mean flow equation, the frazil concentration equation, and the water temperature equation. In their

model frazil ice particles are assumed to be thin circular disks with a constant ratio of 1:10 (thickness to the face diameter). The frazil ice size distribution is described using eight logarithmically spaced size groups. The size of the groups range from 4 μm to 1.432 mm (radius); the seed crystals and secondary nucleation are assumed to occur in the lowest size group. The formulation of frazil ice evolution includes thermal growth, secondary nucleation, and flocculation. The flow turbulence was simulated by a typical $k-\varepsilon$ model and all the equations are finally solved using the PHONIEX commercial software.

1.5 Research at Hydraulics Research and Testing Facilities

Because of the significant effect of ice on hydraulic facilities in Manitoba, especially on hydropower stations, the Hydraulics Research and Testing Facility (HRTF) at the University of Manitoba started to explore some of the intriguing questions related to frazil ice formation using the unique counter-rotating flume available at the HRTF. Numerous experimental studies and some mathematical modeling have been undertaken. (Doering and Morris, 2002; Clark and Doering, 2002, 2004; Ye and Doering, 2004; Clark and Doering, 2006)

Doering and Morris (2002) developed a digital image processing system to characterize frazil ice. The system used cross-polarized light and a CCD camera coupled to a frame grabber to acquire gray-scale images of frazil ice particles. The digital images were manipulated by the processing system to derive a binary image showing the frazil ice

particles. The binary images were subsequently analyzed to characterize the particles. Based on this system a frazil ice distribution was identified.

Clark and Doering (2002) recognized several different types of frazil ice formations using an updated version of the above digital image processing system. They found that needle shaped particles occurred first, followed by disk-shaped particles, stars, and hexagons. The maximum size of uniform frazil disks was observed to be about 5 mm in diameter, after which they become unstable, non-uniform, and jagged. They also found that the size distribution of frazil ice can be well described by a lognormal distribution at different times during supercooling. The variation of the mean size of the ice particles seems to follow a common tendency, which increases in the principal supercooling process and reaches a plateau in the period of residual supercooling (Clark and Doering, 2004).

Ye and Doering (2004) conducted more than forty experiments to examine the effect of different hydraulic parameters on the supercooling process and frazil ice evolution. In addition, a mathematical model was developed to model the supercooling process and frazil ice evolution.

Clark and Doering (2006) conducted a series of experiments in a counter rotating flume at the Hydraulics Research and Testing Facility, University of Manitoba. A high-precision thermometer and recently improved digital image processing system were used to acquire

data from these experiments, which will hopefully aid in the development of numerical models. The effects of air temperature, water velocity, and bottom roughness on the formation of frazil ice are discussed. It is concluded that a lognormal distribution appears to provide a reasonable fit to the observed frazil particle size distributions.

1.6 Objectives of this Research

Although a lot of effort has been put into the study of frazil ice formation by ice researchers, there is still more that needs to be done. The mathematical model developed previously have some shortcomings such as not considering all of the physical processes of ice formation, or were not verified by experimental data, etc. Therefore, comprehensive mathematical models are required and needed to be experimentally verified in order to be used in practice. The counter-rotating flume at the HRTF has provided a lot of experimental data for model calibration and verification.

The objectives of this research are:

a) to develop a zero-dimensional mathematical model which considers the complicated physical processes of ice formation to simulate the supercooling process and the evolution of frazil ice number during the supercooling process;

b) to develop a vertical one-dimensional mathematical model to simulate the vertical distribution of flow turbulence and frazil ice number concentration;

c) to develop an extended one-dimensional mathematical model by combining the zero-dimensional and one-dimensional model;

d) to investigate the effects of different turbulence models on frazil ice formation; and

e) to compare simulation results from the mathematical model with experimental data.

1.7 Thesis Organization

This document is organized to eight chapters. In chapter 2, a general mathematical model is formulated based on the theories of open channel flow, heat transfer and mass transfer. Chapter 3 introduces some methodologies for modeling the different physical processes of frazil ice formation. In chapter 4 a zero-dimensional mathematical model is developed and used to simulate frazil ice formation in a well-mixed water body. Chapter 5 presents a mathematical model with the vertical space dimensions considered that simulates the supercooling process and the distribution of frazil ice number during the supercooling process. In chapter 6 an extended mathematical model is formulated by considering the size distribution of frazil ice and the physical processes of ice formation. Chapter 7 investigates the effects of different turbulence models on frazil ice formation. Finally in chapter 8 the work of this study is summarized and some conclusions are presented and some recommendations for future study are also suggested.

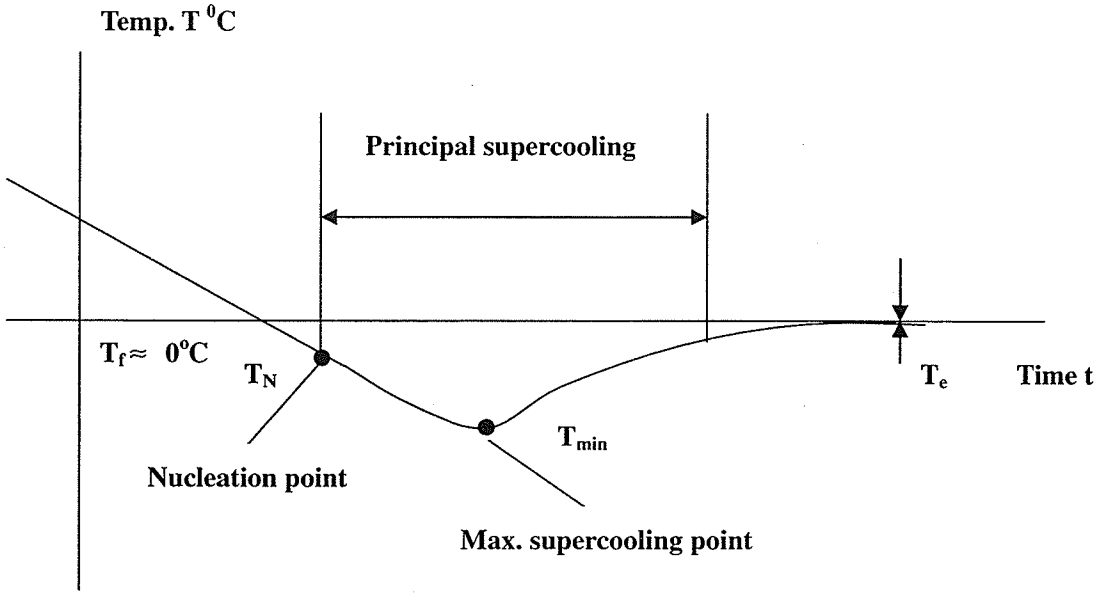

Figure 1.1 Typical supercooling processes.

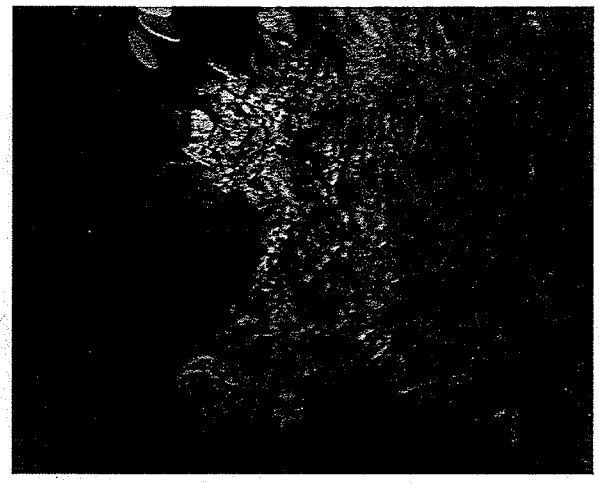

Figure 1.2 An observed sintered ice mass (Clark and Doering, 2004).

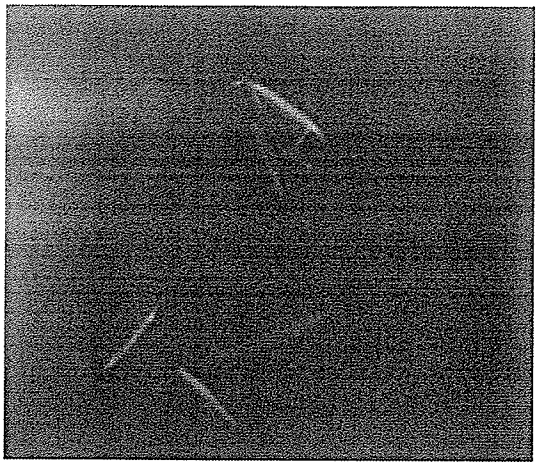

Figure 1.3 Needle ice formed in the counter-rotating flume at the HRTF (Clark and Doering, 2002).

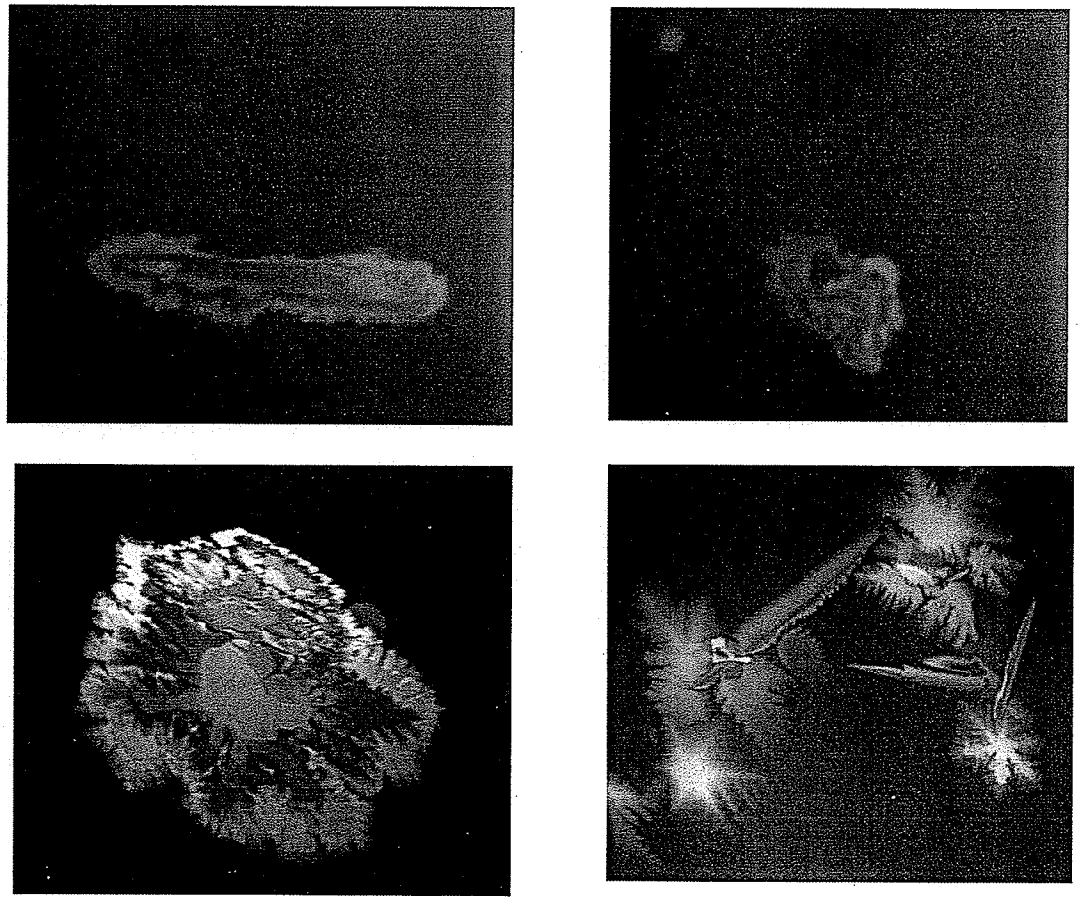

Figure 1.4 Irregularly shaped particles (Clark and Doering, 2002).

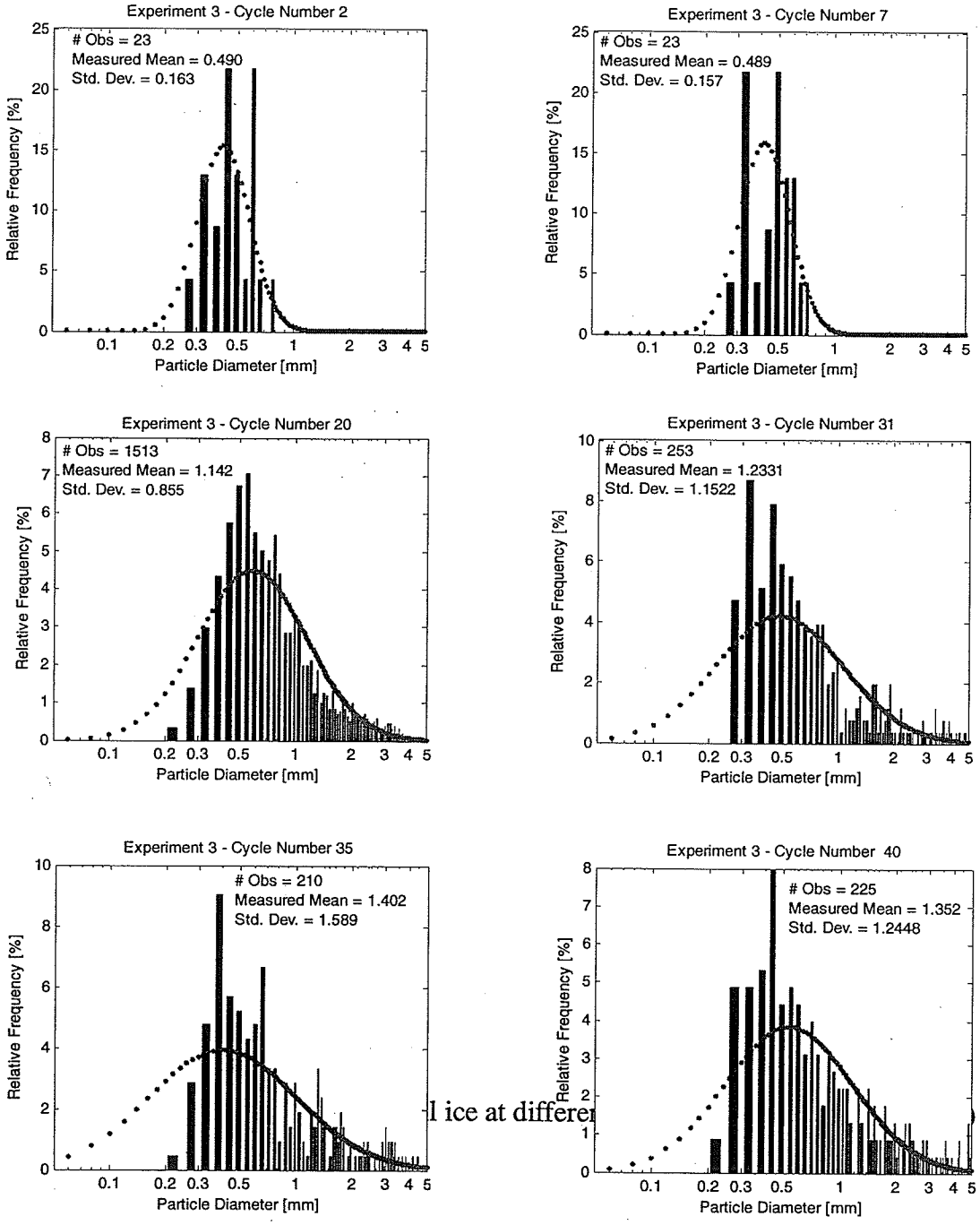

Figure 1.5 Distribution of frazil ice at different times (Clark and Doering, 2004).

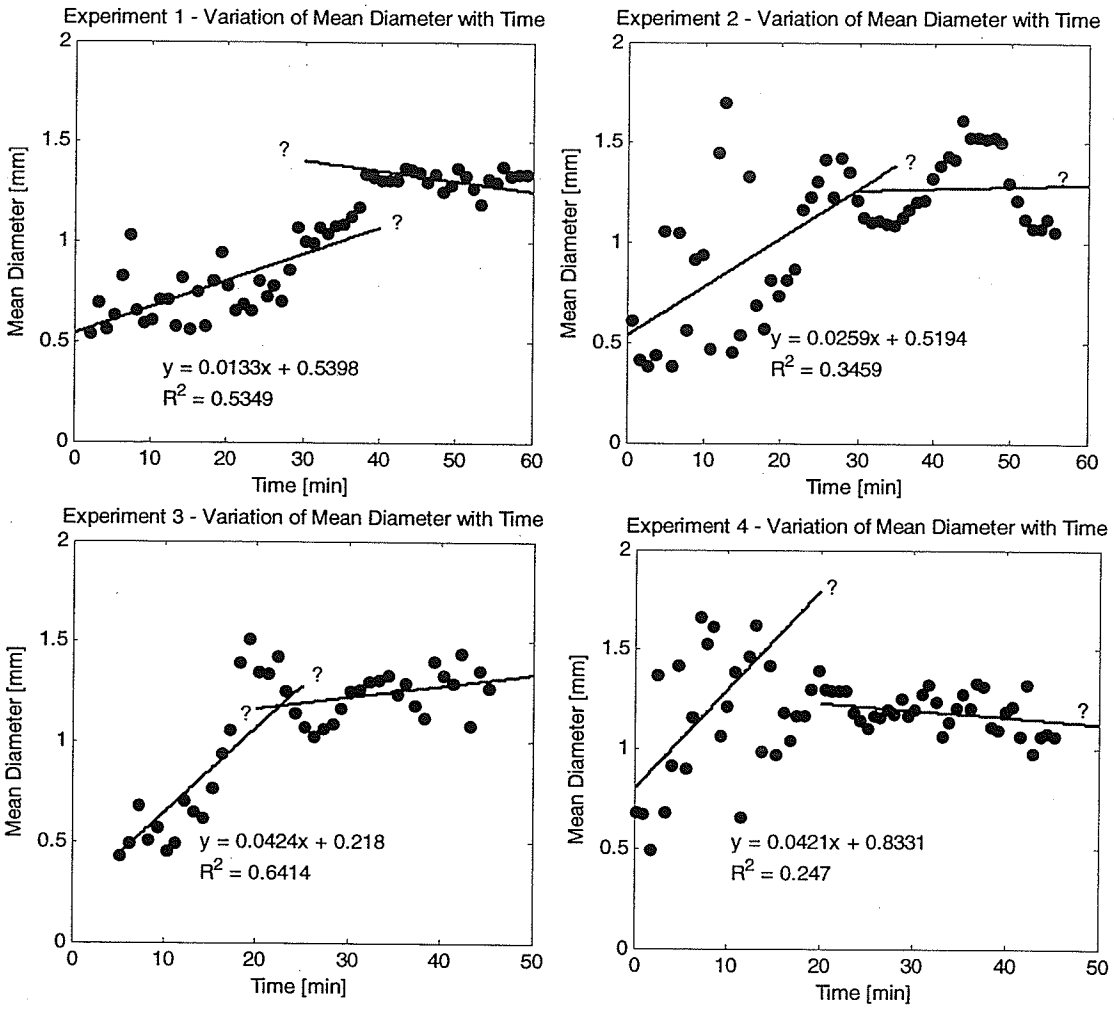

Figure 1.6 Variation of mean size of frazil ice particles (Clark and Doering, 2004).

CHAPTER 2

A General Mathematical Model for Frazil Ice Evolution In Turbulent Water

2.1 Introduction

The process of frazil ice formation, involving flow turbulence, heat transfer between ice particles and the ambient flow, and the transport of frazil ice in water, is a very complicated phenomenon. Theoretically, frazil ice formation can be categorized as a typical two-phase flow problem. The modeling of two-phase flow has been a very prevalent and challenging subject in the field of computational fluid mechanics over the past decades (R. Scardovelli and S. Zaleski, 1999).

Different approaches have been developed to formulate two-phase flow (Tryggvason et al., 2001). The main focus has been on the treatment of the interface that separates the phases. Since the detailed knowledge of the position of the phase interface is not always known and it is very costly to obtain it computationally, the so-called homogenized or averaged mixture

models are put forward as an alternative to the interface methods (Ishii, 1975). The system of governing equations for such models is obtained by the volume and time averaging of the single phase equations. The averaging of the single phase equations results in additional terms, which describe the interaction between the two phases.

In the frazil ice formation process, frazil ice concentration is usually very small both in a natural water body and in the experiments. It has been found that the frazil crystal concentrations range from about 10^4 to 10^6 crystals/m^3 in a natural river (Schaefer, 1950; Oskerkamp and Gosink, 1982), and from 1.8×10^5 to 9.82×10^5 crystals/m^3 in a laboratory flume (Daly and Colbeck, 1986). The upper limit of frazil concentration formed in a supercooled water stream is of the order of 0.5% by weight (Tsang, 1986). Therefore, the assumption that the influence of frazil ice on flow turbulence can be neglected appears reasonable. The density difference between the water and the frazil ice is quite small and the relative velocity of the frazil ice to the ambient water is also quite small, so the flow equations are only considered in the modeling of frazil ice formation.

2.2 Modeling of the Flow and the Turbulence

The flows in most natural rivers are turbulent flow and can be described by time dependent Navier- Stokes equations (i.e., N-S equations). N-S equations can be solved directly with supercomputers; however, it is very time-consuming and sometimes not necessary if the

detailed turbulence structure is not of interest. The mean-flow equations that are derived by statistically averaging the N-S equations are usually used for turbulent flow simulations. The derived Reynolds equations are no longer closed when the Reynolds stress term is introduced, therefore a turbulence model is necessary to close the system.

2.2.1 Flow Equations

The continuity equations for the mean flow can be written as,

$$\frac{\partial U_i}{\partial x_i} = 0. \tag{2.1}$$

The momentum equation can be described by,

$$\frac{\partial U_i}{\partial t} + U_j \frac{\partial U_i}{\partial t} = \frac{1}{\rho_m}\frac{\partial P_w}{\partial x_j} + \frac{\partial}{\partial x_j}\left(\nu \frac{\partial U_i}{\partial x_j} - \overline{u_i u_j}\right) + g_j, \tag{2.2}$$

where ρ_m is the density of the mixture, $\rho_m = \rho_w + (\rho_i - \rho_w)\sum C_k$, ρ_i and ρ_w are the densities of ice and water, respectively, U_i is the i_{th} component of the mean velocity, $\overline{u_i u_j}$ is the Reynolds stress, P_W is the mean water pressure, ν is the molecular viscosity, ν_t is the kinematic eddy viscosity, and g_j is the j^{th} gravity component.

2.2.2 Turbulence Modeling

Generally, two approaches are suggested to deal with the Reynolds stress term and close the system mathematically. One is the eddy viscosity approach and the other is the stress equation approach. The latter is rarely applied to open channel flow. The eddy-viscosity model is formulated based on the assumption that the turbulent stresses are proportional to

the mean velocity gradients, which is analogous to the viscous stresses in a laminar flow. A variety of turbulence models have been suggested (Rodi, 2000) for the eddy viscosity concept such as the zero-equation model, the one-equation model, the two-equation $k-\varepsilon$ model, the two-equation $k-kl$ model, etc. The $k-\varepsilon$ two-equation model is the most commonly used turbulence model for the simulation of open channel flow

2.2.2.1 The two-Equation $k-\varepsilon$ Model

The turbulent energy k characterizes the intensity of the fluctuating motion and represents the velocity scale of the fluctuation. The k equation and the ε equation in the $k-\varepsilon$ model are as follows,

$$\frac{\partial k}{\partial t}+U_i\frac{\partial k}{\partial x_i}=\frac{\partial}{\partial x_i}\left(\frac{\nu_t}{\sigma_k}\frac{\partial k}{\partial x_j}\right)+P+G-\varepsilon \tag{2.3}$$

$$\frac{\partial \varepsilon}{\partial t}+U_i\frac{\partial \varepsilon}{\partial x_i}=\frac{\partial}{\partial x_i}\left(\frac{\nu_t}{\sigma_\varepsilon}\frac{\partial \varepsilon}{\partial x_i}\right)+C_{1\varepsilon}\frac{\varepsilon}{k}(P+G)-C_{2\varepsilon}\frac{\varepsilon^2}{k} \tag{2.4}$$

where k is the turbulent kinetic energy and ε is the energy dissipation rate, P is the generation of turbulent energy, $P=\nu_t\left(\frac{\partial U_i}{\partial x_j}+\frac{\partial U_j}{\partial x_i}\right)\frac{\partial U_i}{\partial x_j}$, G is the buoyant production/destruction, $G=\nu_t g\left(\frac{1}{\sigma_T}\frac{\partial T}{\partial z}+\frac{1}{\sigma_C}\frac{\rho_i-\rho_0}{\rho_0}\frac{\partial C}{\partial z}\right)$, ρ_i is the density of the frazil ice, ρ_0 is the density of the water, and ν_t is the eddy viscosity, $\left(\nu_t=C_\mu\frac{k^2}{\varepsilon}\right)$, T is the water temperature, C is the concentration of the frazil ice, σ_T and σ_C are the

Prandtl/Schmidt number. Several empirical constants such as C_μ, $C_{1\varepsilon}$, $C_{2\varepsilon}$, σ_k and σ_ε are included in the above equations, and the values of these constants as recommended by Lauder and Spalding (1974) are given in Table 2.1.

Table 2.1 Values of the constants in $k-\varepsilon$ model

C_μ	$C_{1\varepsilon}$	$C_{2\varepsilon}$	σ_k	σ_ε
0.09	1.44	1.92	1.0	1.3

Now the mean flow equations together with the $k-\varepsilon$ model become a closed system, and the system can be numerically solved with the proper boundary conditions.

The mathematical formulation for the flow (equations (2.1), (2.2)) and turbulence (equation (2.3)) can be simplified into two-dimensional or one-dimensional cases (horizontal or vertical direction) according to what terms can be neglected in the controlling equations in terms of physical importance.

2.2.2.2 Zero-Equation Model

In a relatively simple turbulence model, i.e., a zero-equation model, the eddy viscosity can be easily obtained from the expressions of k and ε. The typical distribution of the eddy viscosity in an open channel flow is given by Nezu and Nakagawa (1993). Several expressions for k and ε are available (Nezu and Nakagawa, 1993) in the zero-equation model. A typical vertical distribution of the turbulent energy dissipation in an open channel

flow is described by (Mercier, 1984; Hammar and Shen, 1995)

$$\varepsilon(z)=\frac{u_*^3}{\kappa z}(1-\frac{z}{H}). \tag{2.5}$$

The turbulent kinetic energy can be approximated by

$$k(z)=\frac{u_*^{2\text{-}}}{0.3}(1-\frac{z}{H}), \tag{2.6}$$

where u_* is the friction velocity, κ is the Karman constant, z is the vertical distance measured from the bed, and H is the water depth. Hereafter, this model is called turbulence model I in this study.

The eddy-viscosity is

$$\nu_T=C_\mu\frac{k^2}{\varepsilon}, \tag{2.7}$$

$$\nu_T=C_\mu\frac{\left[\frac{u_*^2}{0.3}\left(1-\frac{z}{H}\right)\right]^2}{\frac{u_*^3}{\kappa z}\left(1-\frac{z}{H}\right)}=\frac{C_\mu}{0.09}u_*\kappa z\left(1-\frac{z}{H}\right). \tag{2.8}$$

Normally taking $C_\mu=0.09$ then

$$\nu_T=\frac{C_\mu}{0.09}u_*\kappa z\left(1-\frac{z}{H}\right)=u_*\kappa z\left(1-\frac{z}{H}\right). \tag{2.9}$$

Another zero-equation model was suggested by Nezu (1977) and is called turbulence model II in this study. The expressions for k and ε are

$$\frac{k(z)}{u_*^2} = 4.78\exp\left(\frac{-2z}{H}\right) \tag{2.10}$$

and

$$\frac{\varepsilon(z)*H}{u_*^3} = E_1\left(\frac{z}{H}\right)^{-1/2}\exp\left(\frac{-3z}{H}\right) \tag{2.11}$$

yielding,

$$\nu_T = C_\mu\frac{k^2}{\varepsilon} = C_\mu\frac{4.78^2}{E_1}(zH)^{1/2}u_* e\,\mathrm{xp}\left(\frac{-z}{H}\right). \tag{2.12}$$

Taking $C_\mu = 0.09$ and $E = 9.8$ (if Reynolds number is about $10^4 \sim 10^5$), then

$$\nu_T = 0.2098(zH)^{1/2}u_* e\,\mathrm{xp}\left(\frac{-z}{H}\right). \tag{2.13}$$

These two simple turbulence models are usually used in the vertical one-dimensional mathematical model to simulate the flow and turbulence characteristics.

2.3 Modeling of the Heat Transfer in Turbulent Water

Frazil ice formation results from the comprehensive heat transfer process between the water and its ambient environment (air, and river bank, etc.), and between the water and the exsisting frazil ice. The water temperature variation can be modeled based on the thermal dynamics of frazil ice and the turbulent heat transfer at the water surface. The thermal dynamics of frazil ice is a key factor in the modeling of the water temperature.

The turbulent heat convection equation for water is given by

$$\frac{\partial T}{\partial t}+U_i\frac{\partial T}{\partial t}=\frac{\partial}{\partial x_i}\left(\left(\frac{\nu_t}{\sigma_t}+\frac{\nu}{P_r}\right)\frac{\partial T}{\partial x_j}\right)-S_b+S_f, \qquad (2.14)$$

where U_i is the i_{th} component of the mean velocity, ν is the molecular viscosity, ν_t is the kinematic eddy viscosity, and σ_t are Prandtl/Schmidt numbers, P_r is Prandtl number, T is the water temperature, S_b, S_f are source terms due to the heat loss at the channel boundaries and the latent heat release from the frazil growth. The term S_f can be determined by frazil thermal dynamics.

2.4 Modeling of Frazil Ice Formation and Transport

Once frazil ice formation is initiated in supercooled turbulent water, more frazil ice particles are produced as the water temperature is lowered. Due to the turbulent mixing and buoyancy effect, frazil ice will be distributed throughout the water depth and will be carried downstream by the flow. These phenomena can be mathematically described by the following mass advection-diffusion equation

$$\frac{\partial C_k}{\partial t}+U_i\frac{\partial C_k}{\partial t}=\frac{\partial}{\partial x_i}\left(\left(\frac{\nu_t}{\sigma_c}+\frac{\nu}{S_n}\right)\frac{\partial C_k}{\partial x_j}\right)-\varpi_k\frac{\partial C_k}{\partial x_3}+S_{c_k}+S_{floc,k}, \qquad (2.15)$$

where U_i is the i_{th} component of the mean velocity, σ_c is turbulent Prandtl number for

frazil ice concentration, S_n is the turbulent Schmidt number, C_k is the volumetric concentration of the frazil ice in the k[th] size fraction, ϖ_k is the frazil buoyant velocity of the k^{th} size fraction, S_{c_k} is the source term due to the thermal growth of the frazil ice and $S_{floc,k}$ is the source/sink term due to secondary nucleation and flocculation. The determination of these two terms S_{c_k} and $S_{floc,k}$ will be discussed in the chapters 5 and 6 when the specific mathematical model is formulated.

The mathematical formulation for water temperature (equation (2.14)) and frazil ice transport (equation (2.15)) can be simplified into two-dimensional or one-dimensional cases (horizontal or vertical direction), when only a certain space of ice formation is of interest.

2.5 Boundary Conditions

A general mathematical model for frazil ice formation was formulated in the above section. Boundary conditions are needed in order to find numerical solutions. Usually there are four boundary conditions for the unknown variables, i.e., inflow, outflow, rigid wall and free surface conditions.

2.5.1 Inflow and Outflow Boundaries Conditions

At the inflow boundary, prescribed values are given to all the dependent variables. The outflow conditions depend on the control structure of the outflow. A zero normal gradient of

a dependent variable such as velocity, water temperature, and concentration of frazil ice are applied at the outflow.

2.5.2 Free Surface Boundary Condition

For all the variables except for the turbulent energy dissipation rate ε, usually a zero flux or specific amount of flux at the water surface is enforced. The expression for ε suggested by Celik and Rodi (1984) and presented by Nezu (1993) is usually applied for the free boundary condition, i.e.,

$$\varepsilon_w = \frac{k_w^{3/2}}{\alpha_w H} \tag{2.16}$$

in which, k_w is the value of k at the water surface, H is the water depth, and α_w is the constant with a value of 0.18.

2.5.3 Rigid Wall Condition

The boundary condition at the bed or the banks of the river are usually not specified at the wall itself in an open channel simulation, but rather at the first grid point z_1^+, ($z^+ = zu_* / \nu$). and the zero flux boundary condition is used for the water temperature and the frazil ice concentration. The following relations for k and ε are specified at the first grid point outside the viscous layer,

$$k_1 = \frac{1}{\sqrt{C_\mu}} u_*^2 = 3.33 u_*^2 \quad \text{and} \quad \varepsilon_1 = \frac{u_*^3}{\kappa z_1},$$

where κ is the Karman constant.

2.6 Model Applicability in a Counter-Rotating Flume

A general mathematical model is formulated based on open channel flow theory. The model is then used to simulate the flow turbulence, the water temperature variation, and frazil ice formation in a counter-rotating flume at the Hydraulics Research and Testing Facility at the University of Manitoba.

The counter-rotating flume is specially designed to simulate frazil ice formation in an open channel flow. It has improved the flow characteristics over the circular flume used by Tsang (1994) where only the bed rotated. The flow in a counter-rotating flume is driven by a bed and walls that rotate in opposite directions and at a proper rate to minimize the effect of a secondary current created by centrifugal forces. The velocity calibration to determine the rates of counter-rotation was completed by Clark and Doering (2006). The flume is located in a temperature controlled cold room creating an ideal environment for frazil ice formation. The flow with respect to the bed in the counter-rotating flume simulates prototype open channel flow in a river.

The flow in open channels is driven by a pressure gradient $\frac{\partial P_w}{\partial x}$, i.e., the gravity component along the channel. When applying the open channel flow equations to a counter-rotating flume, the bed and wall effect can be considered as boundary conditions if three-dimensional flows are considered. When a vertical one-dimensional model is considered, the

pressure gradient term $\frac{\partial P_w}{\partial x}$ can be intentionally used to simulate the resultant force produced by the walls and the bed, similar to how Omstedt (1985a) used the pressure gradient to simulate the force from a propeller in his experiments. This term should be calibrated in order to allow the flow to reach a steady state.

The temperature of the water in the flume is measured with a high resolution thermometer, which is recorded by a data acquisition system. The temperature data is useful for the calibration of the model. Frazil ice is detected by using a cross-polarized lighting technique (Doering and Morris, 2003; Clark and Doering, 2004). A high resolution CCD camera is used to collect images of the frazil ice and these digital images are used to determine the frazil ice characteristics. The detailed descriptions of the counter-rotating flume and the algorithms used to detect the frazil ice were introduced by Morris and Doering (2003), Clark and Doering (2004) and Ye and Doering (2004).

CHAPTER 3

Mathematical Modeling of the Physical Processes of Frazil Ice Formation

3.1 Introduction

As described in previous chapters, the physical process of frazil ice formation consists of the initial seeding, secondary nucleation, flocculation/break up and buoyancy removal. To better model frazil ice formation it is necessary to understand the basic theory of each process, and to develop mathematical formulation for these mechanisms.

3.2 Seeding

Seeding is required to start heterogeneous nucleation, and therefore it is an important factor for frazil ice formation. The source of seeding could be from mass transfer between water surface and air, crystal dust washed off from large crystal, or microscopic crystals fallen into the melt (Andreas Muller, 1978). However, it is difficult to quantify and to measure experimentally due to its extensive origins. In mathematical simulation, seeding should be

defined to initiate the simulation process, and it usually considers the seeding as a calibration parameter in most mathematical models, including this one.

3.3 Thermal Growth of Ice Particles

The growth rate of ice particles depends on the transfer rate of the latent heat from the particles to the ambient turbulent flow. The heat transfer rate from ice particles to the turbulent flow is influenced by many factors and also varied for different ranges of turbulence. Since the density of the ice particles is different from that of the water, the ice particles are subject to gravitational and inertial forces that give them a gravitational motion relative to the water, but it has been found that the translational motion caused by inertia and gravity can be neglected in determining the heat transfer (Daly, 1984).

The rate of heat transfer from an ice particle surface to the water body per unit area, q, can be estimated as

$$q = h_w(T_i - T). \tag{3.1}$$

The heat transfer coefficient, h_w, can be expressed in its dimensionless form as a Nusselt number defined by

$$N_u = \frac{h_w l}{k_w}, \tag{3.2a}$$

where k_w is the conductivity of the water. Equation (3.2a) can be rearranged to give

$$h_w = N_u \frac{k_w}{l}. \tag{3.2b}$$

The face radius of an ice particle is used as the characteristic length (Daly 1984).

The Nusselt number depends on the flow conditions and the particle size (Daly, 1984). It is defined as the ratio of the actual heat transfer to that due to conduction alone. In this study an actual Nusselt number is used instead of the turbulent Nusselt number that was used by Hammar and Shen (1995). A detailed discussion of the Nusselt number and the turbulent Nusselt number can be found in Daly's report (1984).

The actual Nusselt number is defined by the turbulent Nusselt number, N_{u_T}, multiplied by the term $m^* = r/\eta$, i.e., $N_u = N_{u_T} m^*$. This relationship can be derived by comparing equations (49), (50) and (60) (Daly 1984) with the equations given in Daly's (1984) summary. The formulation for the turbulent Nusselt number developed by Batchelor (1980) and Wadia (1974), which is summarized by Daly (1984), is described as follows

$$N_{u_T} = \left(\frac{1}{m^*}\right) + 0.17\,\mathrm{Pr}^{1/2} \quad \text{if} \quad m^* < \frac{1}{\mathrm{Pr}^{1/2}} \tag{3.3}$$

and

$$N_{u_T} = \left(\frac{1}{m^*}\right) + 0.55\left(\frac{\mathrm{Pr}}{m^*}\right)^{1/3} \quad \text{if} \quad \frac{1}{\mathrm{Pr}^{1/2}} < m^* < 10, \tag{3.4}$$

where $m^* = r/\eta$, is the ratio between the face radius of an ice particle and the Kolmogorov length scale.

For large particles, i.e., $m^* > 1$

$$N_{u_T} = 1.1\left[\left(\frac{1}{m^*}\right) + 0.80\alpha_T^{0.035}\left(\frac{\mathrm{Pr}}{m^*}\right)^{1/3}\right] \quad \text{if} \quad \alpha_T m^{*4/3} < 1000 \tag{3.5}$$

and

$$N_{u_T} = 1.1\left[\left(\frac{1}{m^*}\right) + 0.80\alpha_T^{0.24}(\mathrm{Pr})^{1/3}\right] \quad \text{if} \quad \alpha_T m^{*4/3} \geq 1000, \tag{3.6}$$

where $\alpha_T = \sqrt{2k}/U$ is the turbulence intensity, and U is the mean flow velocity. It should be noted that when m^* increases, N_{u_T} decreases, while N_u increases.

3.3.1 Thermal Growth of a Single Ice Particle

Disk shaped frazil ice is the most dominant shape of frazil ice formed. If the size of a frazil disk is defined by its radius r, the ice particle growth rate can be modeled by (Daly, 1984)

$$\frac{dr}{dt} = \frac{h_w}{\rho_i L}(T_i - T_w), \tag{3.7}$$

where h_w is the heat transfer coefficient and can be calculated from equation (3.2b). Equation (3.7) will be used herein to simulate the mean size variation during the supercooling process.

3.3.2 Thermal Growth of Ice Particles in Volumes

The ice volume produced per unit time by thermal growth can be computed from the following

$$\frac{dM}{dt} = \frac{Q_{iw}}{\rho_i L_i} \tag{3.8a}$$

or $$\frac{d}{dt}\left(\rho C_p (1-M)T\right) = Q_{iw} - Q_{aw}, \qquad (3.8b)$$

in which, ρ is the density of water, L_i is the latent heat of the water, T is the ambient water temperature, M is the volume concentration of the frazil ice, Q_{iw} is the total heat transfer between the ice and water, and Q_{aw} is the heat exchange between the water and the air and is given by $Q_{aw} = \phi(T_a - T)$, ϕ is the heat transfer coefficient and is constant for a given air temperature and wind speed. However, Q_{aw} can also be computed from the cooling rate of the water neglecting the heat transfer from a river bank

$$Q_{aw} = \rho C_p \frac{dT}{dt}, \qquad (3.9)$$

where C_p is the specific heat of the water, and $\frac{dT}{dt}$ is the cooling rate measured from the $T-t$ history curve.

3.4 Secondary Nucleation

The mechanism of secondary nucleation has been studied by several researchers (Daly, 1984; Mercier, 1984; Svensson and Omsted, 1994). Accordingly, some mathematical representations have been formulated already based on a limited understanding; although this complicated process was not well characterized. These formulations have been used in some mathematical modeling of frazil ice formation. The formulation given by Svensson and Omsted (1994) is used in this study.

3.4.1 Daly's Formulation

Based on the kinetics of secondary nucleation, a theoretical formulation of the secondary nucleation rate was suggested by Daly (1984) as follows

$$\dot{N}_t = \left(\dot{E}_{t1} + \dot{E}_{t2} + \dot{E}_{t3} + \ldots \right) S_N \left(\theta_t, \varepsilon, etc. \right), \qquad (3.10)$$

where $\dot{N}_t$ is the secondary nucleation rate, $\dot{E}_{ti}$ is the rate of the energy transfer, which can be determined by the different mechanisms of collision. S_N is the product of two functions F_1 and F_2. F_1 represents the number of particles produced per unit of collision energy and F_2 represents the number of particles surviving to become crystals. S_N largely depends on the supercooling of the water and less on the level of turbulence (Daly 1984).

The expression for $\dot{E}_{ti}$ is given by Daly (1984) based on the collision between particles and the collision between particles and the boundary, however, a description for S_N is not presented as it is hard to determine.

3.4.2 Evan et al. and Mercier's Formulation

The procedure put forward by Evans et al. (1974a, b) for the secondary nucleation is summarized by Mercier (1984) and adopted in his model. Furthermore, Hammar and Shen (1995) used Mercier's formulation in their mathematical model to simulate frazil ice formation.

Formulation by Evan et al. (1974) is derived based on the fact that breeding is the primary mechanism of secondary nucleation. The number of nuclei produced by the collision between particles of size v_i and v_j is

$$I(v_i, v_j) = \int_{v_{i-1/2}}^{v_{i-1/2}} \int_{v_{i-1/2}}^{v_{i-1/2}} ZC_E\left(v_i, v_j\right) dv_i dv_j , \tag{3.11}$$

where $I(v_i, v_j)$ is the number of nuclei produced per unit time, v_i and v_j are the volumetric sizes of the colliding particles, Z is the number of nuclei produced per unit collision energy, and $C_E\left(v_i, v_j\right)$ is the rate of the collision energy transferred to the crystals per unit volume of fluid (it can be expressed in terms of the collision frequency and the collision efficiency). The collision frequency function is the collision probability of two non-interfering particles of size v_i and v_j in a unit time. Typically the turbulent shear and the differential rising are the main contributors for $C_E\left(v_i, v_j\right)$, which is given by

$$\begin{aligned} C_E\left(v_i, v_j\right) = 0.5\rho_i \frac{v_i v_j}{v_i + v_j} \Bigg\{ & b\left(v_i^{1/3} + v_j^{1/3}\right)^5 \left(\frac{\varepsilon}{\nu}\right)^{3/2} E_{sh} + \\ & 0.00076\left(\frac{g}{\nu}\frac{\left|\rho_i - \rho_w\right|}{\rho_w}\left|v_i^{2/3} + v_j^{2/3}\right|\right)^3 \left(v_i^{1/3} + v_j^{1/3}\right)^2 E_{dr} \Bigg\} g\left(v_i\right) g(v_j). \end{aligned} \tag{3.12}$$

ε is the mean energy dissipation rate, ν is the kinematic viscosity of water, $b = 0.0066 / K_u^{3/4}$, K_u is the kurtosis of the velocity derivative (Mercier 1984), and $g\left(v_i\right)$ are the frazil ice number density functions. The collision efficiency functions for the differential rising and the turbulent shear, E_{dr} and E_{sh}, respectively, are introduced to account for the particle interference effects, which are evaluated according to the procedure described by Pearson et al. (1984).

3.4.3 Svensson and Omstedt's Formulation

A simple formulation for secondary nucleation was suggested by Svensson and Omstedt (1994) based on the assumption that breeding by collision is the dominant process. Consider the relative movement of a particle in a volume Δ_i in a time interval dt, $\Delta_i = U_r \pi r_i^2 dt$, for which U_r is the crystal velocity relative to the fluid. A collision frequency for n_i particles in a radius interval i can then be formulated as

$$f_{colli}^{i} \sim \bar{n} \Delta_i n_i / dt, \tag{3.13}$$

where $\bar{n}$ is the average number of particles per unit volume. The relative velocity is assumed to be related to the turbulent fluctuations and gravitational rise, $U_r = \sqrt{U_l^2 + U_{rise}^2}$, where $U_l = \left(1/15\right)^{1/2} \left(\varepsilon/\nu\right)^{1/2} d$, note that ε is the turbulent dissipation rate, ν is the kinematic viscosity, d is the particle diameter, and U_{rise} is the rise velocity of frazil ice in water. If a calibration factor is introduced by setting an upper limit on $\bar{n}$, then

$$\bar{n} = \min\left(\sum_{i=1}^{n} n_i, \bar{n}_{\max} \right). \tag{3.14}$$

The upper limit $\bar{n}_{\max}$ is introduced because the frequency of the collisions may be reduced since the concentration of frazil ice is increasing in the supercooling process and it will dampen the flow turbulence. It seems logical to limit $\bar{n}$ by the calibration factor $\bar{n}_{\max}$ as this will restrict the collision frequency. Then a coefficient α_j, which represents the rate of secondary nucleation, can be formulated as follows

$$\alpha_j = \frac{\bar{n} \Delta_i}{dt}. \tag{3.15}$$

3.5 Flocculation and Break up

Modeling flocculation is not easy since its mechanism is not clear yet (Daly, 1991). Sintering is considered the primary mechanism of flocculation. Some simple formulations are given and applied in the mathematical modeling by Svensson and Omstedt (1994) and Hammar and Shen (1995).

3.5.1 Svensson and Omstedt's Formulation

Svensson and Omstedt (1994) assumed that the transport to larger scales is the net effect of flocculation, and it is more effective for larger particles. A linear relation was suggested (Svensson and Omstedt, 1994) to describe the flocculation in the principal supercooling process

$$\beta_i = \alpha_{floc} \frac{r_i}{r_1}, \tag{3.16}$$

where β_i is the rate of flocculation of the frazil ice particles, and α_{floc} is a calibration parameter.

3.5.2 Hammar and Shen's Formulation

According to Mercier's (1984) stochastic coagulation theory, Hammar and Shen (1995) put forward a method to calculate the flocculation for frazil ice particles. For the particles in i^{th} size and j^{th} size group, the expected number of instantaneous collisions per unit volume

per unit time is

$$F_n = \beta(v_i, v_j)E(v_i, v_j)\phi_i\phi_j, \tag{3.17}$$

where ϕ_i and ϕ_j are the number concentrations of the i^{th} and j^{th} size particles, respectively. If each collision per unit volume reduces the local number concentration in the i^{th} and the j^{th} size group by one, then it will create a new particle in the volume $v_{new} = v_i + v_j - v_{Sec}$ by merging, where v_{Sec} is the volume contributed to secondary nuclei production. It is assumed that the merged particles will be distributed to the two neighboring size groups. Based on conservation of volume, a fraction $f = {(v_{k+1} - v_{merge})}/{(v_{k+1} - v_k)}$ of F_n is assigned to the k^{th} size group, and a fraction (1- f) is assigned to $(k+1)^{th}$ size group. When the merged particle size is larger than the size of the last size group m, then the fraction $f = {v_{merge}}/{v_m}$ of F_n is assigned to the m^{th} size group.

3.6 Buoyancy Removal

Svensson and Omstedt (1994) assumed that buoyancy force removes some particles located throughout the volume $A_{sw}U_{rise}dt$ in a time step dt, where A_{sw} is the water surface area. The removal per unit time and volume is ${A_{sw}U_{rise}dt}/{A_{sw}Hdt}$. The removal per unit time and volume is thus:

$$\gamma_i = \frac{U_{rise}}{H}, \tag{3.18}$$

where γ_i is the rate of the buoyancy removal, and H is the depth of the well mixed flume.

Note that $U_{rise} = 30 r_i^{1.2}$, where r_i is the radius of the disc (Daly, 1984). It should be recognized in the calculation of the rise velocity ($U_{rise} = 30 r_i^{1.2}$) that the units for the radius and the rise velocity are cm and cm/s, respectively.

CHAPTER 4

A Zero-Dimensional Model of Frazil Ice Formation and Evolution

4.1 Introduction

A zero-dimensional model for frazil ice formation and evolution is developed based on the assumption that the water is well-mixed and that flow stratification can be neglected, and as such that vertical spatial resolution is not required.

The model formulated in this chapter is based on combination of Daly's (1984) model and Svensson and Omstedt's (1994) model. The physical process of the initial seeding, ice particle growth, secondary nucleation, flocculation/break up and buoyancy removal are implemented in this model. Furthermore, several modifications and improvements are made including the use of a variable Nusselt number related to the flow turbulence, the modification of the coefficient for secondary nucleation and buoyancy removal and the introduction of an additional coefficient for the secondary nucleation to allow for the formation of larger ice particles. This model can simulate the supercooling process, the

variation of frazil number with time, and the size distribution of frazil ice.

4.2 Model Formulation

The model formulated consists of two equations: a general heat balance equation and a number continuity equation. If the size range of frazil ice particles is divided into N discrete radius intervals, then all the particles are assumed to be of an equal radius in each interval. The overall heat transfer for the water and the frazil ice particles is described by

$$\frac{d}{dt}(\rho C_p(1-M)T) = -Q_{aw} + \sum_{i=1}^{N-1} Q_i \tag{4.1}$$

and

$$\frac{dM}{dt} = \frac{H_{wi}}{\rho_i L_i}(T_i - T), \tag{4.2}$$

where $Q_{aw} = \phi(T_a - T) = \rho_w C_p \left.\frac{dT}{dt}\right|_{coolingrate}$, $Q_i = h_{wi}(T_i - T)$, $H_{wi} = \sum_{i=1}^{N-1} h_{wi}$, and $h_{wi} = h_w A_i n_i$, $h_w = \frac{N_u k_w}{l}$. Q_i is the release of heat due to the freezing for the radius interval $i(i=1\ldots N-1)$, n_i is the number of crystals in the interval class i, A_i is the active freezing frazil ice area, k_w is the thermal conductivity, and l is the characteristic length of the ice particle. N is the total number of bins into which the frazil ice is discretized. h_{wi} is the heat transfer coefficient for all the ice particles in the interval class i, H_{wi} is the heat transfer coefficient for all the ice particles, and h_w is the heat transfer coefficient.

The number continuity equation describes the dynamic evolution of the frazil ice number as suggested by Daly (1984)

$$\frac{\partial n_c}{\partial t} + \frac{\partial}{\partial r}(G n_c) + D_i - B_i + \nabla(\overline{V_e} n_c) = 0\,, \qquad (4.3)$$

where n_c is the crystal size distribution along the crystal size axis r and at a time t, D_i is the death function which allows for the sudden disappearance of the crystals such as the break up of crystals, B_i is the birth function which accounts for the sudden appearance of crystals due to initial seeding and secondary nucleation, G is the growth rate of the ice particles, $\overline{V_e}$ is the external convective velocity, and r is the radius of an ice particle.

When the frazil ice particles are divided into several groups with the same size, and the physical processes such as the initial seeding, ice particle growth, secondary nucleation, flocculation and gravitational removal are considered, Daly's general equation can be simplified to the equation used in Svensson and Omstedt's (1994) model, which is easier to understand from a physical perspective.

In the model developed in this chapter, an additional parameter ζ_i is introduced into the secondary nucleation term in the equation of Svensson and Omstedt (1994) to allow for the formation of larger ice particles. It is assumed that secondary nucleation is a source for the smallest radius interval and a sink for the rest. The number of the smallest ice particles increases due to collisions, whereas the number of larger particles should be reduced by the

ratio of ζ correspondingly, therefore,

$$\frac{dn_i}{dt} = \left(\sum_{j=2}^{N}\alpha_j n_j\right) - \zeta_i\alpha_i n_i \quad - \beta_i n_i + \delta\beta_{i-1}n_{i-1} \quad - \gamma_i n_i \quad - \tau_i n_i + \tau_{i-1}n_{i-1}.$$

$(1 \le i \le N)$ $(i = 1)$ $(2 < i \le N)$ $(1 \le i \le N-1)$ $(2 \le i \le N)$ $(1 \le i \le N)$ $(1 \le i \le N)$ $(2 \le i \le N)$

change in number secondary nucleation flocculation/break up gravity crystal growth

(4.4)

α_j, β_i, γ_i, τ_i are the coefficients to describe secondary nucleation, flocculation/break up, gravitational removal, and ice particle growth, respectively. These coefficients are determined in the following sections.

4.2.1 Initial Seeding

As described in chapter 3, a certain number of particles are evenly presented in each interval at the time when supercooling begins. The number of frazil ice particles from the point of initial seeding is one factor to be calibrated in the simulation.

4.2.2 Ice Particle Growth

The ice volume produced per unit time by the ice particle growth for the interval i can be calculated as

$$\frac{\partial V_i}{\partial t} = N_u \frac{k_w}{l}(T_i - T)\frac{A_i n_i}{\rho_i L_i}, \tag{4.5}$$

where A_i is the active freezing area per ice particle. The area of a frazil ice particle's edge, i.e., $2\pi r_i t_i$, is considered as the active freezing area for a disk shaped ice particle, where t_i

is the thickness of an ice particle. The Nusselt number, N_u, can be calculated from the methods introduced in chapter 2. By considering the volume difference between the ice particles in the neighboring radius interval, the number of ice particles to be moved to the higher radius interval can be calculated. Hence the parameter τ_i in equation (4.5) is

$$\tau_i = \frac{\frac{\partial V_i}{\partial t}}{\Delta_{vi} n_i} = N_u \frac{k_w}{l}(T_i - T)\frac{A_i}{\rho_i L_i \Delta_{vi}}, \tag{4.6}$$

where Δ_{vi} is the difference in the particle volumes for the two neighboring radius intervals.

4.2.3 Secondary Nucleation

The formulation suggested by Svensson and Omstedt (1994) is used in this model. Accordingly the coefficient of α_j, the rate of secondary nucleation, can be formulated as follows

$$\alpha_j = \frac{\bar{n}\Delta_i}{dt}. \tag{4.7}$$

ζ_i is introduced to the secondary nucleation term to allow for larger ice particles. It can be determined from $\zeta_i = V_1/V_i \quad (i = 2....N)$, where V_1 is a single particle volume in the first interval and V_i is the single particle volume for other intervals.

4.2.4 Flocculation/Break up

A relationship suggested by Svensson and Omstedt (1994) is implemented in this model as follows

$$\beta_i = \alpha_{floc} \frac{r_i}{r_1}, \tag{4.8}$$

where α_{floc} is a calibration parameter.

4.2.5 Buoyancy Removal

An expression derived by Svensson and Omstedt (1994) is modified and used to calculate the buoyancy removal factor. The factor is assumed to be proportional to the frazil ice concentration as shown

$$\gamma_i = \frac{U_{rise}}{H} M .$$

4.3 Discretization of the Governing Equation

The number continuity equation (4.4) can be discretized and reorganized into the following equation. A detailed derivation is shown in Appendix A.

$$A \begin{Bmatrix} n_1(t+\Delta t) \\ n_2(t+\Delta t) \\ \vdots \\ n_N(t+\Delta t) \end{Bmatrix} = D \tag{4.9}$$

where

$$A = \begin{bmatrix} 1+\Delta t(\beta_1+\gamma_1+\tau_1)\theta & -\Delta t\alpha_2\theta & \cdots & -\Delta t\alpha_N\theta \\ 0 & -\Delta t(\tau_1+\delta\beta_1)\theta & 1+\Delta t(\zeta\alpha_2+\beta_2+\gamma_2+\tau_2) & 0 \\ & \vdots & \vdots & \vdots \\ 0 & 0 & -\Delta t(\tau_{N-1}+\delta\beta_{N-1})\theta & 1+\Delta t(\zeta\alpha_N+\gamma_N) \end{bmatrix}$$

and

$$D=\begin{Bmatrix} n_1(t)-\Delta t\left(\beta_1+\gamma_1+\tau_1\right)\left((1-\theta)n_1(t)\right)+\Delta t\sum_{j=2}^{N}\alpha_j\left((1-\theta)n_j(t)\right) \\ n_2(t)-\Delta t\left(\zeta\alpha_2+\beta_2+\gamma_2+\tau_2\right)\left((1-\theta)n_2(t)\right)+\Delta t(1-\theta)\left(\tau_1+\delta\beta_1\right)n_1(t) \\ \vdots \\ n_{N-1}(t)-\Delta t\left(\zeta\alpha_N+\gamma_N\right)\left((1-\theta)n_N(t)\right)+\Delta t(1-\theta)\left(\tau_{N-1}+\delta\beta_{N-1}\right)n_{N-1}(t) \end{Bmatrix}.$$

Then the frazil ice number at the subsequent time step can be obtained from equation (4.9).

Combining equation (4.1) with

$$Q_n=\phi(T_a-T)=C_p\rho\, dT/dt\Big|_{coolingrate}, \text{ and } \sum_{i=1}^{N-1}Q_i=\sum_{i=1}^{N-1}n_i h_w A_i(T_i-T), \text{ then}$$

$$dT=dt\frac{\left(-C_p\rho\left.\frac{dT}{dt}\right|_{coolingrate}+\sum_{j=1}^{N-1}n_i h_w A_i(T_i-T)\right)}{\rho C_p\left(1-M\right)}. \tag{4.10}$$

The water temperature can be calculated from $T(t+dt)=T(t)+dT$.

4.4 Model Programming

The above algorithm was programmed using MATLAB®. Forty intervals were selected to discretize for the frazil ice size. A time step of 1 second was used. The program readily converges because a differential method with an implicit scheme was used, the flow chart for the programming is shown in figure 4.1.

4.5 Application of the Model

In order to apply the model, the range of frazil size and the size distribution must first be determined. The critical size of frazil ice is considered to be the minimum size in the simulation, which is calculated according to Lal Mason's et al. (1969) survival theory

$$r_c = \frac{2\gamma_{wa}}{\rho_i L_i}\left(\frac{T_e}{T_e - T}\right), \tag{4.11}$$

where γ_{wa} is the ice-water interfacial tension, T_e is the equilibrium temperature of the ice-water mixture. The critical size of frazil ice is on the order of 4 μm (Mercier 1984). The maximum size of a frazil ice particle typically ranges from 1-5 mm (Clark and Doering, 2004); herein it is taken as 5 mm.

The size distribution suggested by Mercier (1984) is used

$$g_n(l) = \frac{dC_n(l)}{dl} = al^{-b}. \tag{4.12}$$

During the simulation, α_{floc} is the most likely factor to control the distribution of frazil ice size, which was already calibrated in term of the size distribution spectra, with a value of 0.0001 proposed by Svensson and Omstedt (1994); this calibrated value will be used in this model.

There are two additional parameters in this model: the initial seeding and the parameter $n_{\max}$. The initial seeding is governed by many factors such as the mass transfer between the air and

the water surface, the impurities in water, etc. Therefore, it can vary for different experiments. Parameter n_{max} was introduced to limit secondary nucleation by constraining the collision frequency between ice particles. An effort has been made in the present model to find a general value for the parameter n_{max} in order to avoid the specification of two variables in the simulation, but it was found that it is difficult to use only one value of n_{max} for all experiments. This is probably because the parameter n_{max} is affected by turbulence intensity and it will be investigated hereinafter based on the simulations results. The data from Carstens (1966) and Clark and Doering (2004) are used to check the validity of the present model.

4.5.1 Carstens' Data

The two cases presented by Carstens can be regarded as well-mixed flows. Table 4.1 gives the flow parameters and the heat loss rates for Carstens' experiments. $\alpha_{floc} = 0.0001$ is used for both cases. $n_{max} = 1.5\times10^6$ and $n_{max} = 8\times10^5$ were used for case I and case II, respectively. The initial seeding of the total frazil ice number takes the values of 40000 and 32000 for these two cases, respectively.

Table 4.1 Parameters of Carstens' (1966) Experiments

Case	U [m/s]	K [m^2/s^2]	ε [m^2/s^3]	Cooling rate [°C/min]	H [cm]
I	0.50	0.00096	0.00120	0.0240	20
II	0.33	0.00048	0.00038	0.0078	20

Figure 4.2 shows the simulated and measured water temperature history for Carstens Case I. The simulation fits the experimental data quite well and supports the validity of the simulation model. Figure 4.3 shows the frazil ice concentration variation with time; it increases during supercooling so as to provide enough latent heat to balance the heat loss from the water surface. Figure 4.4 shows that the total number of frazil ice particles increases much faster during the principal period of supercooling ($t < 400$ s) than during the residual period of supercooling ($t > 400$ s). The size distribution of frazil ice at different times during the experiment is shown in figure 4.5. It seems that the smaller frazil ice particles increase faster than do the larger particles. Figures 4.6 to 4.9 show the results for Carstens Case II, which indicates the same tendency as figures 4.2 to 4.5 and suggested that the model can provide reasonable predictions.

4.5.2 Clark and Doering's Data

To further examine the applicability of the present model, the experimental data from Clark and Doering (2004) was used. Their experiments were conducted in a counter-rotating flume and the turbulence was generated by shear as in open channel flow. Since water depth (0.15 m) used in their experiments was very small, and the temperature was measured at only one point, it was assumed in this simulation that the well-mixed water condition is a reasonable assumption. Table 2 gives the parameters for their four experiments. $\alpha_{floc} = 0.0001$ (same as for Carstens' data) was used to model the frazil ice distribution as suggested by Svensson

and Omstedt (1994). Different values of the initial seeding and the n_{max} parameter were used in their simulations, and these values are summarized in table 4.2. The detailed results from the simulation of the experiment conducted on Dec 18 is given and discussed herein. The results are shown in figures 4.10 to 4.13.

Table 4.2 Parameters of Clark and Doering's (2004) Experiments

Case	U [m/s]	H [cm]	T_{air} [°C]	Cooling rate [°C/hour]	d_s [mm]
Dec 18	0.7	15	-10.0	0.234	3.5
Dec 17	0.6	15	-15.0	0.437	3.5
Dec 23	0.6	15	-7.5	0.063	3.5
Nov 5	0.6	15	-10.0	0.142	3.5

Note: d_s is the absolute roughness

Table 4.3 Summarization of Calibrated Parameters

Case	n_{max}	Initial Seeding	Cooling rate [^{0}C/min]	α_T
Case I	1500000	40000	0.0200	0.0876
Case II	800000	32000	0.0078	0.1030
Dec 18	150000	3200	0.0039	0.1340
Dec 17	200000	12000	0.0073	0.1157
Dec 23	2000	4800	0.0010	0.1340
Nov 5	2000	6400	0.0024	0.1350

The predicted water temperature (figure 4.10) closely matches that obtained by Clark and Doering (2004). Figure 4.11 shows that the simulated frazil ice concentration increases during the supercooling. Figure 4.12 shows the variation of the total frazil ice number with

time during the supercooling process. The total frazil ice number from the simulation predictions are larger than those observed. The discrepancy probably occurs because the frazil ice particle detection system can not recognize very small particles, as well as the larger particles can not be counted accurately due to the overlapping that occurs in two-dimensional digital images of frazil ice particles. Figure 4.13 shows the simulated distribution of frazil ice at different times. It is clear that the small and intermediate size of the ice particles is dominant at different times during the supercooling process.

Figures 4.14 to 4.16 show the predicted frazil size distribution compared with the experimental data (the bar) and a lognormal distribution; these figures show that the shapes of the distribution curves are generally consistent among the three results. The falling limb of the size distribution for the simulation is not inconsistent with that from the experimental data and a standard lognormal distribution. Nevertheless, there is some difference in the rising limb for the size distribution and it indicates that the size distribution used in this simulation may not adequately simulate the number of small ice particles. A lognormal distribution, which was suggested by Daly and Colbeck (1986), and Clark and Doering (2004), should be considered to simulate the size distribution of frazil ice as long as the standard deviation is defined.

4.5.3 Initial Seeding and n_{max}

The six simulations listed in table 4.3 were used to develop relationships for the initial

seeding and parameter n_{max} as a function of the turbulent intensity; this would be useful in helping to choose the values for these two parameters in the practical application of this mathematical model.

Figure 4.17 shows the relationship between the initial seeding and the turbulence intensity; the initial seeding is inversely proportional to the turbulence intensity, and is defined as $\alpha_T = \sqrt{2k}/U$, where k is the kinematic energy, and U is the average velocity. Figure 4.18 gives the relationship between the parameter n_{max} and the turbulence intensity. If the two relationships were fit with a straight line, the values of R^2 are above 0.80. These relations give some general guidance for helping to calibrate these two parameters in the practical application of this model.

4.5.4 Sensitivity Analysis

To investigate the sensitivity of the two calibrated parameters, the initial seeding and the parameter n_{max}, to the supercooling process, additional simulations were performed using this model for Carstens' Case I. The number of the seeding particle was assumed evenly distributed in each size groups in the simulation. As expected, if the other parameters don't change, increasing the initial seeding will decrease the maximum supercooling and will shorten the duration of the principal period of supercooling as shown in figure 4.19. The variation of the parameter n_{max} also influenced the supercooling process in terms of

affecting secondary nucleation. An increase of the parameter n_{max} reduced the maximum amount of supercooling and shortened the duration of the principal supercooling process as shown in figure 4.20.

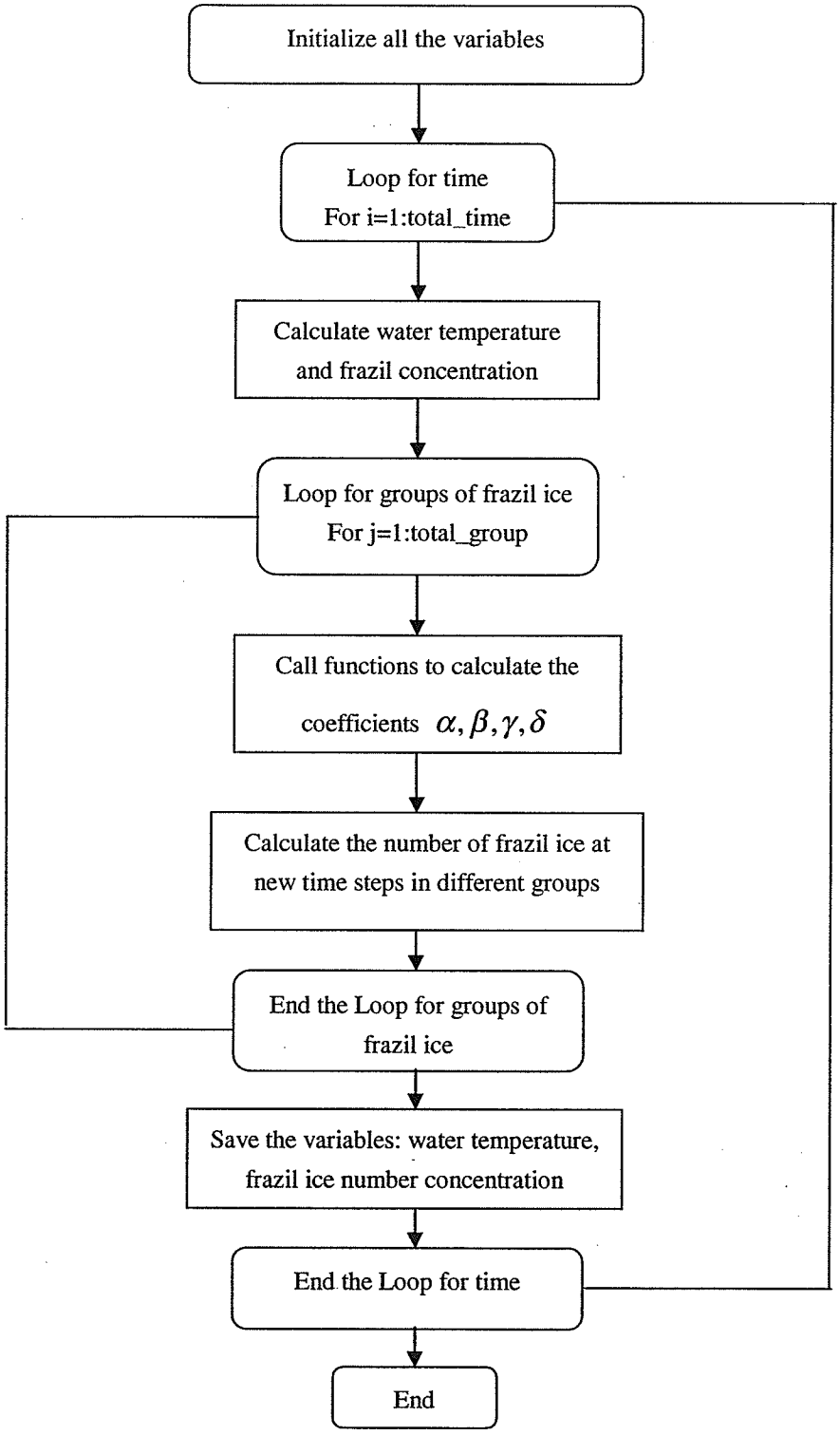

Figure 4.1 Flow chart of the MATLAB program

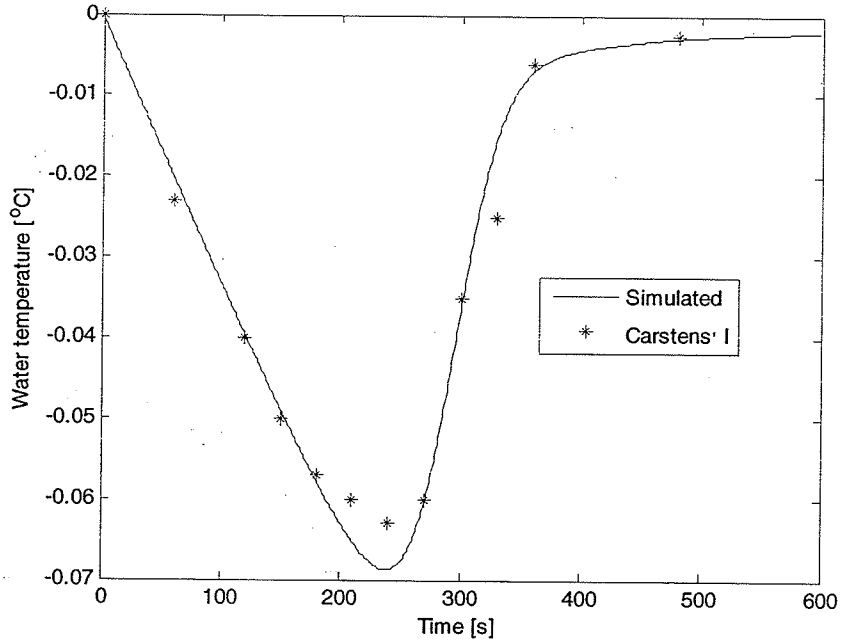

Figure 4.2 Water temperature vs. time (Carstens' case I).

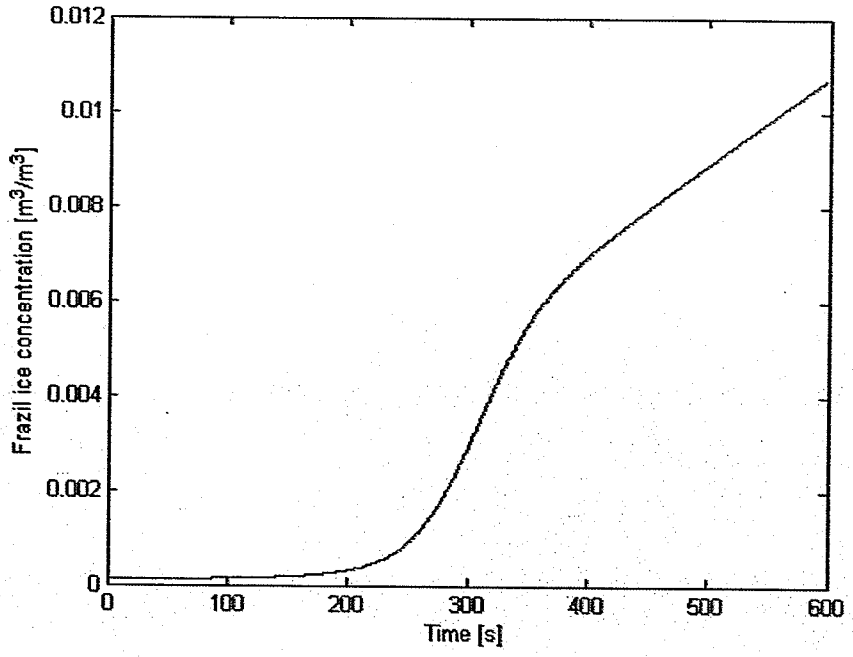

Figure 4.3 Frazil ice concentration vs. time (Carstens' case I).

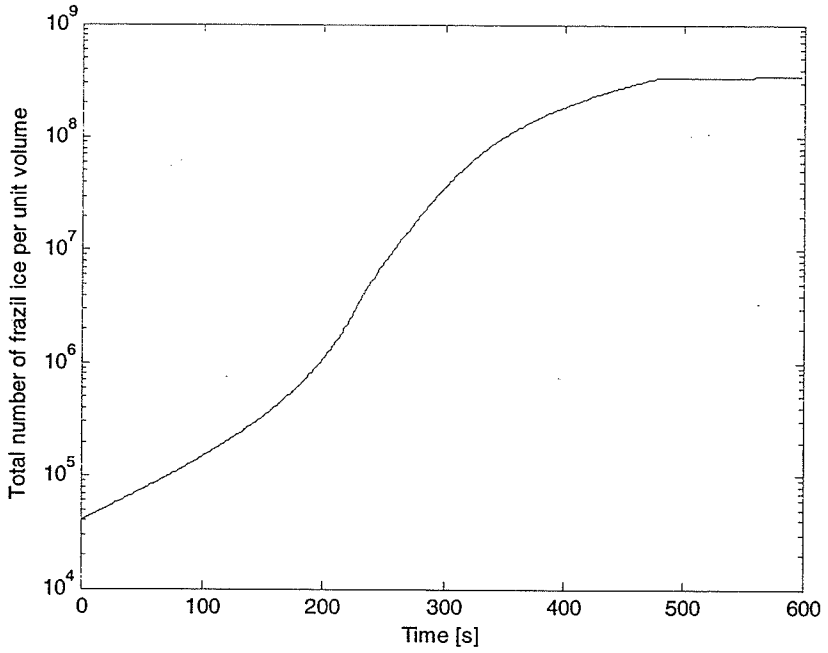

Figure 4.4 Total number of frazil ice vs. time (Carstens' case I).

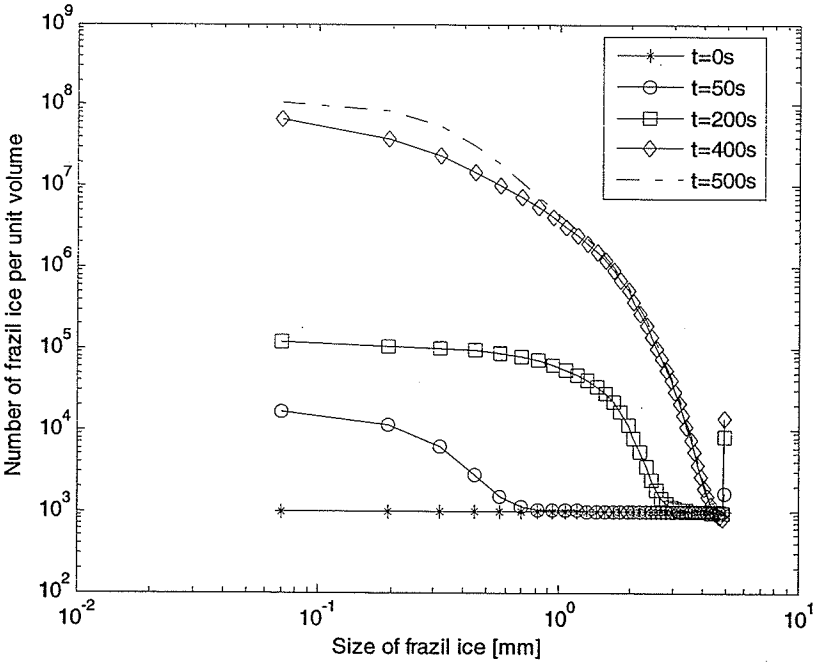

Figure 4.5 Frazil ice size distributions (Carstens' case I).

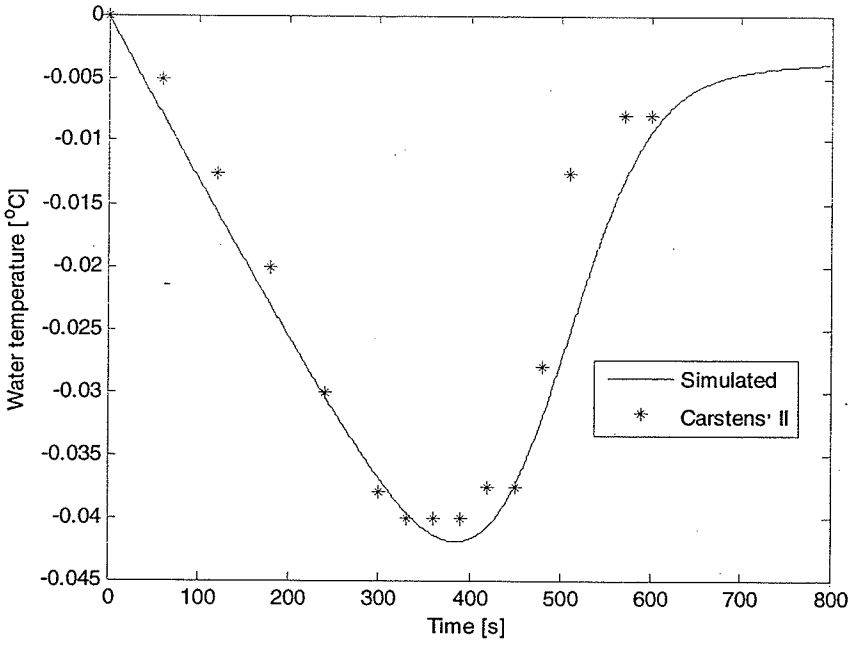

Figure 4.6 Water temperatures vs. time (Carstens' case II).

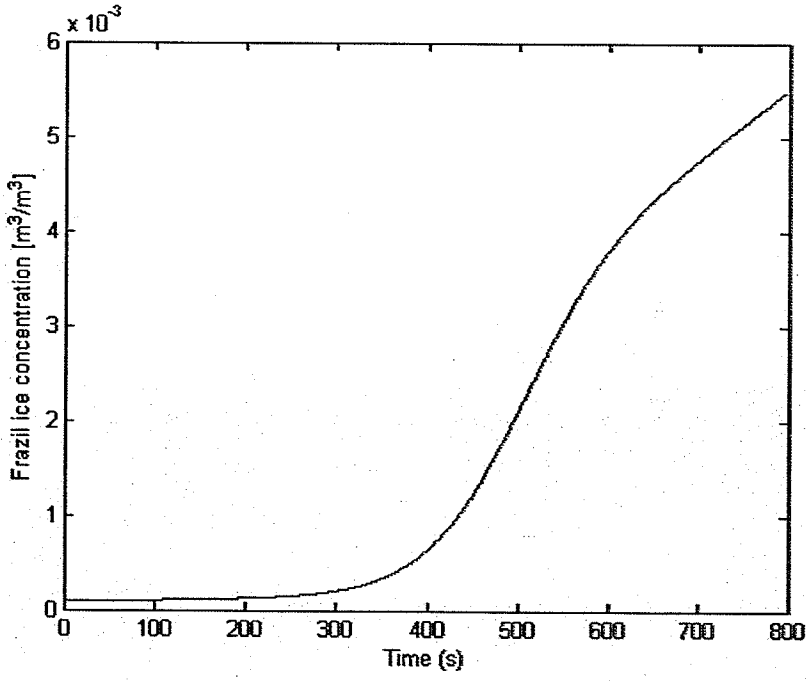

Figure 4.7 Frazil ice concentrations vs. time (Carstens' case II).

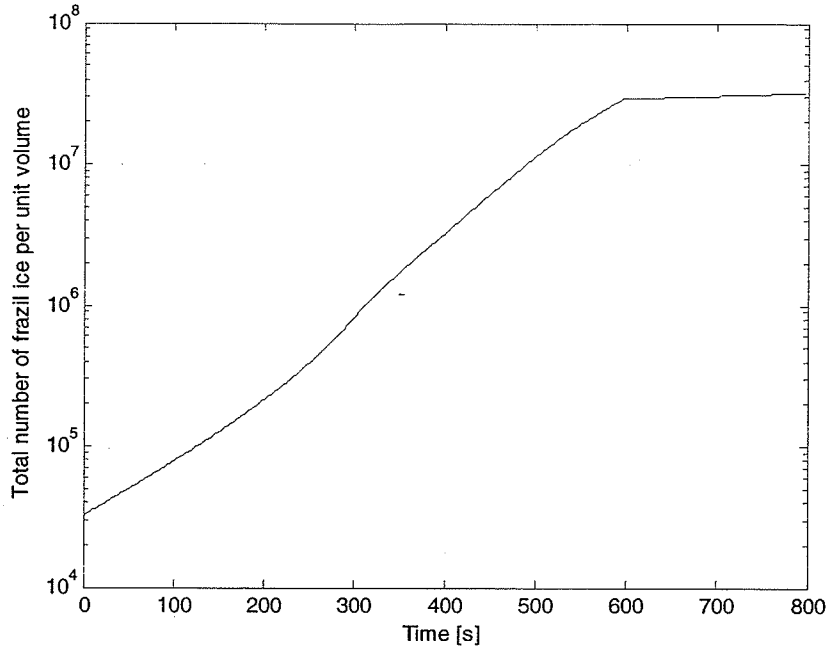

Figure 4.8 Total number of frazil ice vs. time (Carstens' case II).

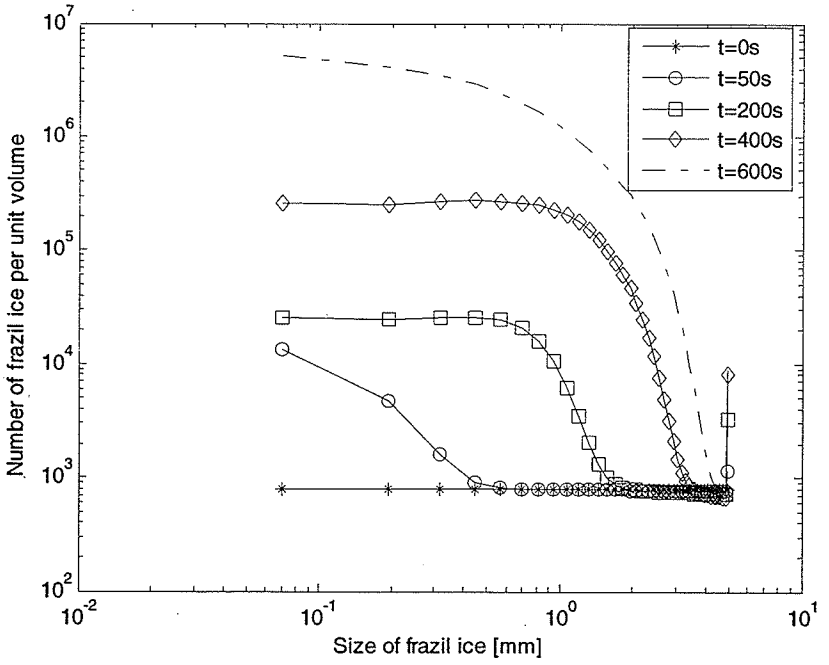

Figure 4.9 Frazil ice size distributions (Carstens' case II).

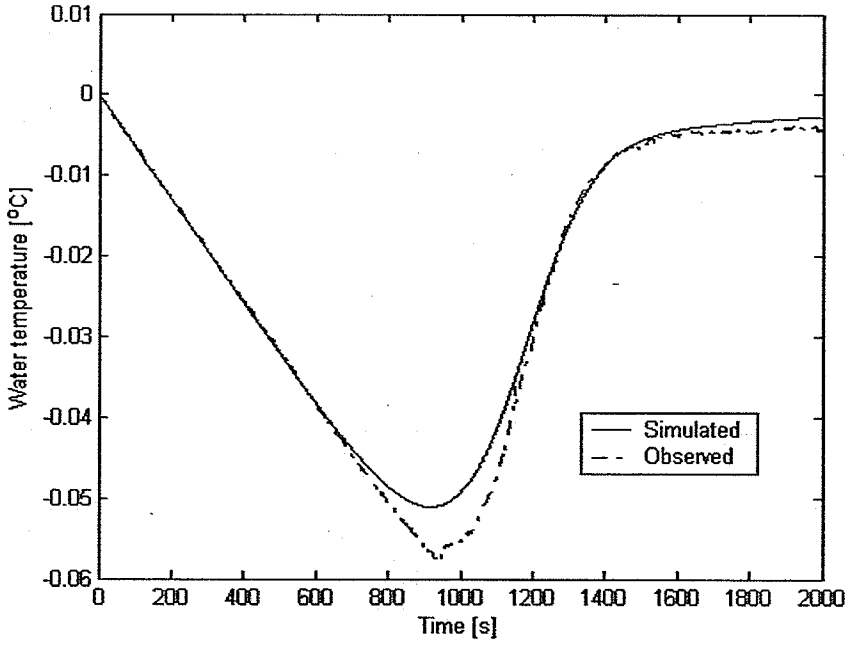

Figure 4.10 Water temperature vs. time (Clark and Doering, 2004).

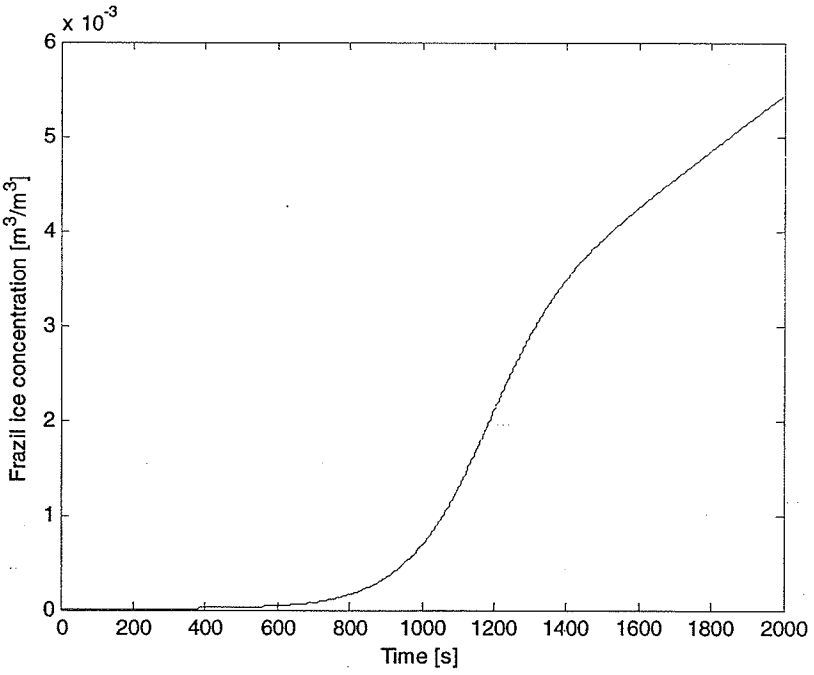

Figure 4.11 Frazil ice concentration vs. time (Clark and Doering, 2004).

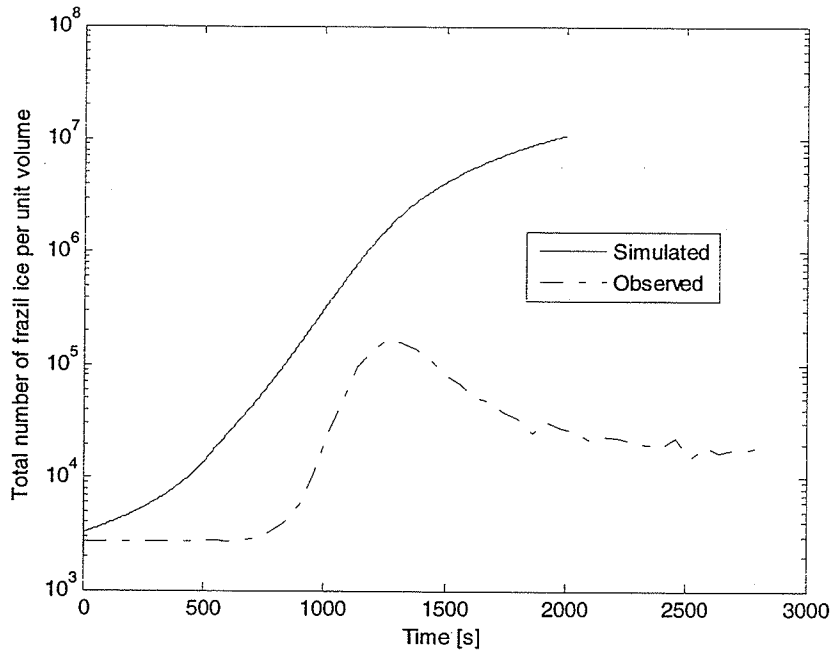

Figure 4.12 Total frazil ice number vs. time (Clark and Doering, 2004).

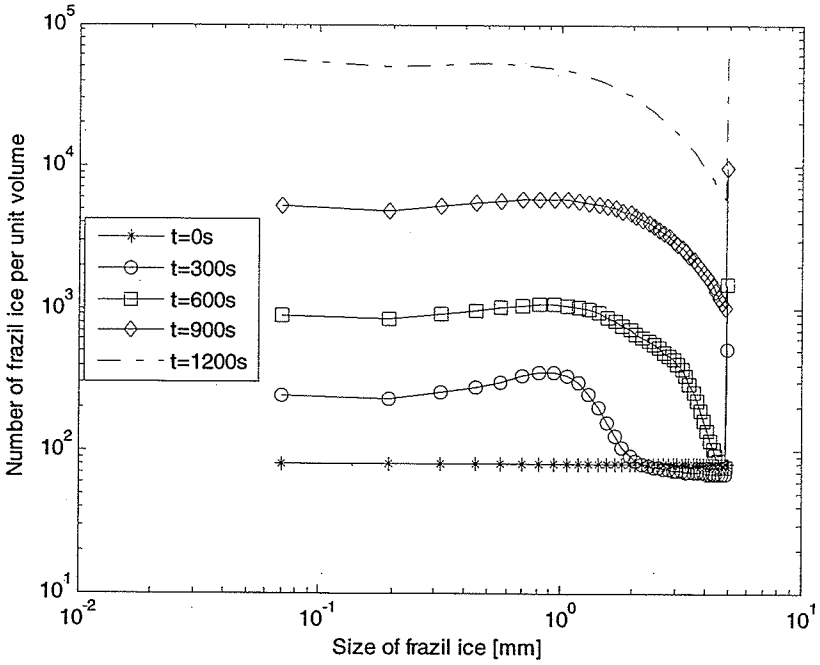

Figure 4.13 Frazil ice size distributions (Clark and Doering, 2004).

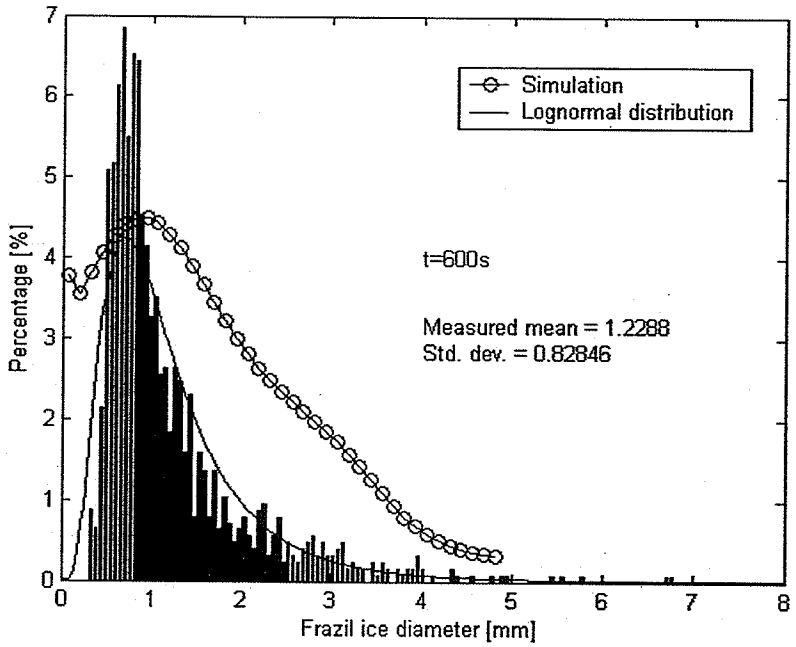

Figure 4.14 Frazil ice size distributions (t=600s) (Clark and Doering, 2004).

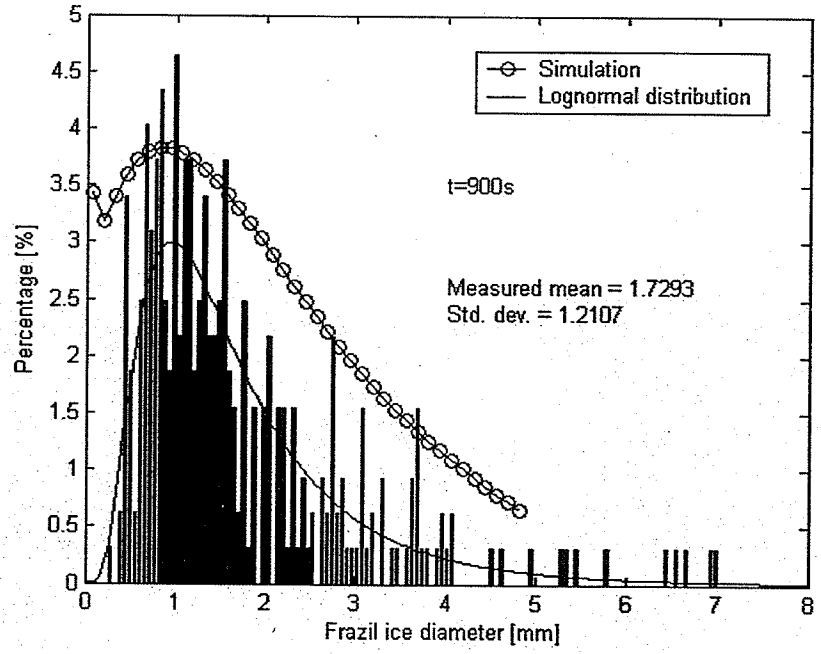

Figure 4.15 Frazil ice size distributions (t=900s) (Clark and Doering, 2004).

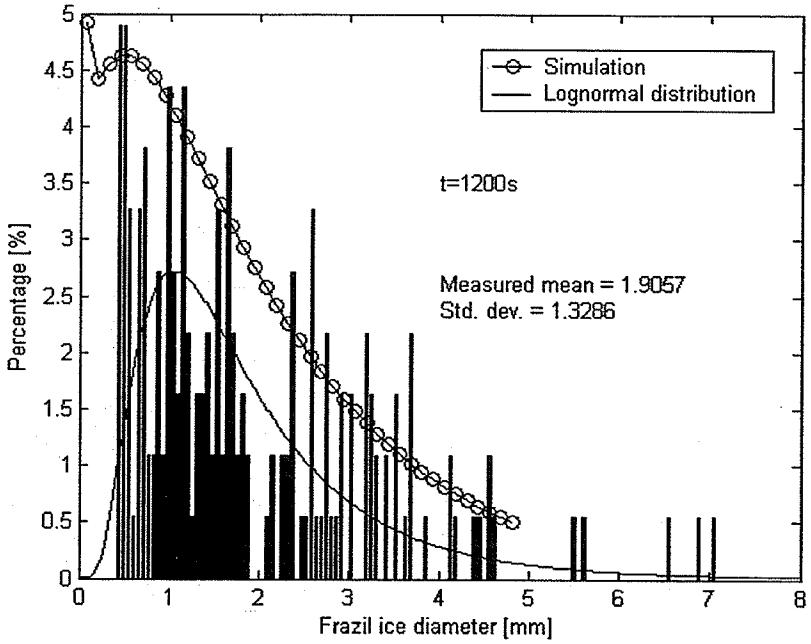

Figure 4.16 Frazil ice size distributions (t=1200s) (Clark and Doering, 2004).

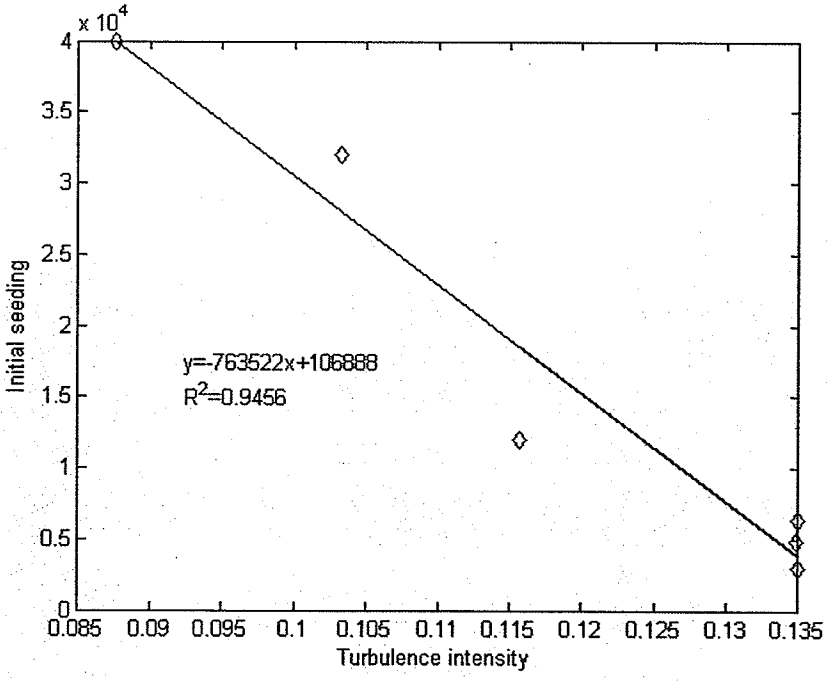

Figure 4.17 Relationship between initial seeding and turbulence intensity.

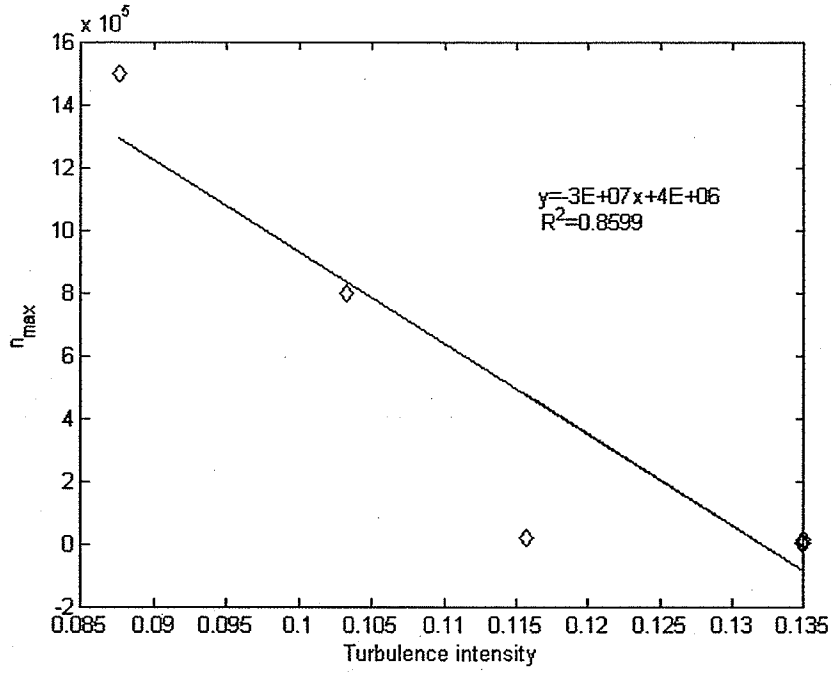

Figure 4.18 Relationship between parameter n_{max} and turbulence intensity.

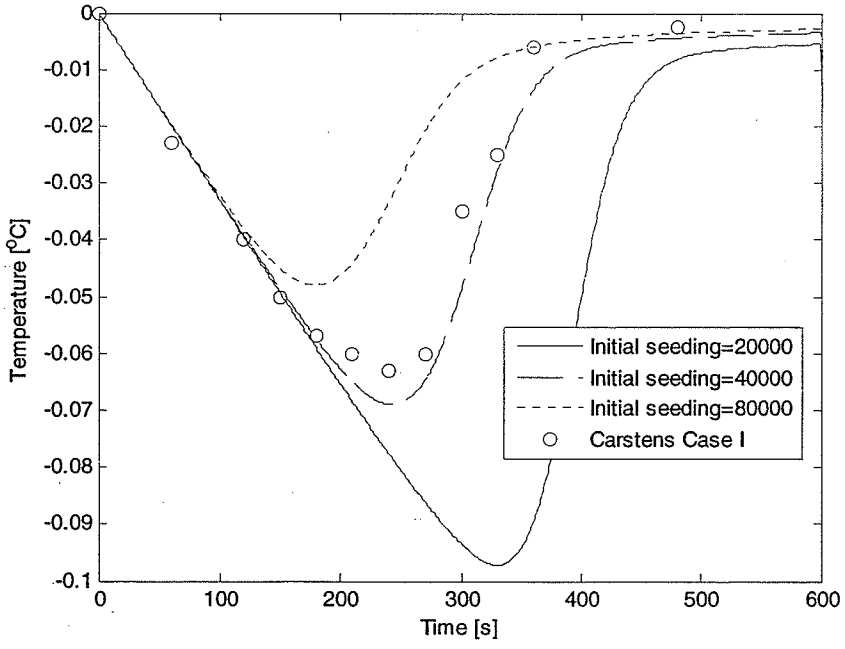

Figure 4.19 Sensitivity analysis for initial seeding.

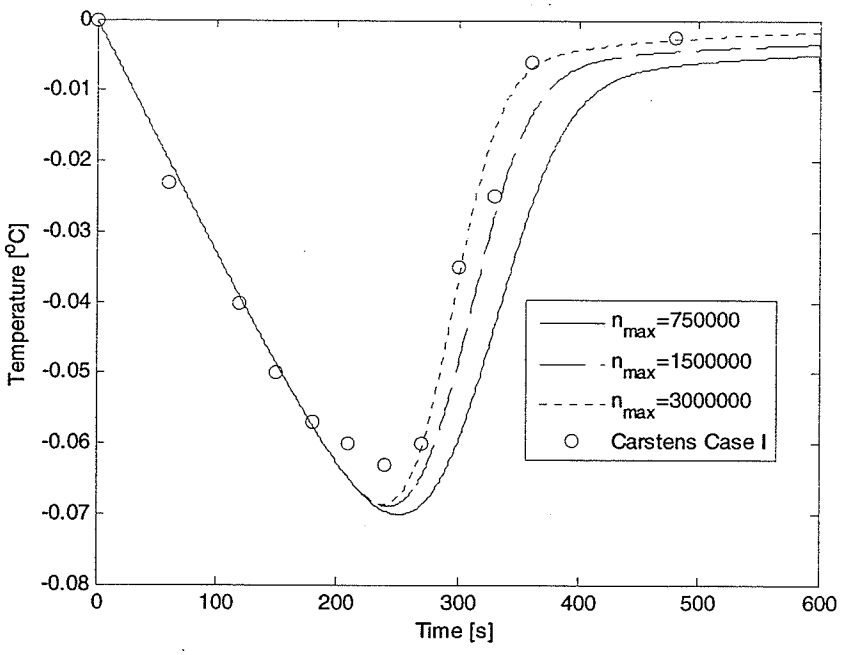

Figure 4.20 Sensitivity analysis for parameter n_{max}.

CHAPTER 5

A Vertical One-Dimensional Model of Frazil Ice Growth and Evolution

5.1 Introduction

In a river the flow is not always well-mixed and therefore the flow turbulence is not uniformly distributed throughout the water depth. Vertical stratification and mass transport should therefore be considered in such cases. The distribution of water temperature and frazil ice concentration throughout the water depth is an important factor in frazil ice evolution and anchor ice formation. Therefore, the development of a vertical one-dimensional model is necessary. This vertical one-dimensional model considers the interaction among the flow turbulence, heat transfer and frazil ice transport. The governing equations are solved by using implicit differential schemes. The vertical distributions of the flow, the turbulence parameters, as well as the frazil concentration are simulated in this model.

The one-dimensional model developed in this chapter is used to simulate the formation of

frazil ice in a counter-rotating flume. The results are then compared with the experimental data. This model was developed from Hammar and Shen (1995) model and from Omstedt and Svensson's (1984) model.

5.2 Mathematical Formulation

Assuming the mean vertical flow velocity is negligible and the flow is horizontally homogeneous, then the flow can be treated as one-dimensional turbulent flow. This assumption is reasonable in laboratory experiments, but may not always be true in a natural river. However, it can be approximately applied to river flow and some basic information about the ice formation can be obtained.

The governing equations for the mean flow can be simplified from equation 2.2, they then take the form

$$\frac{\partial U}{\partial t} = \frac{\partial}{\partial z}\left((\nu_T + \nu)\frac{\partial U}{\partial z} \right) - \frac{1}{\rho_w}\frac{\partial P_w}{\partial x}. \qquad (5.1)$$

In a similar way, the heat transfer and the frazil ice number can be described by

$$\frac{\partial T}{\partial t} = \frac{\partial}{\partial z}\left(\left(\frac{\nu_T}{\sigma_T} + \frac{\nu}{P_r} \right)\frac{\partial T}{\partial z} \right) + G_T \qquad (5.2)$$

and $$\frac{\partial n}{\partial t}=\frac{\partial}{\partial z}\left(\left(\frac{\nu_T}{\sigma_n}+\frac{\nu}{S_n}\right)\frac{\partial n}{\partial z}\right)-W_i\frac{\partial n}{\partial z}+G_n, \tag{5.3}$$

where z is the vertical space coordinate (positive upwards), t is the time coordinate, W_i is the frazil ice rise velocity, ρ_w is the density of water, and T is the water temperature. ν_T is the kinetic eddy viscosity while ν is the molecular viscosity. Since ν is usually much smaller than ν_T it can be neglected in the simulation. σ_n and σ_T are the turbulent Prandtl and Schmidt numbers for frazil ice number and the temperature, while P_r and S_n are Prandtl and Schmidt numbers, respectively. n is the frazil ice number. The mean flow is driven by a pressure gradient denoted by $\frac{\partial P_w}{\partial x}$ in open channel flow. The source terms, because of ice formation, are denoted by G_T and G_n, respectively. G_T represents the latent heat released during ice growth, and G_n represents the number of ice particles produced during ice formation. These two terms can be calculated as follows (Hammar and Shen,1995; Svensson and Omstedt, 1984)

$$G_T = A_i nq(\rho_w C_p)^{-1}, \tag{5.4}$$

where q is the heat transfer for a single ice particle, C_p is the specific heat of the water, and ρ_w is the density of the water. A_i is the active area of frazil ice. G_n is given by

$$G_n = A_i nq(\rho_w L_i)^{-1}/V_i, \tag{5.5}$$

where V_i is the volume of a single ice particle.

The physical processes of secondary nucleation, flocculation, and breakup are not included

in this model formulation. The distribution of frazil ice size during the supercooling process is also not considered, while a varied mean diameter of the frazil ice is used in the simulation instead of using a constant mean diameter as was done by Omstedt (1985a). The evolution of the mean size of frazil ice in the supercooling process can be calculated according to Daly (1984) and Mercier (1984)

$$\frac{dD_m}{dt} = 2\frac{h_w}{\rho_i L}(T_e - T), \tag{5.6}$$

where D_m is the mean diameter of the frazil ice, T_e is the equilibrium temperature of the water-ice mixture, and h_w is the heat transfer coefficient.

5.2.1 Thermal Growth of Ice Particles

The thermal growth of the ice particles can be calculated using the same method described in section 3.3

5.2.2 Turbulence Model

If the effects of frazil ice concentration and water temperature on turbulence are neglected, a simple turbulence model can be used instead of the two equation k-ε model that is described by equations 2.5 and 2.6.

The friction velocity u_* can be computed by $u_* = U(\frac{f}{8})^{\frac{1}{2}}$, where f is a friction factor which has the form

$$\frac{1}{\sqrt{f}} = 2\log(R_h f^{\frac{1}{2}}) - 0.8 \quad \text{(smooth bed)} \tag{5.7}$$

or

$$\frac{1}{\sqrt{f}} = -2.01\log\left(\frac{k_s}{3.71(4R_h)} + \frac{2.51}{R_e\sqrt{f}}\right) \text{ (rough bed).} \tag{5.8}$$

R_h is the hydraulic radius and R_e is the Reynolds number.

5.2.3 Boundary and Initial Conditions

Since the frame of reference for this simulation is the bed of the counter-rotating flume, all the boundary conditions are implemented in terms of open channel flow. The boundary conditions at the surface are specified according to

$$\nu_T \frac{\partial U}{\partial z} = 0, \tag{5.9}$$

$$\frac{\nu_T}{\sigma_n}\frac{\partial n}{\partial z} = W_i n, \tag{5.10}$$

and

$$\frac{\nu_T}{\sigma_T}\frac{\partial T}{\partial z} = F_N/(\rho C_p), \tag{5.11}$$

where F_N is the net heat loss from the water surface. At the lower boundary condition, a zero flux condition is used for all of the variables, except for the velocity. The velocity at the first near wall node is set with the aid of the law of the wall, which reads $U_+ = \frac{1}{\kappa}\ln(z^+) + B$, in which $B = 5.1$, $\kappa = 0.4$ and $z_+ = \frac{zu_*}{\nu}$ =50~100.

The initial flow velocity is set to the measured velocity and the initial temperature is set to 0°C. The initial frazil number is set to zero except for the seeding at the water surface.

5.3 Discretization Scheme

The governing equations (5.1), (5.2), and (5.3) can be discretized using differential schemes, and the details of which are shown in Appendix B.

Note, for equation (5.6)

$$D_m(t+\Delta t) = D_m(t) + 2\Delta t \frac{h_w}{\rho_i L}(-T(t+\Delta t)). \tag{5.12}$$

All of the equations have boundary conditions that consist of a closed system and can be solved numerically.

5.4 Model Programming

The algorithm introduced above is programmed in MATLAB®. The flow chart is shown in figure 5.1.

5.5 Model Application

5.5.1 Carstens' data

Case I presented by Carstens (1966) is considered first to calibrate the model developed in this chapter. The flow parameters and the heat loss rates for Carstens' experiments are given

in Table 4.1.

Some of the simulation results using Carstens data are shown in figures 5.2 to 5.7. Figure 5.2 shows a comparison between the turbulence parameters that are simulated from Hammar and Shen's (1995) model and those simulated in this model. The results for these two models are very close, except for the kinetic energy close to the water surface. The difference between these two models is likely because the $k-\varepsilon$ turbulence model used by Hammar and Shen (1995) requires the boundary conditions at the water surface, which impacts the distribution of the kinetic energy. As Mercier (1984) suggested, the simple turbulence model applied in his (and this) model gives a comparable distribution to the $k-\varepsilon$ model but is much easier to solve. In figure 5.3, the simulated results of water temperatures at different depths are plotted with observed data from Carstens' experiment. The temperature goes down a bit lower and the maximum supercooling occurs roughly one minute later than that of the experimental data. The lag time can be estimated by $T_{lag} = h^2 / \Gamma_{Ave} \approx 1$ min, where Γ_{Ave} is the average eddy diffusivity (Mercier, 1984). This can be explained with reference to the turbulence model that predicts the maximum level of k and ε close to the bottom of the flume where the concentration of the particles is at their minimum (Hammar and Shen, 1995). Figure 5.4 shows the comparison of mean water temperature variation between this model and Hammar and Shen's (1995) model, a discrepancy apparently exists because different Nusselt numbers are used to compute the thermal growth of frazil ice in the two models, as well as the size distribution and the physical processes of secondary nucleation

and flocculation/breakup are not considered in this model.

The temperature distribution throughout the water depth is shown in figure 5.5. Figure 5.6 shows the relative vertical frazil number profiles. The relative vertical frazil number for n_i is defined as $n_i / \bar{n}$, in which $\bar{n} = \int n_i u dy \Big/ \int u dy$ is the depth-averaged valued of n_i. During a cooling down period of supercooling, the frazil ice numbers near the water surface are smaller than that at the rest of the water depth, while during a warming up period of supercooling, the frazil ice numbers at the water surface are larger than other the water depths. This is because the buoyant force overcomes the effect of turbulence mixing as the ice particles become larger. Figure 5.7 shows how the mean diameter of frazil ice varies with time. The diameter of frazil ice increases during the period of primary supercooling and becomes nearly constant during the residual period of supercooling indicating that the heat loss from the water surface and the heat gained from frazil ice formation are in equilibrium.

5.5.2 Clark and Doering's Data

The data from Clark and Doering's (2004) experiments were also used to examine the accuracy of the model developed herein. If a well-mixed case is assumed for their experiments, the simulation results from a vertical one-dimensional model will differ slightly from the experimental data. The parameters used in their two typical experiments are given in Table 4.2.

The simulation results for the experiment conducted on Dec. 17 are shown in figures 5.8 to 5.11 and the results for Dec 18 are shown in figures 5.12 to 5.15. The water temperature variation at different depths is given in figures 5.8 and 5.12 for both experiments, respectively. It seems that the gradient of the water temperature throughout the water depth is very small, and it probably reflects the strong level of turbulence that usually occurs in a well-mixed water mass. The relative frazil ice number distribution is shown in figures 5.9 and 5.13, and the same tendency is observed as was in Carstens' (1966) experiment. During the warm up period of supercooling, the surface frazil ice number is larger than the rest of the water depth. The evolution of the mean size of frazil ice in the supercooling process generally matches the observed data from the experiment (figures 5.10 and 5.14). The total volume of the frazil ice from the simulation is similar to that of the experimental findings (figures 5.11 and 5.15), however there are still some differences. Possible reasons for the differences include: (a) that not all the ice particles formed in the experiment are detected by the image processing technique; and (b) that the use of only the mean size of a frazil particle does not adequately represent the real situation that occurred during the experiment.

5.5.3 Application of the Model to the Downstream Location of the Limestone Generating Station

Limestone Generating Station is located on the Nelson River in Northern Manitoba, and is the largest hydroelectric station in Manitoba Hydro's system. Every winter frazil ice forms a short distance downstream from the dam, and at the same time an anchor ice dam forms at

Sundance Rapids, an area 3 kilometers downstream of the generating station. Since the frazil ice attached to the bed is usually the main mechanism for anchor ice growth, an investigation of frazil ice formation is a very important portion of the study of anchor ice formation and the associated rise in water level at the anchor ice dam.

The mathematical model developed by Lianwu Liu el al. (2004) has been recently used to investigate ice formation at the downstream location of the Limestone Generating Station. Since the model is a depth-averaged two-dimensional plane model, it can not give the vertical distribution of the frazil ice concentration and the water temperature. The vertical one-dimensional model developed in this chapter could function as a supplement to Lianwu Liu's model to investigate the vertical variation of the water temperature and frazil ice concentration downstream of the Limestone Generating Station.

Figure 5.16 shows an aerial view downstream of Limestone Generating Station. The width for the reach from downstream of generating station to Sundance Rapids is about 1500 m, and the bottom slope is approximately 0.1%. The highest discharge was approximately 4500 m^3/s, and lowest discharge was approximately 2000 m^3/s in the winter of 1999. The average discharge of 3000 m^3/s is used in this simulation. The average temperature during the winter is about -15 ^0C and the cooling rate of the water column is $dT/dt = C_0(T - T_0)/\rho C_p H = 3.84\times10^{-5}\ ^0$C/sec, where C_0 is a coefficient from about 15 to 25 $W/m^2 \cdot {}^0C$. Accordingly, the flow parameters can be computed as shown in table 5.1.

Table 5.1 Flow parameters for the downstream of Limestone Generating Station

Water Depth H [m]	Average Velocity U [m/s]	Friction Velocity U_* [m/s]	Reynolds Number
1.87	1.59	0.116	6.9×10^6

The initial seeding of frazil ice was taken as used in Lianwu Liu's (2004) model, and the mean size of the ice particle varied in this model while it stays constant in Lianwu Liu's (2004) model with a default value of 2×10^{-3} m in diameter. The results from this model are shown in figures 5.17 to 5.21. These figures show that the water temperature and frazil ice volumetric concentrations have almost the same magnitude as obtained by Lianwu Liu et al. (2004), although their model only predicts the depth- averaged values.

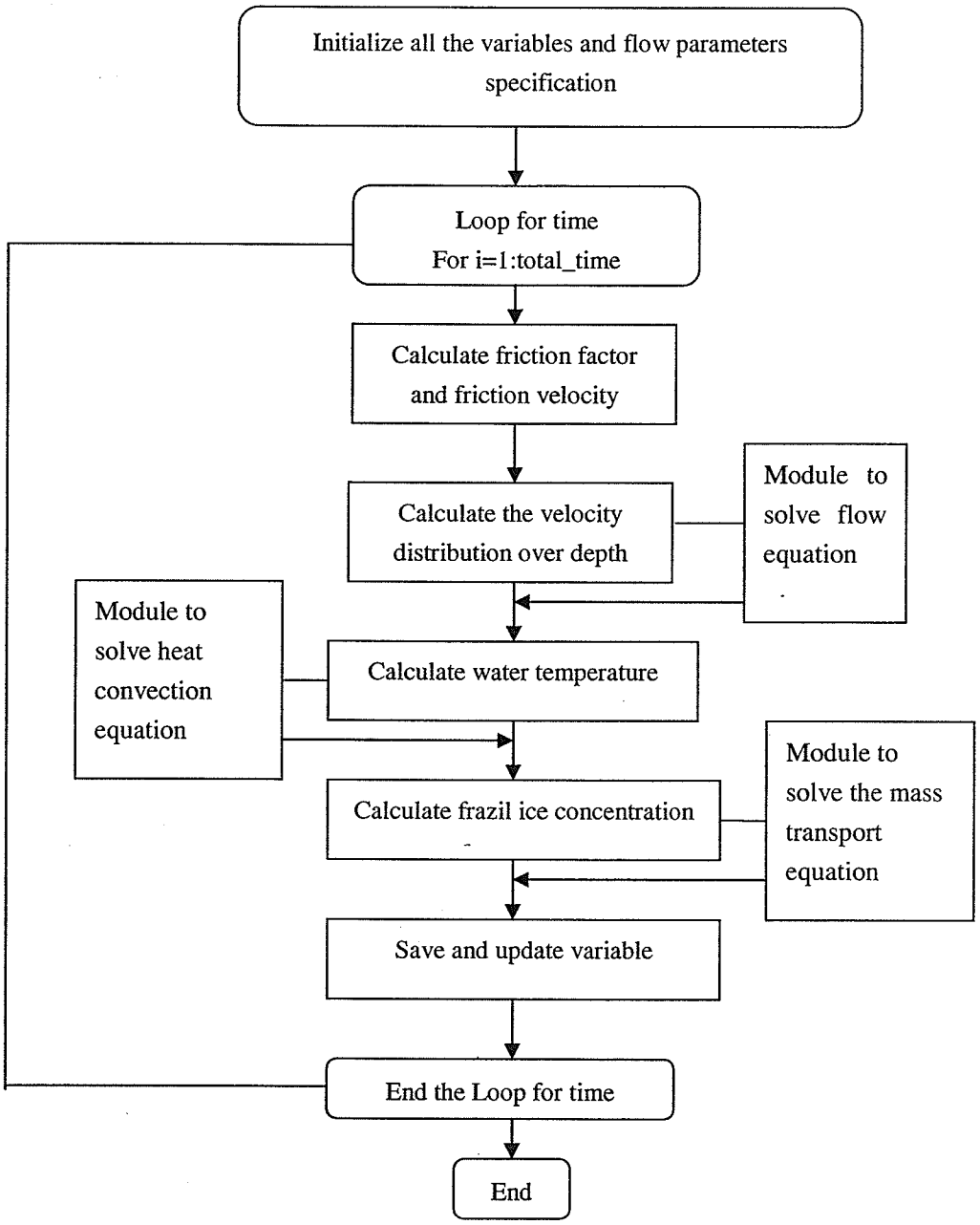

Figure 5.1 Flow chart of the MATLAB program

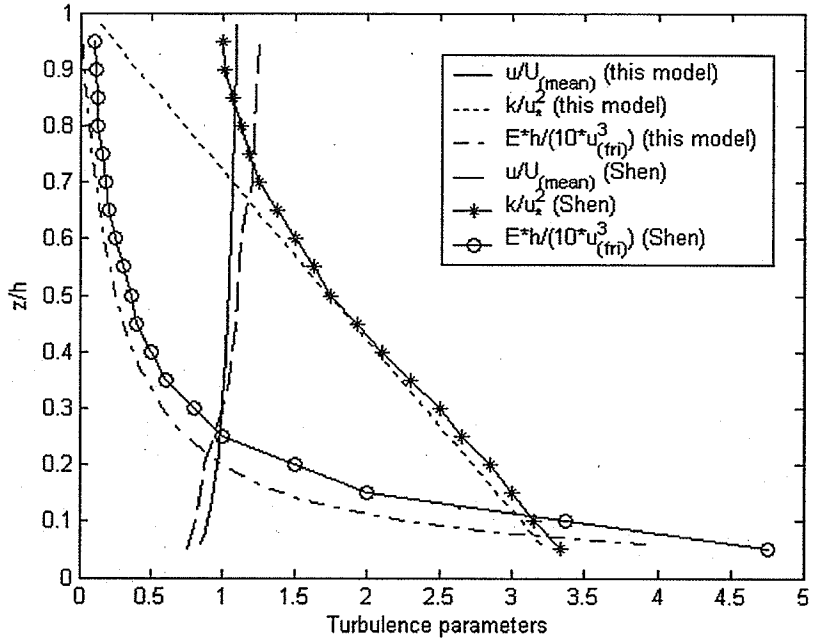

Figure 5.2 Vertical distributions of the turbulence parameters for the flow.

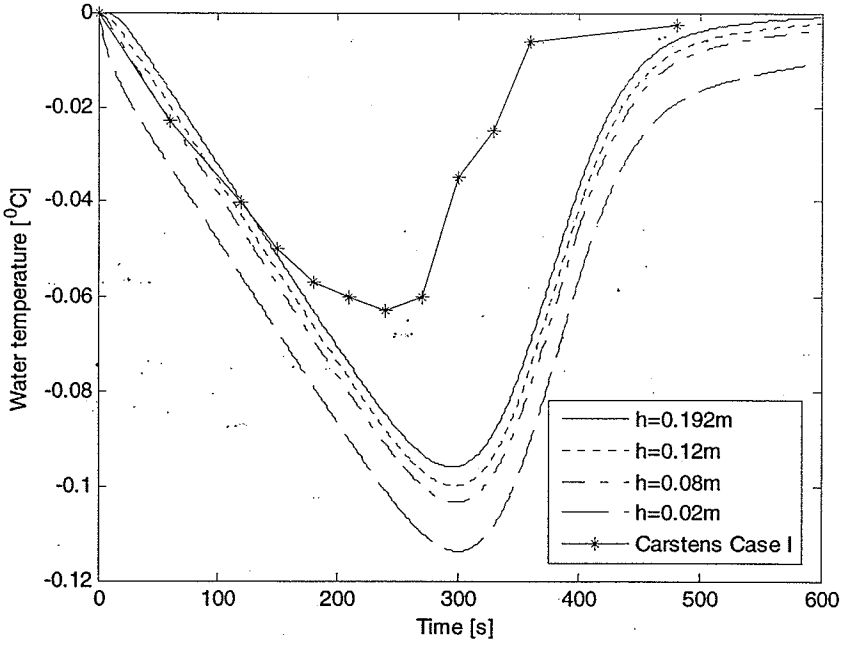

Figure 5.3 Variation of water temperature with time at different depths.

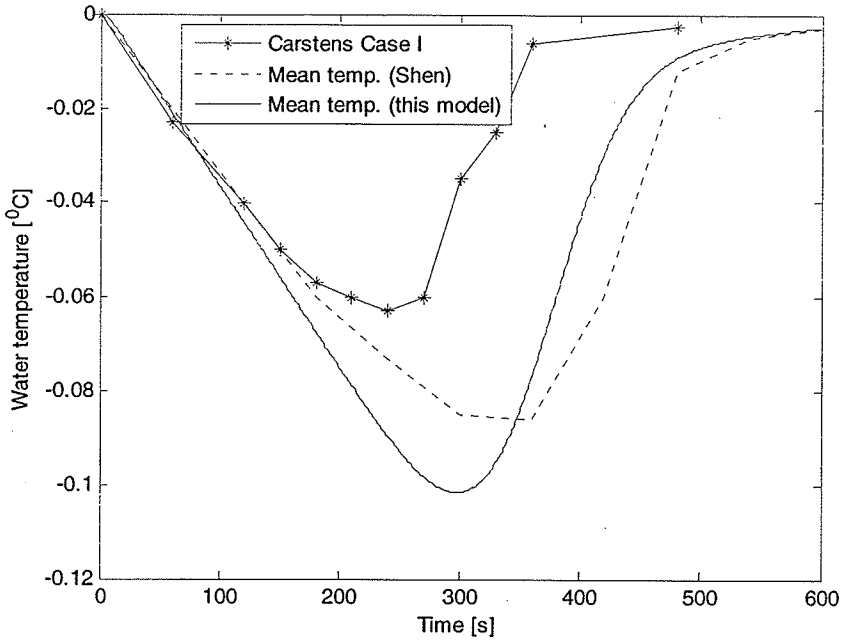

Figure 5.4 Comparison of mean water temperature between this model and Hammar and Shen's (1995) model.

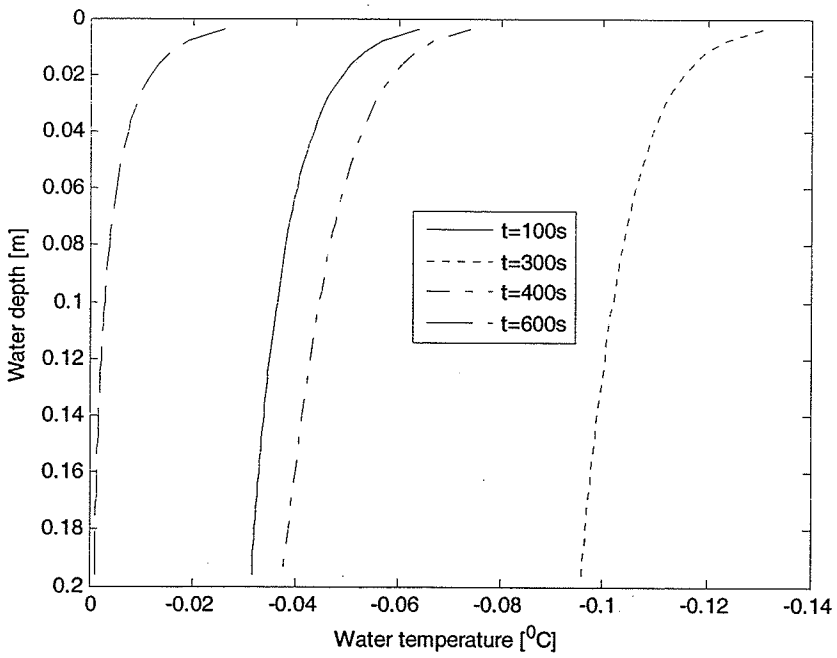

Figure 5.5 Variation of vertical temperature profiles at different times.

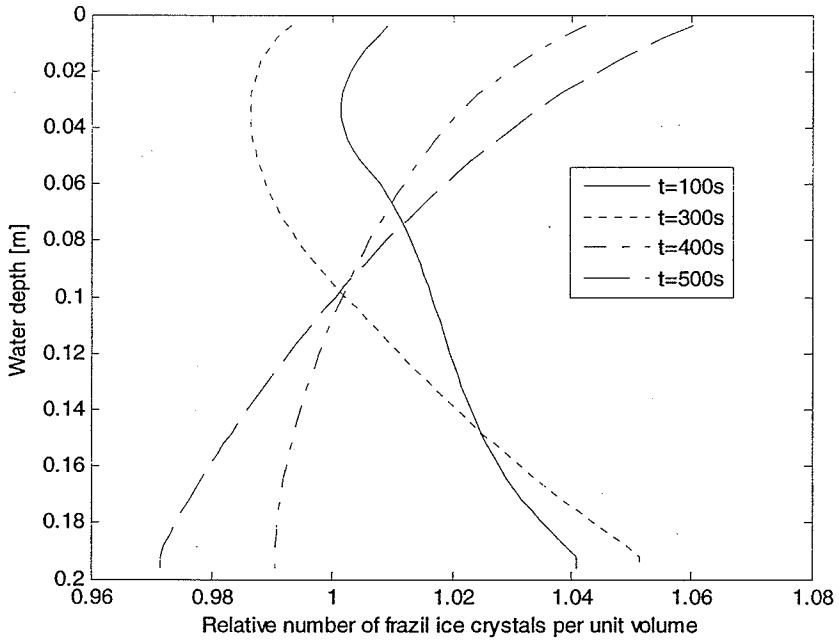

Figure 5.6 Relative frazil ice number profiles.

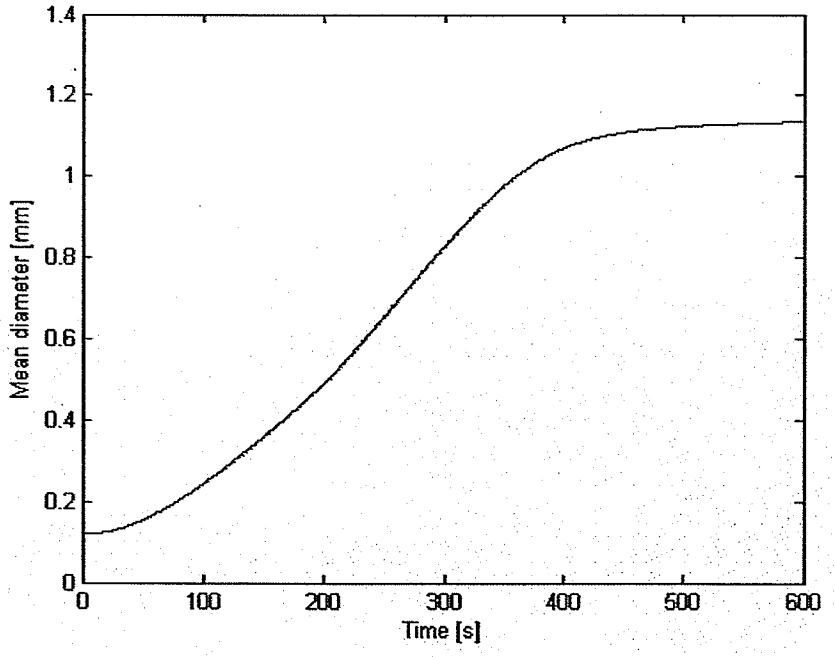

Figure 5.7 Variation of mean frazil ice diameter with time.

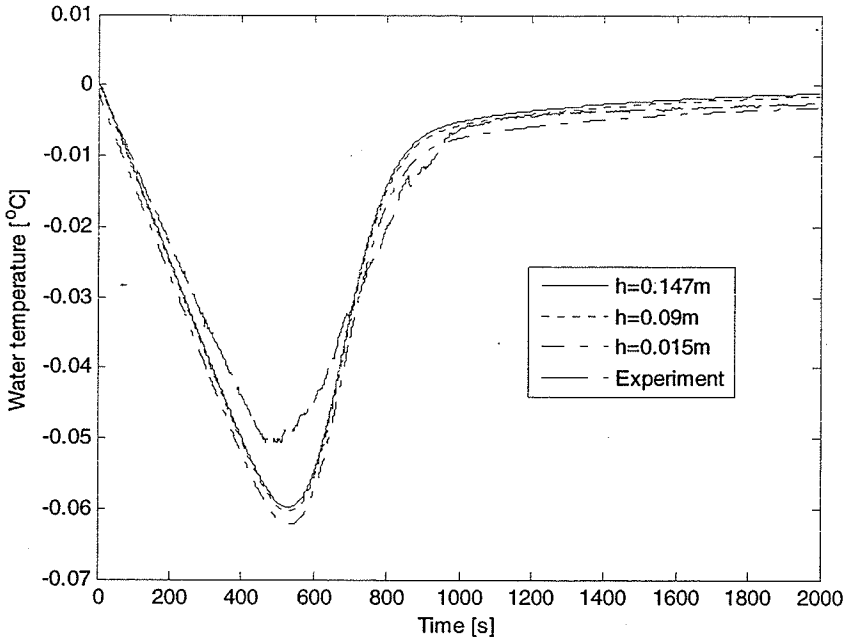

Figure 5.8 Variation of water temperature with time at different depths.

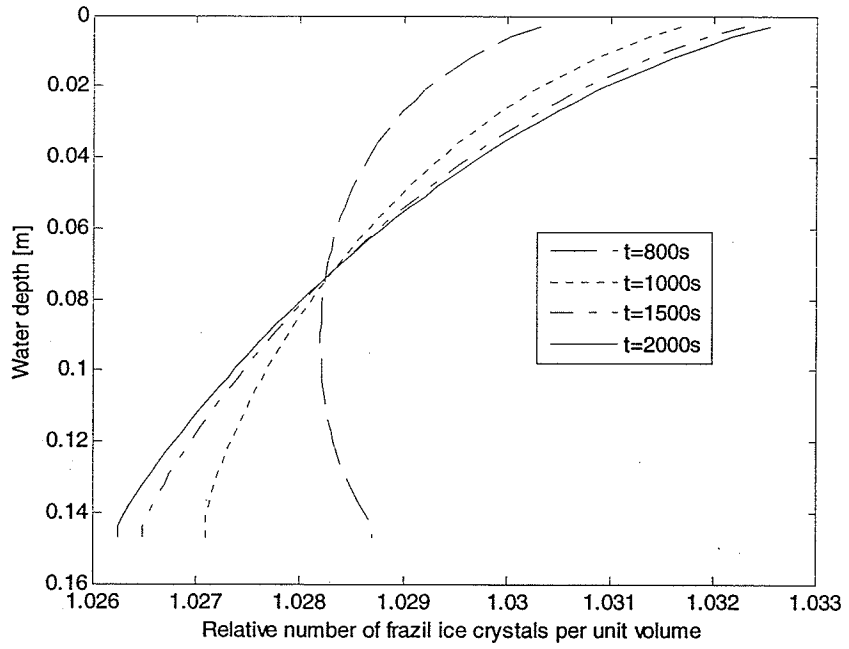

Figure 5.9 Relative frazil ice number profiles.

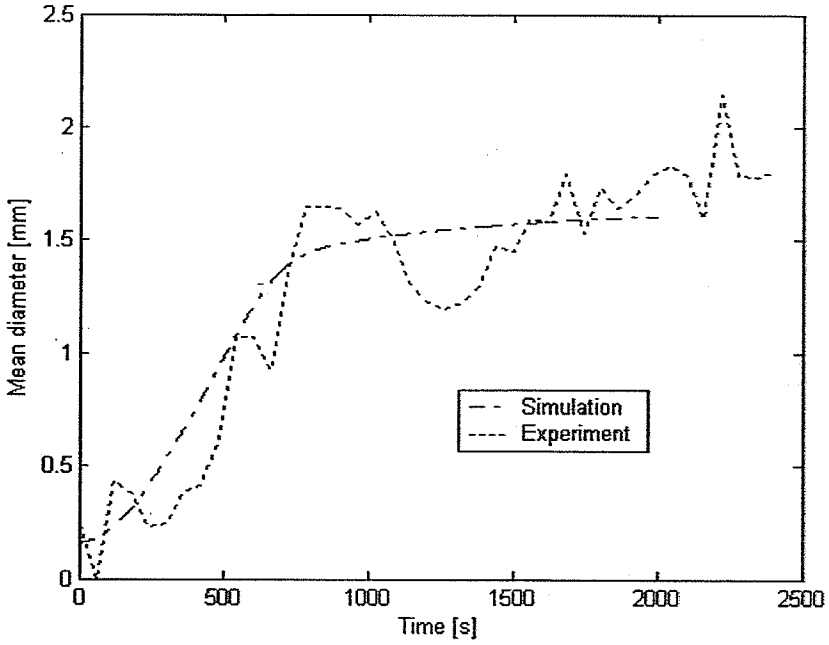

Figure 5.10 Variation of mean frazil ice diameter with time.

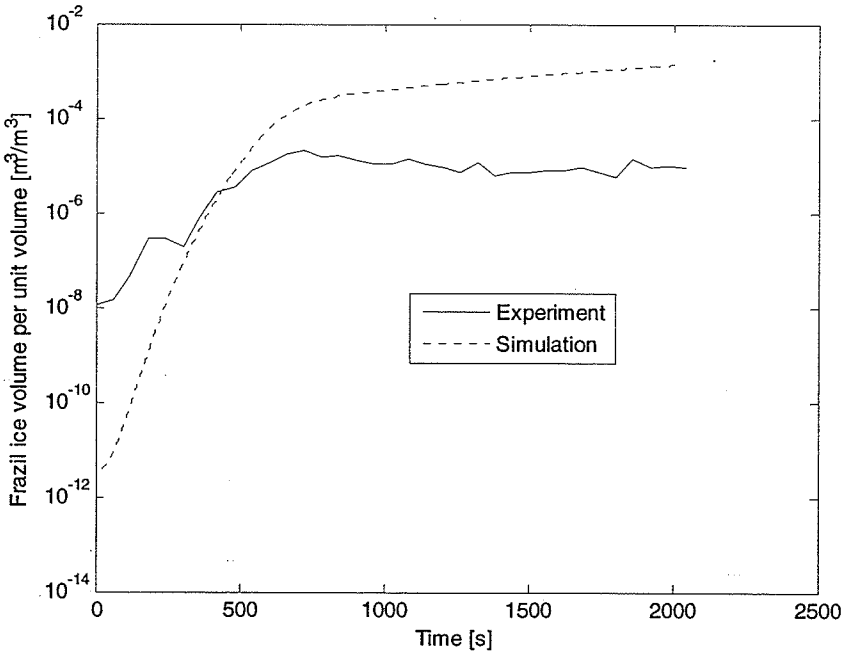

Figure 5.11 Total volume of frazil ice vs. time.

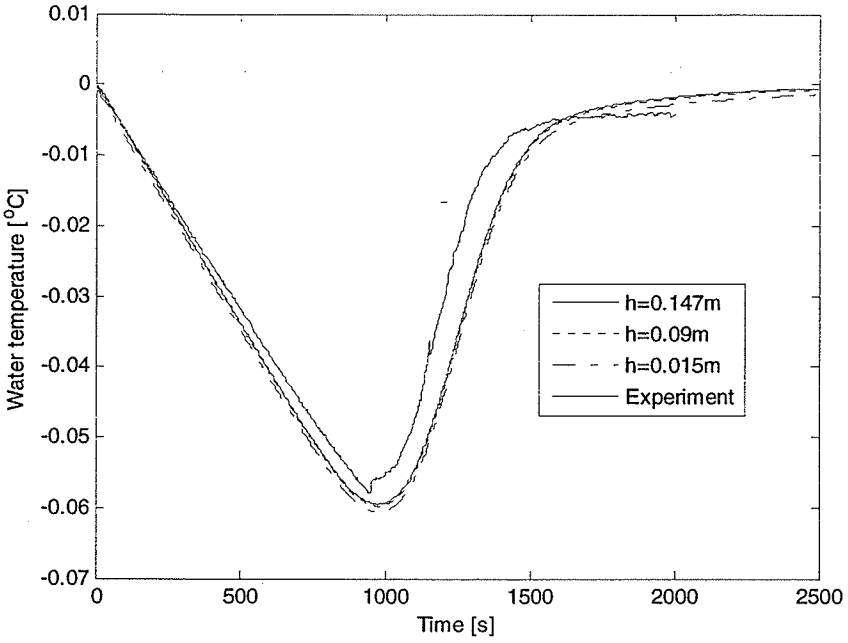

Figure 5.12 Variation of water temperature with time at different depth.

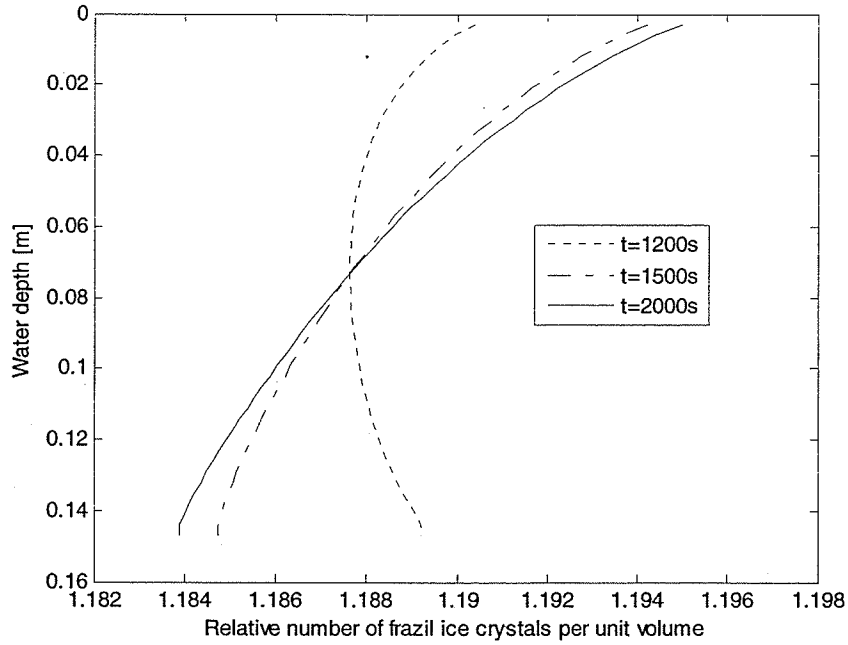

Figure 5.13 Relative frazil ice number profiles.

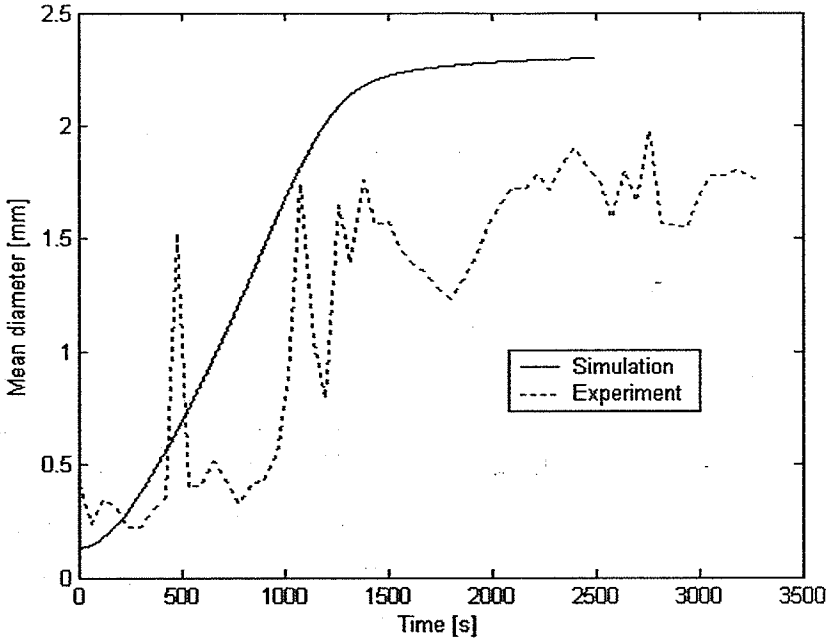

Figure 5.14 Variation of mean frazil ice diameter with time.

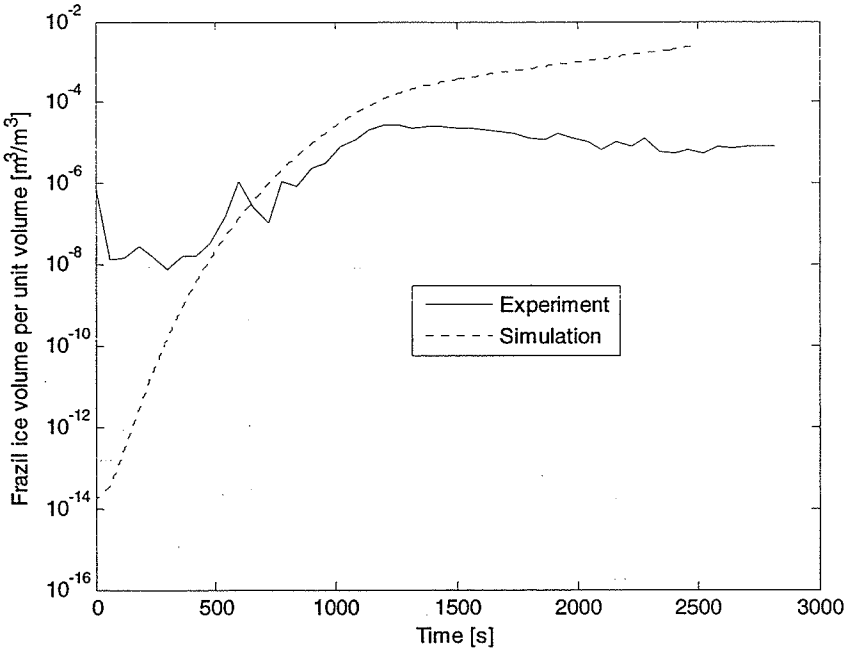

Figure 5.15 Total volume of frazil ice vs. time.

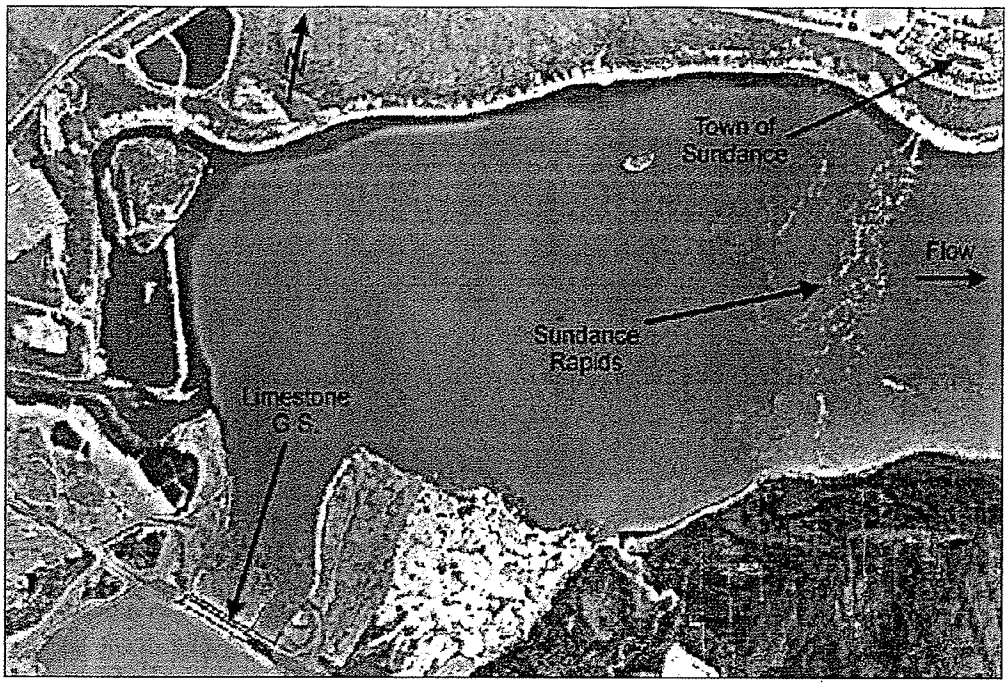

Figure 5.16 Aerial view of the area from the Limestone Generating Station to Sundance Rapids.

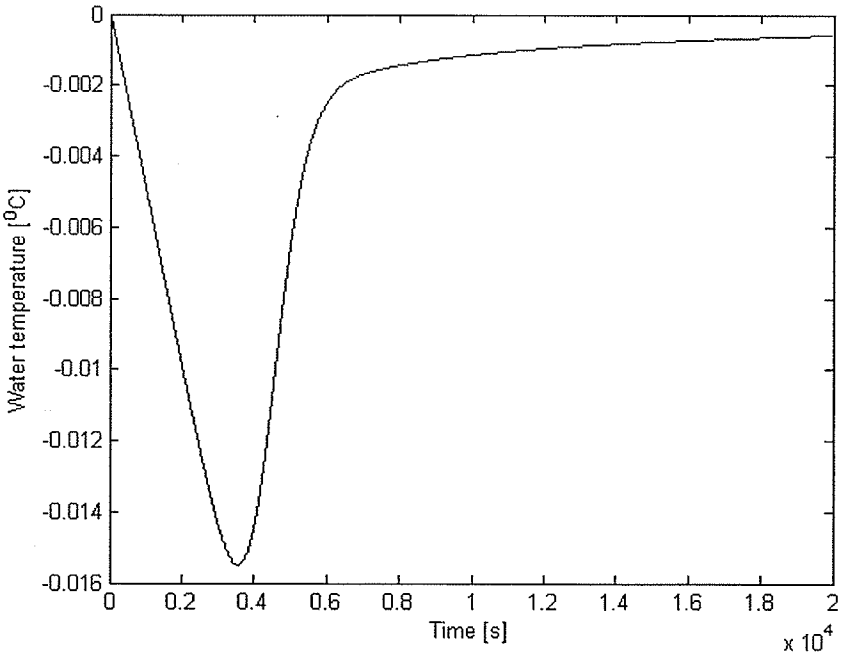

Figure 5.17 Water temperature variation with time at water depth=0.9m.

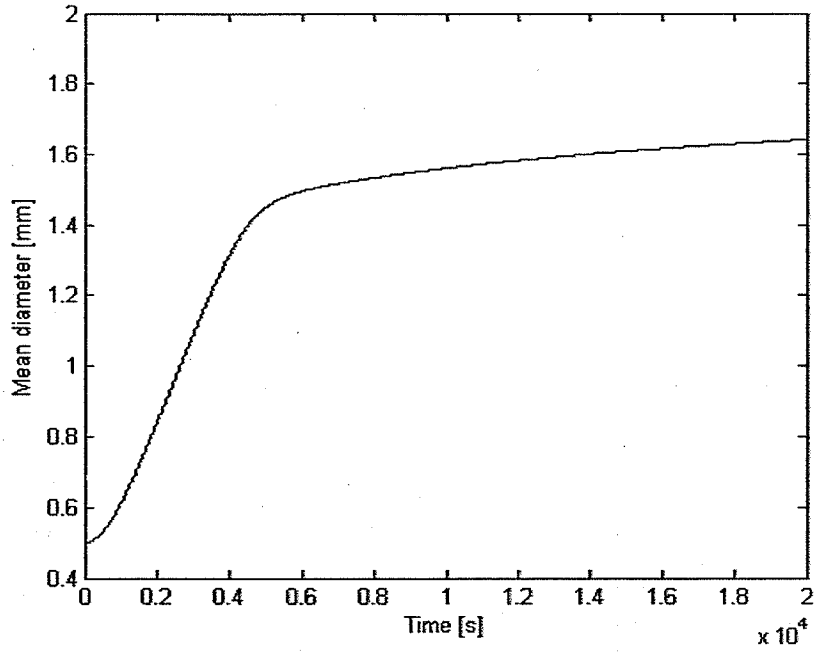

Figure 5.18 Mean size of frazil ice variation with time.

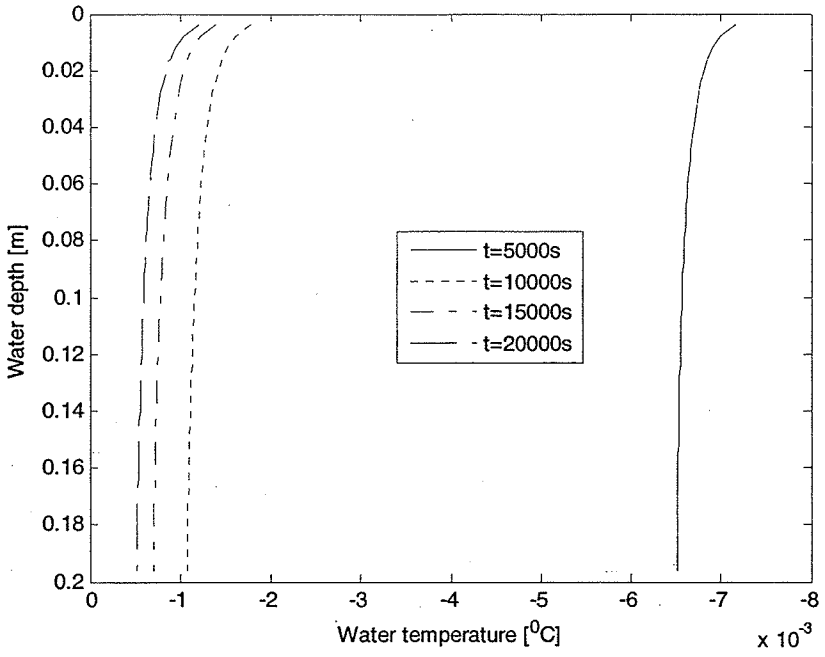

Figure 5.19 Variation of vertical temperature profiles at different times.

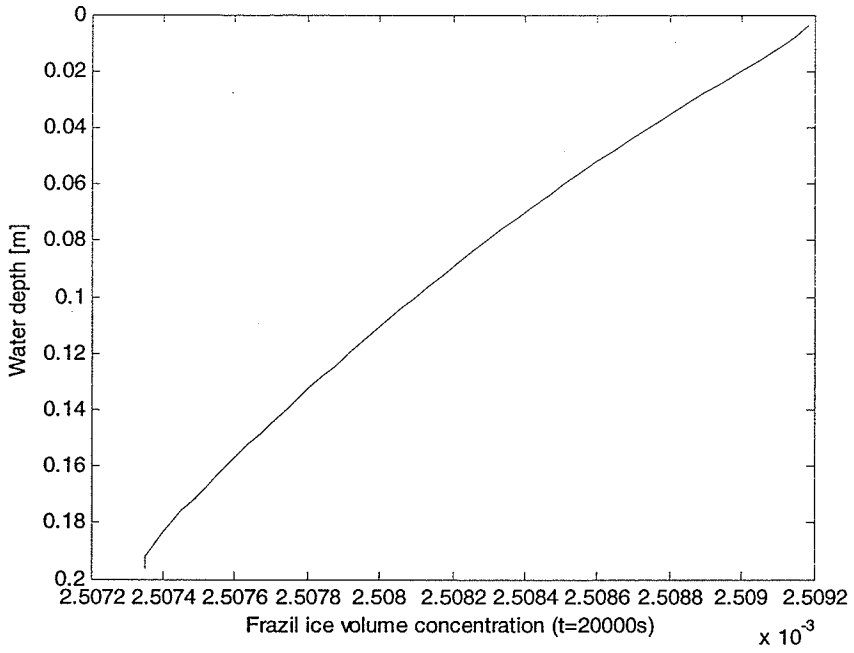

Figure 5.20 Vertical distribution of frazil ice volume concentration at t=10000 s.

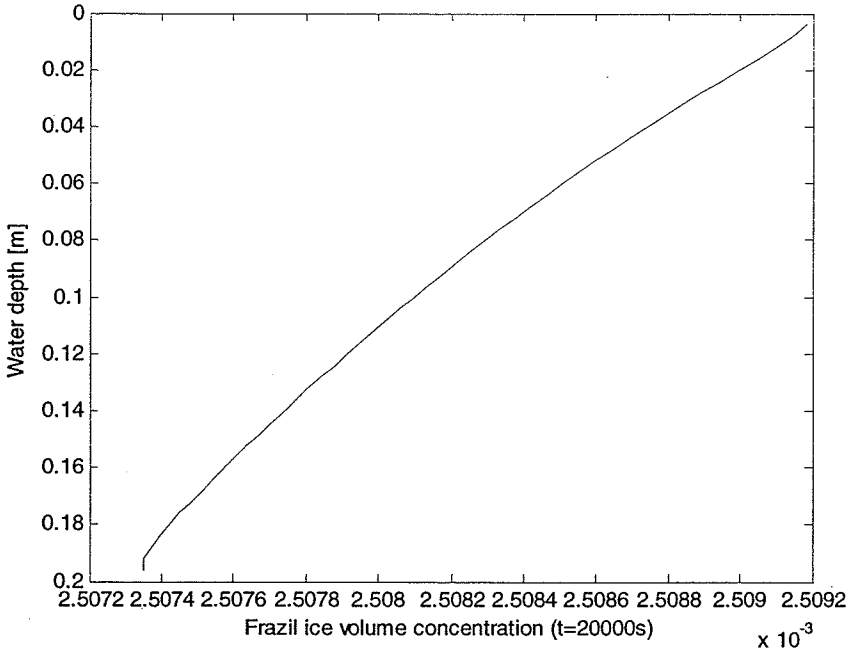

Figure 5.21 Vertical distribution of frazil ice volume concentration at t=20000 s.

CHAPTER 6

An Extended Mathematical Model of Frazil Evolution in A Counter-Rotating Flume

6.1 Introduction

The model in this chapter was extended from the one dimensional model that was developed in the previous chapter by adding the size distribution of the frazil ice instead of using only the mean size of the ice particles. As well, the physical processes of seeding, secondary nucleation, flocculation/break up, and buoyancy removal are considered in this extended model. Seeding is a prerequisite for the initialization of frazil ice. Once the frazil ice regime is established, a small ice particles acts as a nucleus for further growth of an ice particle. The correspondingly large ice particles breed many smaller ice particles through collisions, and this process is known as secondary nucleation and was described in chapter two. The frazil ice size distribution varies with time and is influenced by flocculation and break-up. Buoyancy moves ice particles to the water surface forming surface ice or frazil slush. All of these processes are important physical factors for the modeling of frazil ice evolution. The

model developed in this chapter is used to simulate frazil ice formation in a counter-rotating flume and the results from the model are then compared with the data from experiments conducted in the counter-rotating flume.

6.2 Mathematical Formulation

The governing equations for the mean flow take the same form as those in the vertical one-dimensional model developed in the previous chapter, while the equations for the heat transfer and the frazil ice number equation are slightly different with respect to the source terms, because the size distribution of frazil ice is considered and frazil ice is divided into several size groups

$$\frac{\partial T}{\partial t}=\frac{\partial}{\partial z}\left(\left(\frac{\nu_T}{\sigma_T}+\frac{\nu}{P_r}\right)\frac{\partial T}{\partial z}\right)+G_T \tag{6.1}$$

$$\frac{\partial n_m}{\partial t}=\frac{\partial}{\partial z}\left(\left(\frac{\nu_T}{\sigma_n}+\frac{\nu}{S_n}\right)\frac{\partial n_m}{\partial z}\right)-W_m\frac{\partial n_m}{\partial z}+G_n\,. \tag{6.2}$$

The source terms, because of the ice formation, are denoted by G_T and G_n, respectively. The term G_T represents the latent heat from the ice formation in all group sizes, and the term G_n represents the production of ice particles in different size groups through complicated physical processes such as secondary nucleation, flocculation, etc. These two terms can be calculated as follows (Hammar and Shen, 1995; Svensson and Omstedt ,1984)

$$G_T = \sum_{m=1}^{N} A_m n_m q_m (\rho_w C_p)^{-1}, \tag{6.3}$$

where q_m is the heat transfer for a single ice particle, C_p is the specific heat of water, ρ_w is the density of water, A_m is the active area of frazil ice and N is the number of groups that the frazil ice has been divided into. G_n is given by

$$G_n = \underbrace{\left(\sum_{l=2}^{N} \alpha_l n_l\right)}_{(m=1)} \underbrace{-\zeta \alpha_m n_m}_{(2<m\le N)} \underbrace{-\beta_m n_m}_{(1\le m\le N-1)} + \underbrace{\delta \beta_{m-1} n_{m-1}}_{(2\le m\le N)} \underbrace{-\tau_m n_m}_{(1\le m\le N)} + \underbrace{\tau_{m-1} n_{m-1}}_{(2\le m\le N)} \tag{6.4}$$

secondary nucleation; flocculation/break up; crystal growth

where α_m, β_m, τ_m are the coefficients to describe the secondary nucleation, flocculation/break up, and ice particle growth respectively. The expressions for these coefficients and for their information are given in sections 4.2.2 to 4.2.5. The turbulence characteristics are modeled in the same way as described in section 5.2.2.

6.2.1 Frazil Size Distribution

The size distribution according to Mercier (1994) is used in this model. Although a lognormal distribution seems to be a more reasonable representation for the frazil ice distribution (Daly and colbeck, 1986; Clark and Doering, 2004), both the mean and standard deviation are needed. The mean size of frazil ice could be simulated according to frazil thermal growth, but the variation of the standard deviation has not been defined. Therefore, more research is needed to parameterize the lognormal distribution.

6.2.2 Boundary and Initial Conditions

At the upper boundary of the flow, the same boundary conditions as used in section 5.2.3 can be applied for the flow velocity, turbulence characteristics and the water temperature. The boundary condition for frazil ice number is

$$\frac{\nu_T}{\sigma_n}\frac{\partial n_m}{\partial z} = \varpi_m n_m . \tag{6.5}$$

The initial flow velocity is set to the measured velocity and the initial temperature is set to 0°C. The initial frazil number is set to zero except for the seeding at the water surface.

6.3 Differentiation Scheme of the Governing Equation

The kinematic eddy viscosity is related to the turbulent kinetic energy and the turbulent dissipation rate. The same expression for ν_T and its derivative as used in chapter 5, which is described in Appendix B, are applied herein, and then equations (6.1), (6.2) and (6.4) can be discretized into differential equations. A detailed derivation is shown in appendix C.

All of the resultant equations and their suitable boundary conditions consist of a closed soluble system. A MATLAB® based program was developed to solve the three equations simultaneously.

6.4 Model Programming

The algorithm that is introduced above is programmed in MATLAB®. The flow chart is shown in figure 6.1.

6.5 Model Application

6.5.1 Data from Mercier

A mathematical model was developed by Mercier (1984) to simulate the water temperature variation in the supercooling process, and the vertical distribution of frazil ice. The results from this model are compared with the results from Mercier's model (1984). The parameters used in Mercier's model are given in Table 6.1.

Table 6.1. Parameters of Mercier's model (1984)

U [m/s]	H [cm]	u_* [m/s]	Cooling rate [°C/sec]
1	500	0.1	0.00016

Figure 6.2 shows the variation of water temperature with time at different water depths. The two results agree well except during the warming up period. The difference observed in the warming up period is perhaps induced by using a different formulation to simulate the secondary nucleation and flocculation/break up in the two models, which would produce slightly different number of frazil ice, and subsequently affect the water temperature during

the warming up period. The vertical water temperature profile is depicted in figure 6.3. Figure 6.4 shows how the number of frazil ice particles changes with time at a water depth of 4 m, and it indicates that there is a different increase rate for different size of ice particles. The oscillation of the curve at the beginning is presumably due to a numerical instability. The size distribution of frazil ice at a water depth of 3 m is given in figure 6.5, and it shows that the peak of the curve has shifted to larger frazil ice size as the time of supercooling increases.

6.5.2 Carstens' Data

The flow of Carstens' experiment can be considered as a well-mixed flow (Hammar and Shen, 1995) because the water depth was small and turbulence was produced by a propeller. Therefore, the simulation results from Hammar and Shen's (1995) model and the model developed in this chapter are slightly different from Carstens' experimental results because the two models consider the effect of the vertical stratification of the turbulence parameters. The flow parameters and the heat loss rates for Carstens' experiments are given in Table 4.1.

In figure 6.6, the water temperatures at the different water depths are plotted with Carstens' experimental observations. The water temperature goes down a bit lower and the maximum supercooling occurs roughly one minute later than the experimental result. It illustrates that the peak of the supercooling is reached later and it has a larger magnitude for the case of vertical transport than for the case of complete mixing. The lag time can be estimated by

$T_{lag} = h^2 / \Gamma_{Ave} \approx 1$ min (Mercier, 1984). Figure 6.7 shows the mean water temperature from this model and from Hammar and Shen's model (1995). The temperature distribution throughout the water depth is shown in figure 6.8 and a significant cooling zone is observed close to the water surface. Figure 6.9 shows the relative vertical frazil number profiles at t=400 s. The relative vertical frazil number for n_m is defined as $n_m / \bar{n}$, in which $\bar{n} = \int n_m u dy \Big/ \int u dy$ is the depth-averaged valued of n_m. The frazil ice numbers on the surface are larger than the rest of the water depths for all the frazil ice particles due to the effect of buoyancy removal and seeding. The size distribution of frazil ice at a water depth of 0.12 m at the different times during the experiment is shown in figure 6.10. It is observed that the dominant frazil ice size is the intermediate size. Figure 6.11 shows that the variation of the total number of frazil ice particles with time at a water depth 0.16 m, and it also indicates that the number of frazil ice particles in all the size group increases with supercooling time.

6.5.3 Clark and Doering's Data

Clark and Doering's (2004) experiments, which were conducted in a counter-rotating flume, were also used to investigate the applicability of the present model. Table 4.3 gives the parameters used in their experiments.

The simulation results for the experiment conducted on Dec. 17 are shown in figures 6.12 to 6.15. The water temperature variation with time at different depths is given in figure 6.12.

The maximum supercooling from the simulation is a little lower than the value from the experiment and the time to reach the maximum supercooling is slower by approximately $T_{lag} = h^2/\Gamma_{Ave} \approx 1.3$ min in the simulation (Γ_{Ave} is the average eddy diffusivity). The figure 6.12 also shows that the gradient of the water temperature throughout the water depth is very small, which reflects the strong influence of the turbulence on the heat transfer. The size distribution of the frazil ice at a water depth of H=0.12 m at different times during the experiment is shown in figure 6.13. The sintering of larger frazil ice particles can be observed from the tail of the distribution curve. Figure 6.14 shows how the total number of frazil ice particles changed with time at a water depth of 0.12 m. It also shows that the frazil ice numbers increase during the principal supercooling period and eventually reach a plateau during the residual supercooling period. The vertical distribution of the frazil ice number is shown in figure 6.15, and shows the same tendency as observed in Carstens' (1966) experiment.

6.5.4 Application of the Model to Downstream of the Limestone Generating Station

This extended vertical one-dimensional model was also used to simulate the water temperature variation and the vertical frazil ice distribution in the area downstream of the Limestone Generating Station on the Nelson River. The same flow and thermal parameters as introduced in section 5.5.3 were used in this simulation. The results from this model are shown in figures 6.16 to 6.18. Figure 6.16 shows the supercooling process for the water column in the river. The principal supercooling process lasts about one and a half hour, and it

is much larger than the flow in the experiment. Figure 6.18 and 6.19 give the vertical distribution of frazil ice volume concentration, and indicate that the volume concentration of frazil ice is larger in the area close to the water surface than the rest of the water column. The results of the water temperature and the frazil ice concentration are close to those obtained by Lianwu Liu et al. (2004).

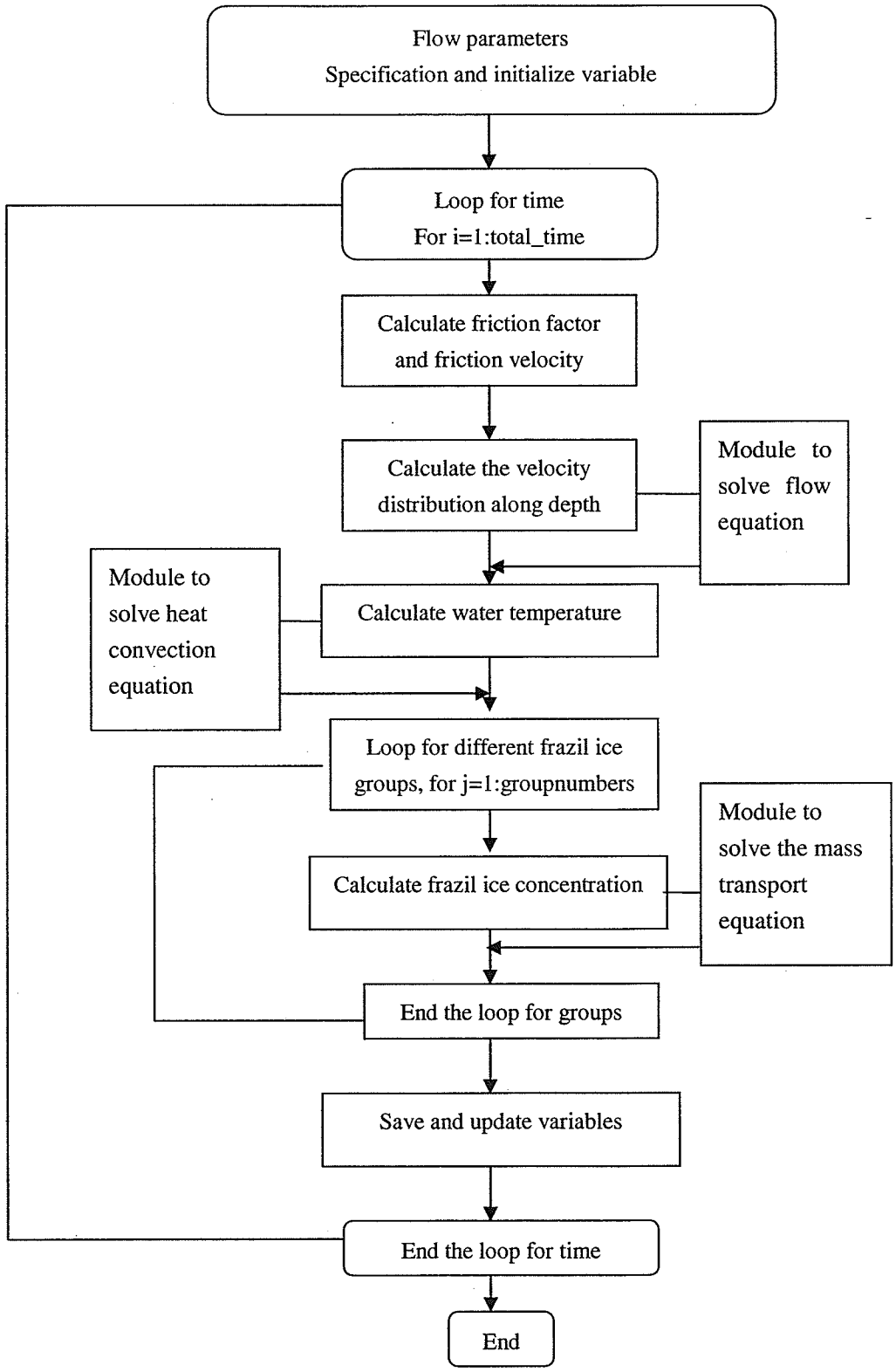

Figure 6.1 Flow chart of the MATLAB program.

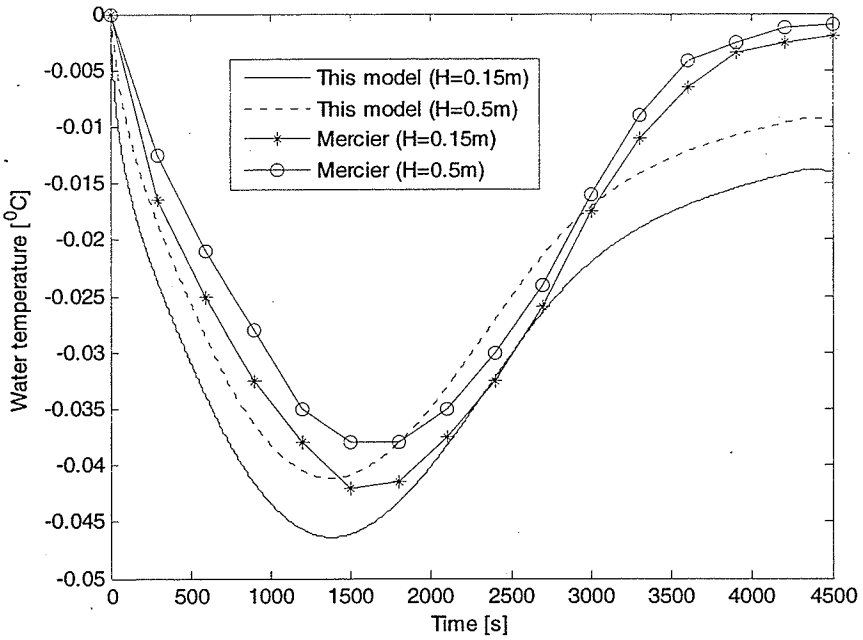

Figure 6.2 Variation of water temperature with time at different depths.

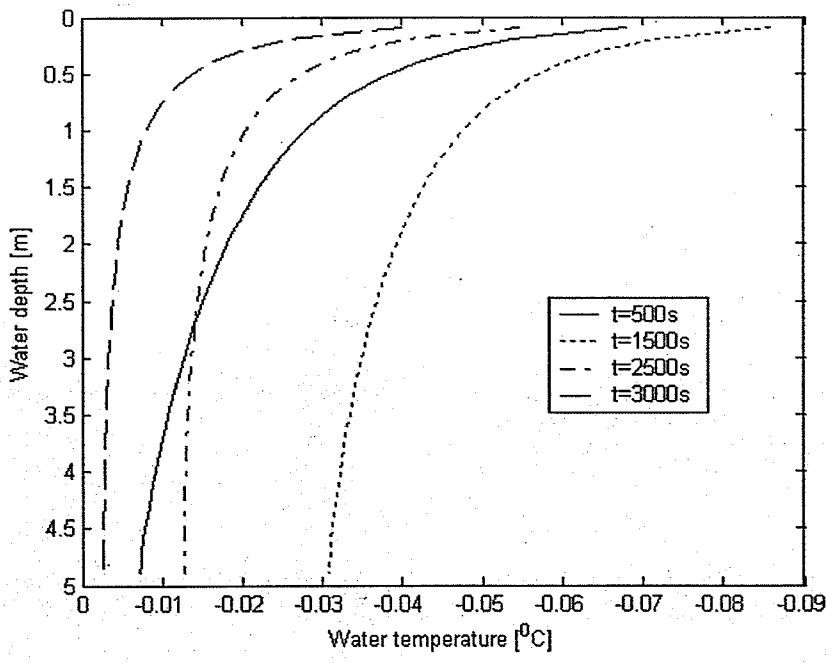

Figure 6.3 Variation of vertical temperature profiles at different times.

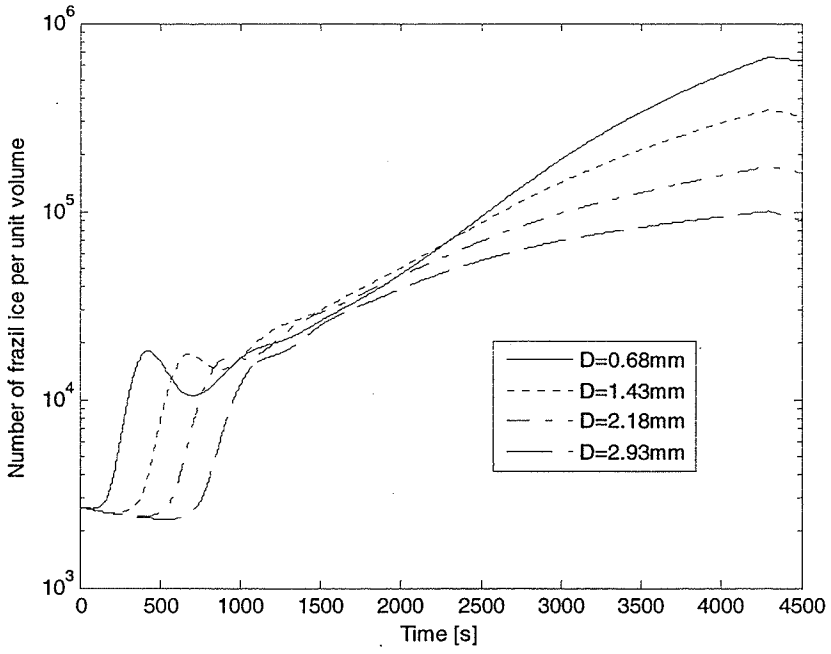

Figure 6.4 Total number of frazil ice particle change with time at water depth 4 m.

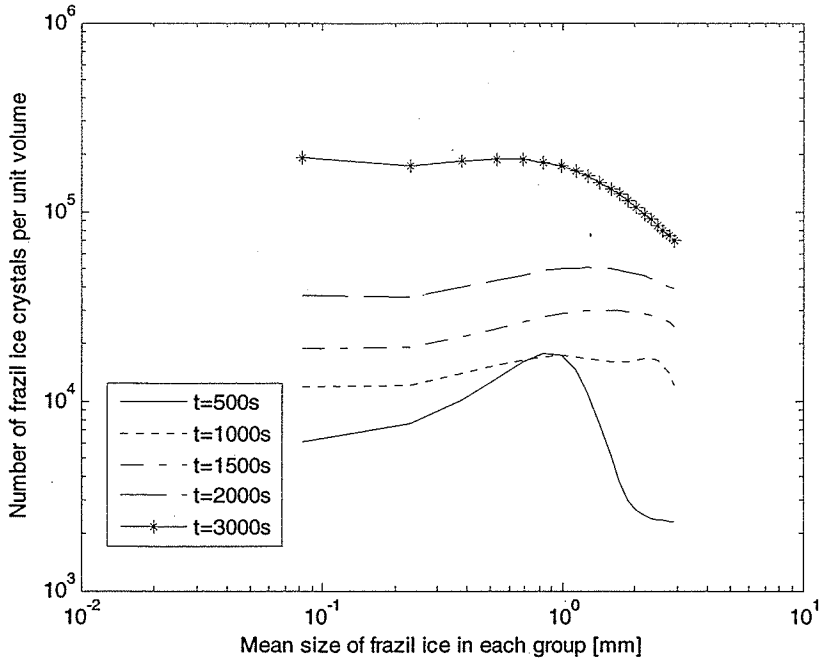

Figure 6.5 Size distribution of frazil ice at water depth 3 m.

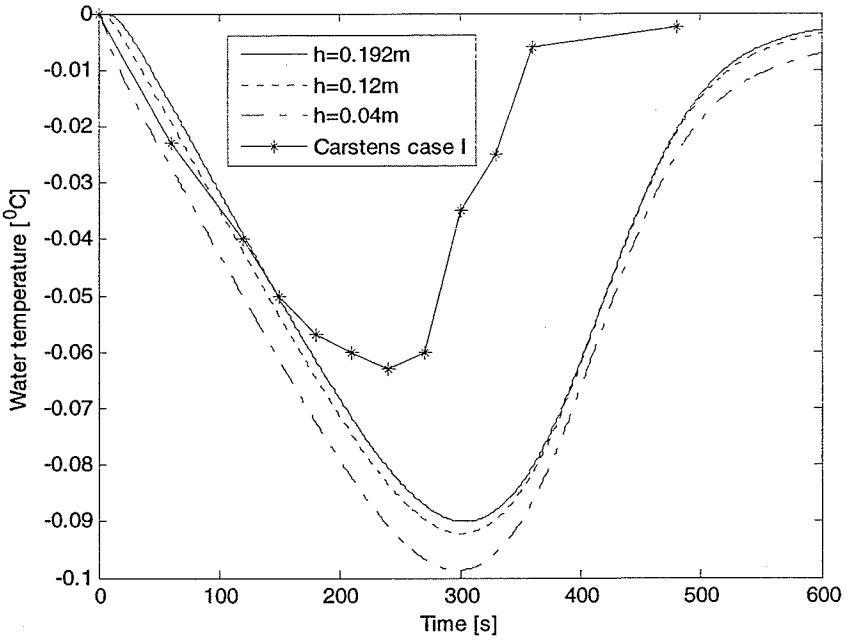

Figure 6.6 Water temperature variations with time at different depths.

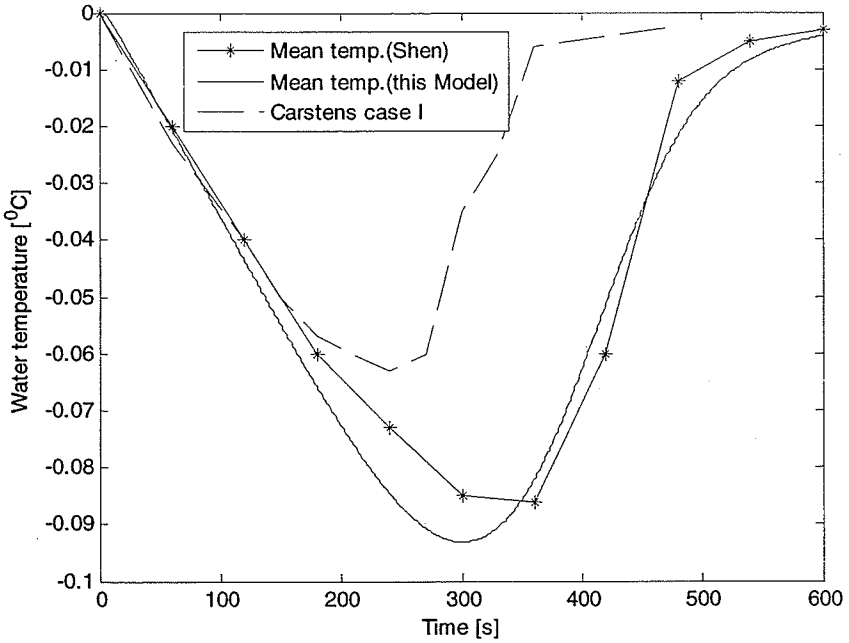

Figure 6.7 Comparison of mean water temperature between this model and Shen's model.

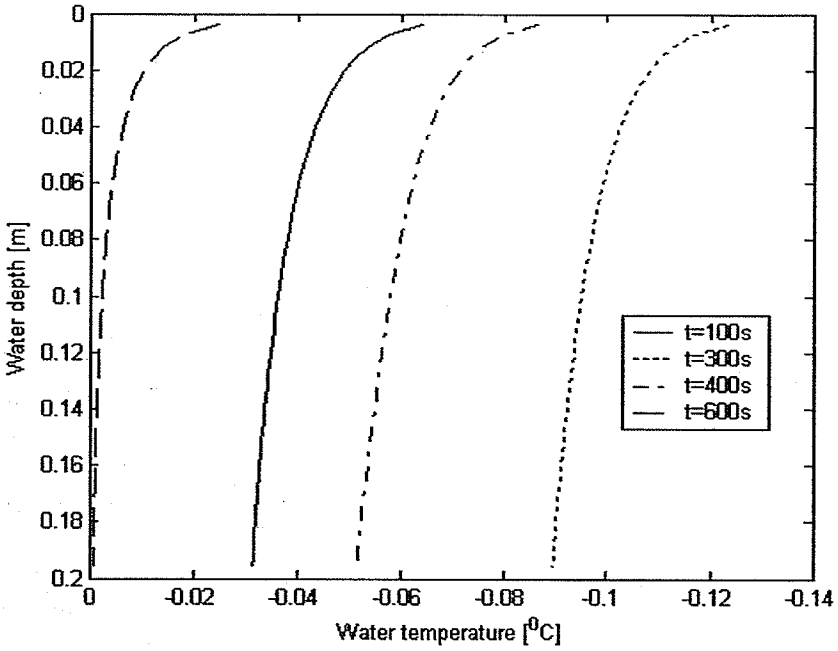

Figure 6.8 Variation of vertical temperature profiles at different times.

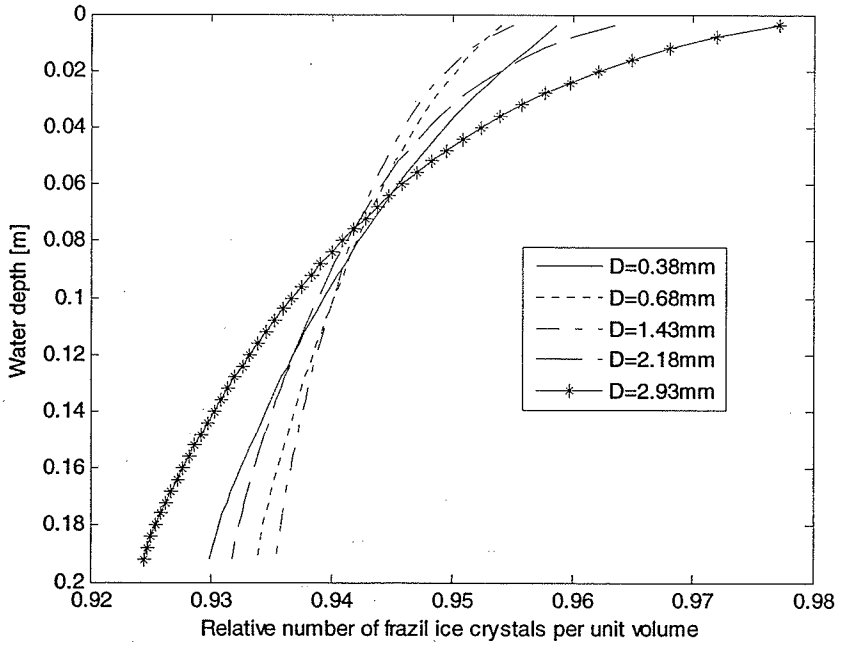

Figure 6.9 Relative frazil ice number profiles at t=400 s.

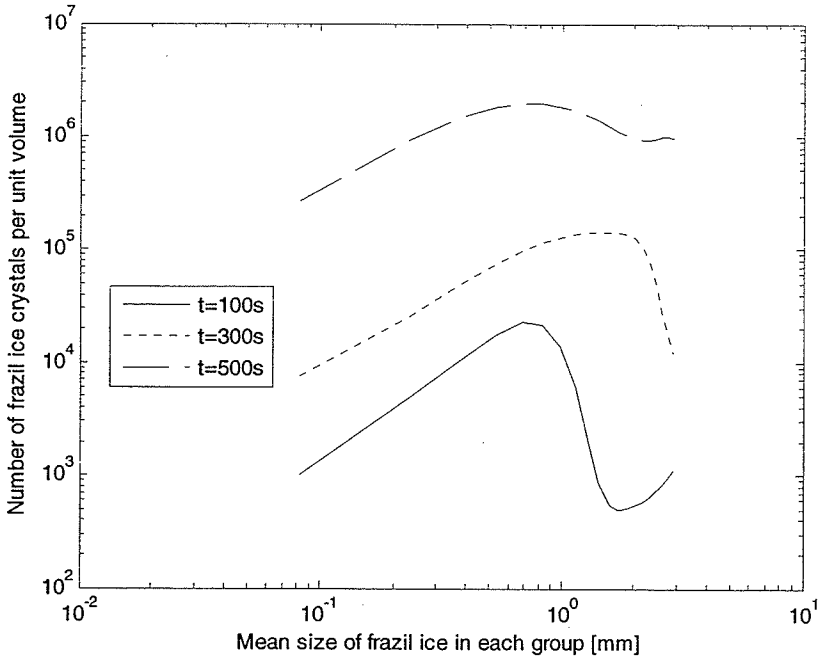

Figure 6.10 Size distribution of frazil ice at water depth 0.12 m.

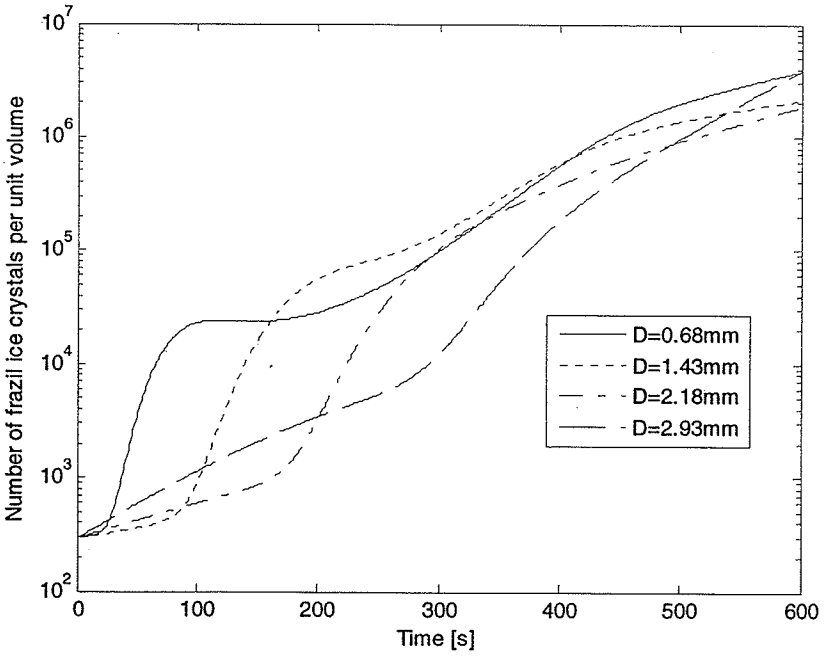

Figure 6.11 Total number of frazil ice particle change with time at water depth 0.16 m.

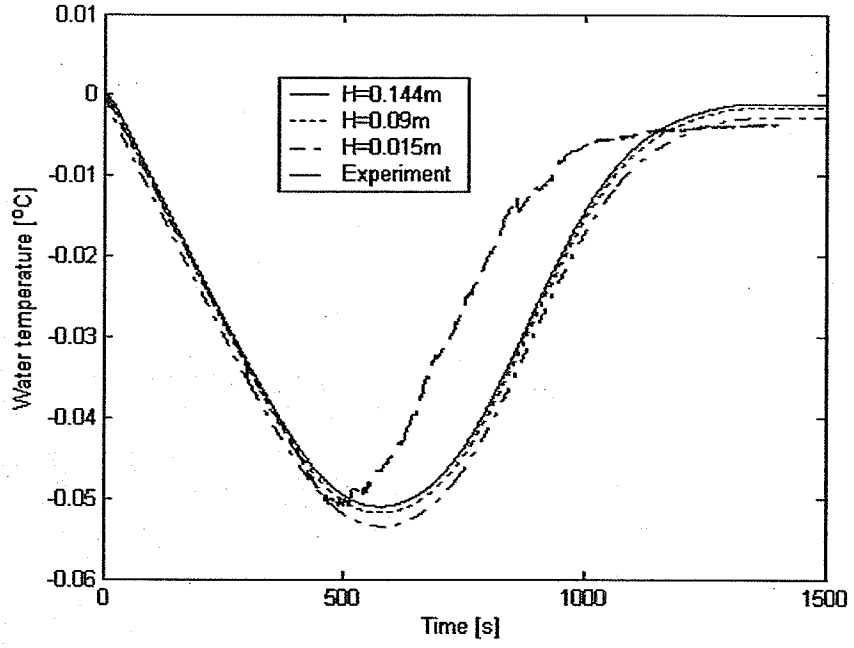

Figure 6.12 Water temperature variation with time at different depths.

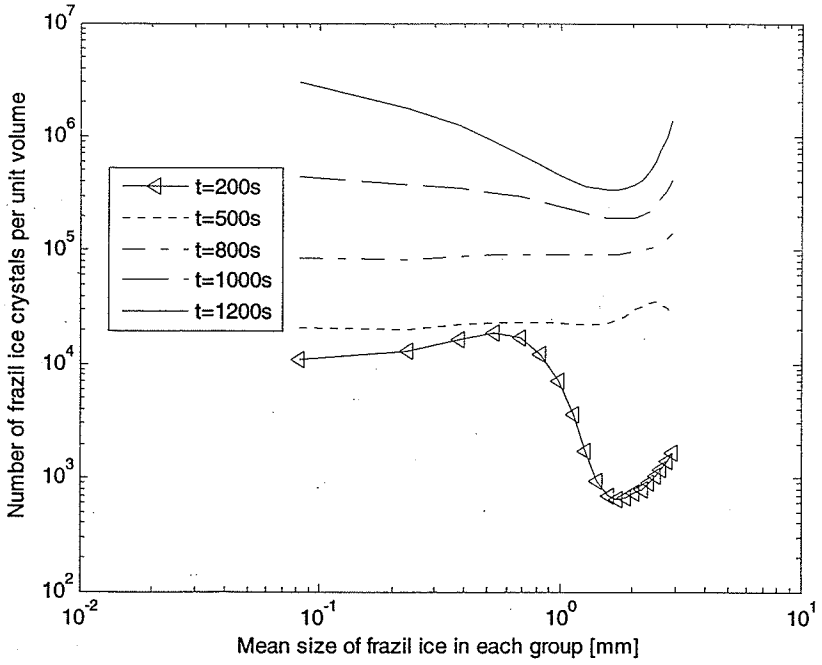

Figure 6.13 Size distribution of frazil ice at water depth 0.12 m.

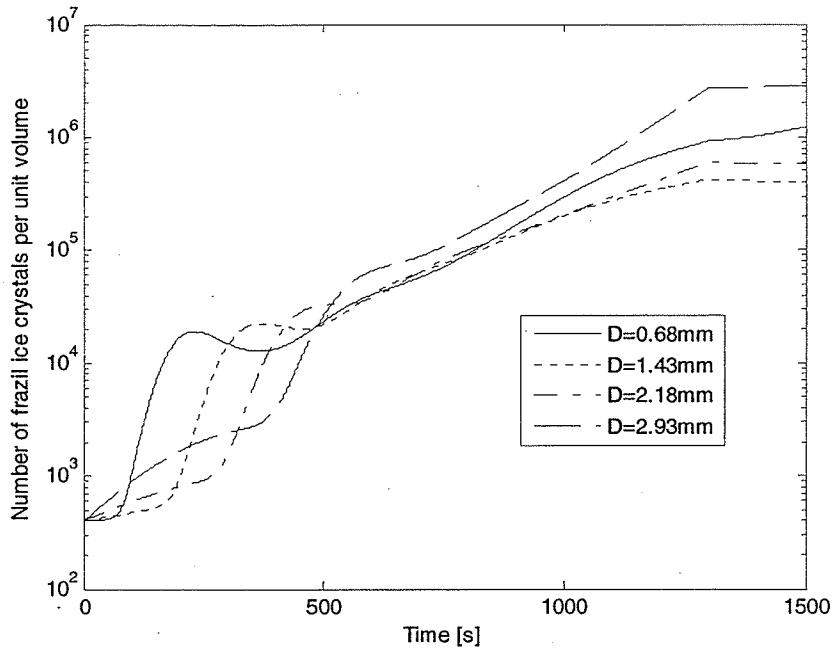

Figure 6.14 Total number of frazil ice particle change with time at water depth 0.12 m.

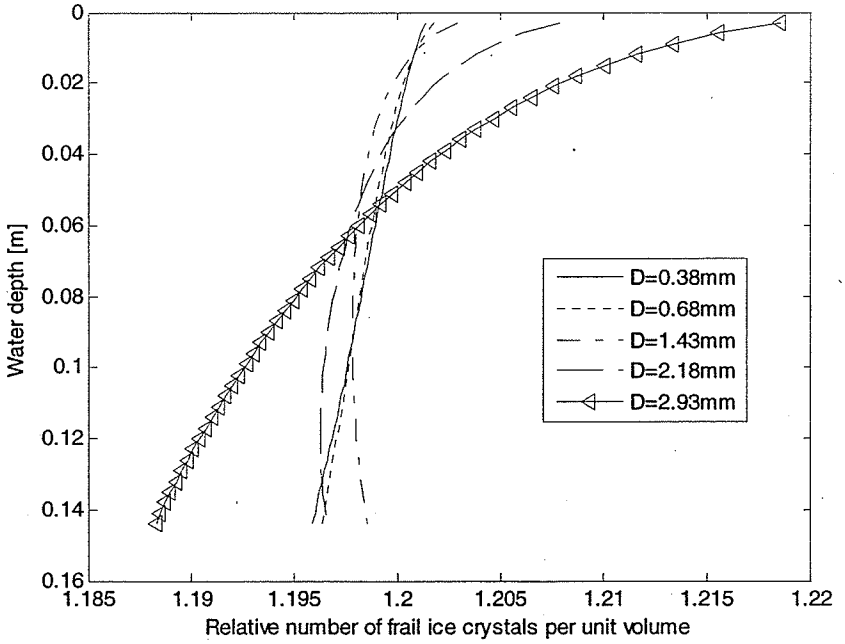

Figure 6.15 Relative frazil ice number profiles at different times.

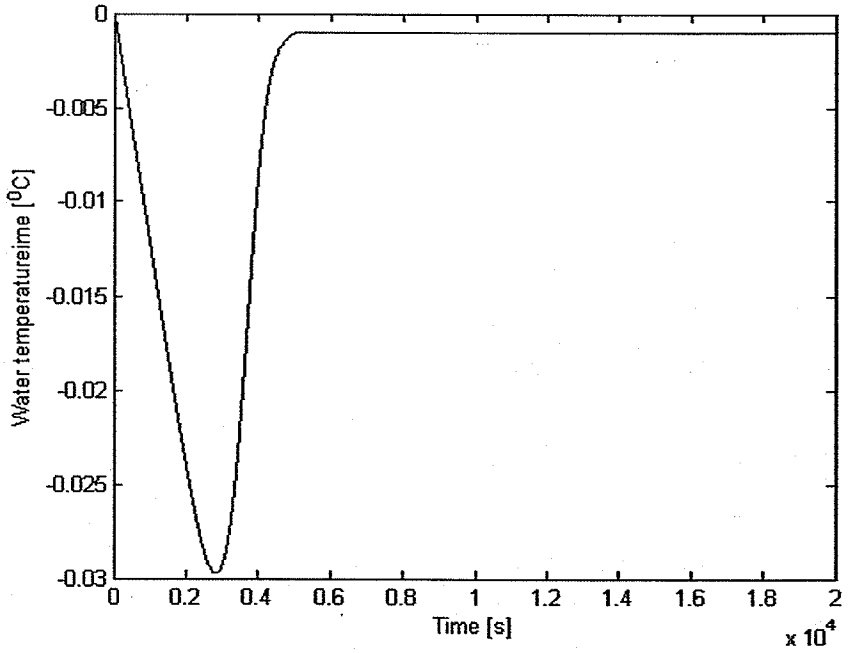

Figure 6.16 Water temperature variation with time at water depth 0.9m.

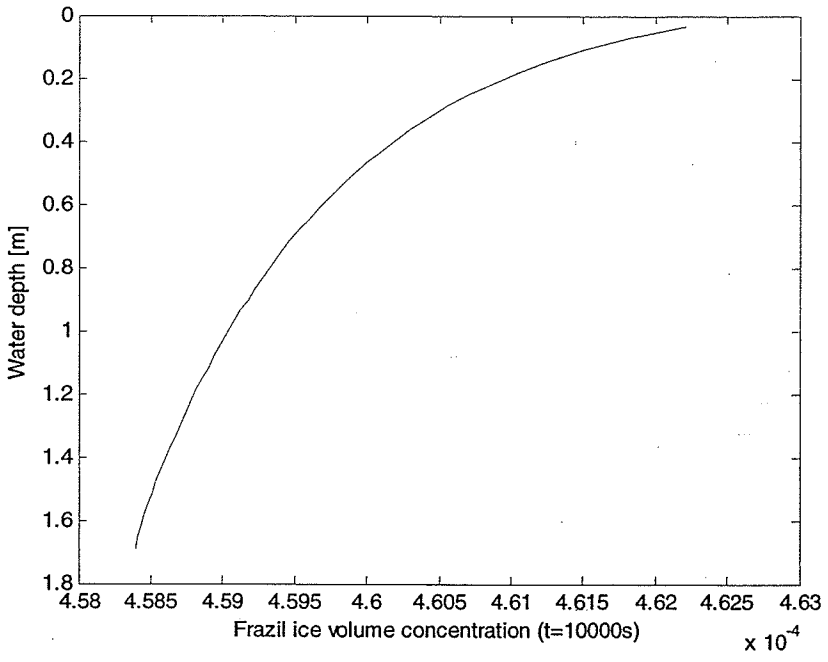

Figure 6.17 Vertical distribution of frazil ice volume concentration at t=10000 s.

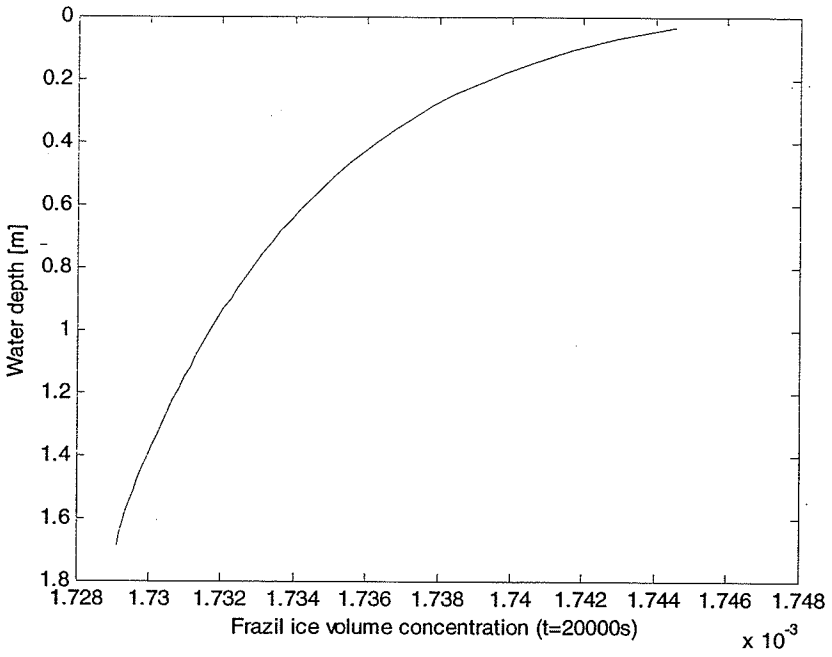

Figure 6.18 Vertical distribution of frazil ice volume concentration at t=20000 s.

CHAPTER 7

Effects of Different Turbulence Models on the Simulation of The Supercooling Process and Ice Formation

7.1 Introduction

Frazil ice usually forms in turbulent supercooled water and the turbulence significantly influences the heat transfer, frazil ice transport, and the distribution of the frazil ice in the water body. Therefore properly simulating turbulence is very important in modeling frazil ice formation and evolution. In this chapter, three different turbulence models are used to investigate turbulence characteristics and their effects on the supercooling process and on the frazil ice formation process. Only the results from the vertical one-dimensional mathematical model in chapter five are given and analyzed herein. However it could be applied to the extended mathematical model in chapter 6.

7.2 Turbulence Models

There are several turbulence models that have been developed so far to simulate the characteristics of turbulence as introduced in chapter two. Three of these models are briefly introduced and then used in this study. Two of the models (turbulence model I and II) are given in an explicit expression in terms of the turbulent energy dissipation rate and the turbulent kinetic energy. The other is the typical $k-\varepsilon$ model and it is extensively used to simulate the turbulence characteristics in open channel flow.

7.2.1 The Two-Equation $k-\varepsilon$ Model

The two equations $k-\varepsilon$ model was given in equations 2.3 and 2.4. These two equations together with equations 5-1, 5-2, and 5-3 can be numerically solved simultaneously.

Discretizing equation (2.3), and (2.4) using the same differential techniques as used in chapter 5, then,

$$\begin{aligned} &-\nu_T(i,j)\Delta t k_{(i+1,j-1)} + \left((\Delta z)^2 + \Delta t(\nu_{T(i,j+1)} - \nu_{T(i,j)}) + 2\Delta t \nu_{T(i,j)}\right) k_{(i+1,j)} \\ &-\left(\Delta t(\nu_{T(i,j+1)} - \nu_{T(i,j)}) + \nu_{T(i,j)}\Delta t\right) k_{(i+1,j+1)} = \Delta z^2 \sigma_k k_{(i,j)} \\ &+ (\Delta z)^2 \Delta t \sigma_k \left(P_{(i,j)} + G_{(i,j)} - \varepsilon_{(i,j)}\right) \end{aligned} \tag{7.1}$$

$$
\begin{aligned}
&-\nu_T(i,j)\Delta t k_{(i+1,j-1)} + \left((\Delta z)^2 + \Delta t(\nu_{T(i,j+1)} - \nu_{T(i,j)}) + 2\Delta t \nu_{T(i,j)}\right) k_{(i+1,j)} \\
&-\left(\Delta t(\nu_{T(i,j+1)} - \nu_{T(i,j)}) + \nu_{T(i,j)}\Delta t\right) k_{(i+1,j+1)} = \Delta z^2 \sigma_k k_{(i,j)} \\
&+ (\Delta z)^2 \Delta t \sigma_k \frac{\varepsilon_{(i,j)}}{k_{(i,j)}} \left(C_{1\varepsilon} P_{(i,j)} + C_{3\varepsilon} G_{(i,j)} - C_{2\varepsilon} \varepsilon_{(i,j)}\right)
\end{aligned}
\tag{7.2}
$$

where $P_{(i,j)} = \nu_{T(i,j)} \left(\frac{U_{(i,j+1)} - U_{(i,j)}}{\Delta z} \right)^2$, $G_{(i,j)} = \nu_{T(i,j)} g \frac{\rho_i - \rho_w}{\rho_w \sigma_C} \frac{C_{(i,j+1)} - C_{(i,j)}}{\Delta z}$ and

$\nu_{T(i,j)} = C_\mu \frac{k_{(i,j)}^2}{\varepsilon_{(i,j)}}$.

The same method used above can be applied to equations (5.1), (5.2), and (5.3). Finally a closed system can be obtained, and the system can be solved numerically with the proper boundary conditions as given in equations (5.9), (5.10) and (5.11). Some coefficients used in the $k-\varepsilon$ equation are given in table 2.1. The term $G_{(i,j)}$ is neglected in this simulation since the concentration of frazil ice is very small.

7.2.2 Zero-Equation Model

Two simple turbulence models were introduced in chapter 2, one of which (turbulence model I) has already been used in chapters 4, 5, and 6. Herein another simple turbulence model (turbulence model II) is applied to the turbulence simulation. Typical expressions for k and ε were suggested by Nezu (1977) and were given by equations 2.10 and 2.11. The kinemetic eddy viscosity is expressed

$$\nu_T = C_\mu \frac{k^2}{\varepsilon} = C_\mu \frac{4.78^2}{E_1} (zH)^{1/2} u_* \exp\left(\frac{-z}{H}\right).$$

Typically, $C_\mu = 0.09$ and if the Reynolds number is around $10^4 \sim 10^5$, then taking $E = 9.8$ (Nezu, 1977), yields,

$$\nu_T = 0.2098(zH)^{1/2} u_* e \exp\left(\frac{-z}{H}\right).$$

Therefore, $\frac{\partial \nu_T}{\partial z} = 0.1049 z^{-1/2} H^{1/2} u_* e \exp\left(\frac{-z}{H}\right) - 0.2098 z^{1/2} H^{-1/2} u_* e \exp\left(\frac{-z}{H}\right)$.

The same procedure as shown in chapter 5 can be applied to equations (5.1), (5.2), and (5.3) to simulate the flow, the water temperature, and the frazil ice number variation.

7.3 Results and Discussions

The three turbulence models are applied to the experiment of Carstens case I. Some results are plotted in figure 7.1 to 7.6. Figure 7.1 shows the vertical velocity distribution from the three turbulence models used in this simulation and from Hammar and Shen's (1995) model. Figure 7.2 and figure 7.3 show the vertical distribution of the turbulence kinetic energy and the turbulent dissipation rate. In general, the results are close, although some slight differences exist in the region close to the water surface and close to the bottom. It indicates that all three turbulence models can be used to calculate the velocity field and the turbulence characteristics if only one dimensional model along vertical direction is of interest. Figure 7.4 shows the comparison of the water temperature history in the supercooling process from the three turbulence models and from Hammar and Shen's (1995) simulation. Figure 7.5 shows how the mean frazil ice size varies with time. The variation of the total frazil ice

volume in the supercooling process is shown in figure 7.6. All of the simulation results in the frazil ice formation from the three turbulence models generally have the same trend.

The results of the velocity distribution, the turbulence kinetic energy and the energy dissipation rate from the three turbulence models are slightly different. The two simple turbulence models seem to overestimate or to underestimate the turbulence kinetic energy and energy dissipation rate in the areas close to the water surface and or close to the bottom of the flume. The reason for this is there is no boundary condition applied in the simple turbulence models, and the impact of boundary layers can not be reflected throughout the water depth. The $k-\varepsilon$ model can consider the impact of the boundary condition and gives a more reasonable solution. A small difference exists between the results from Hammar and Shen's (1995) model and this model, even though both use the $k-\varepsilon$ turbulence model. This is probably caused by neglecting the gradient of frazil ice concentration and water temperature in the turbulence equation (2.4)

The results concerning the water temperature and frazil ice volume variation with time in the supercooling process are also slightly different for the three turbulence models, but in general, the simple turbulence models are good enough to be used to simulate frazil ice formation and evolution compared to the complicated $k-\varepsilon$ equations if only the variables alone vertical direction is of interest.

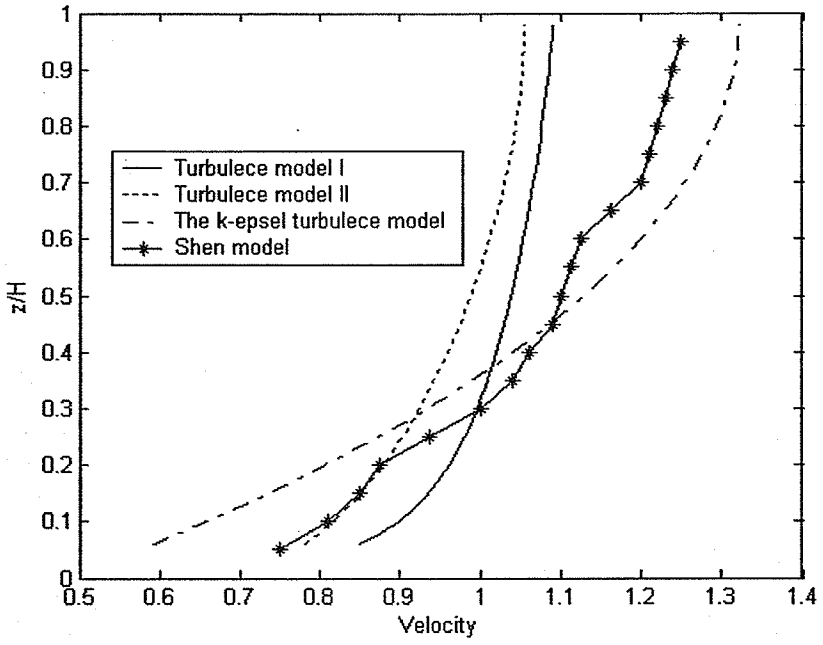

Figure 7.1 Vertical distribution of flow velocity.

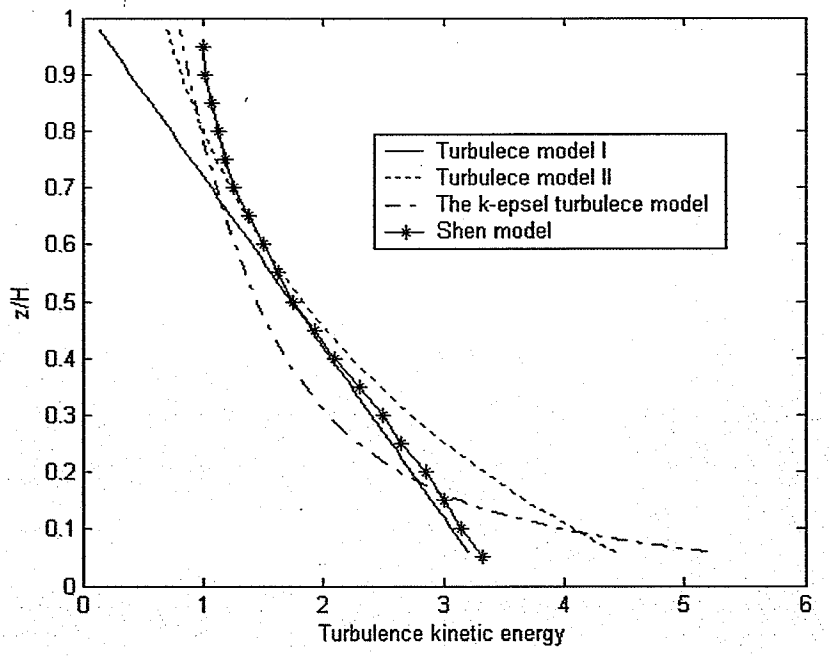

Figure 7.2 Vertical distribution of turbulent energy.

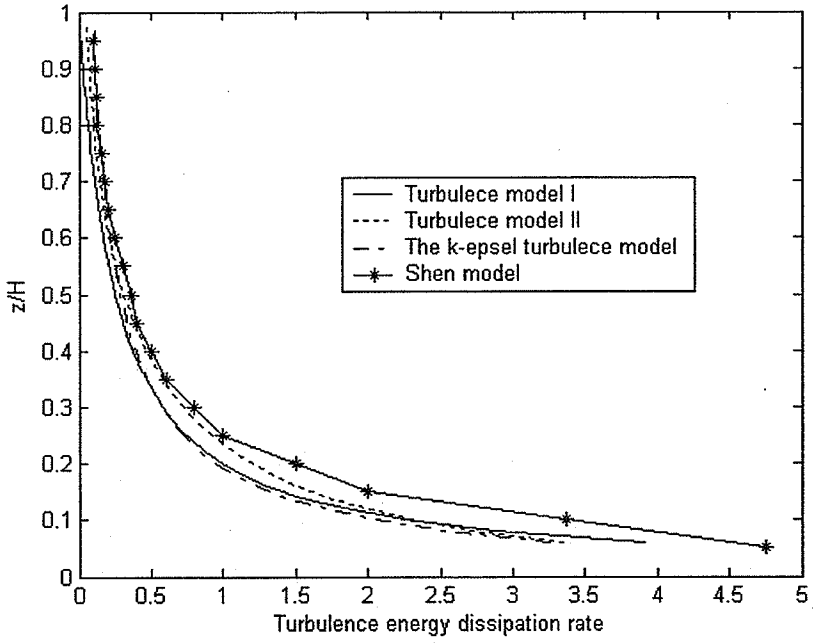

Figure 7.3 Vertical distribution of turbulent energy dissipation rate.

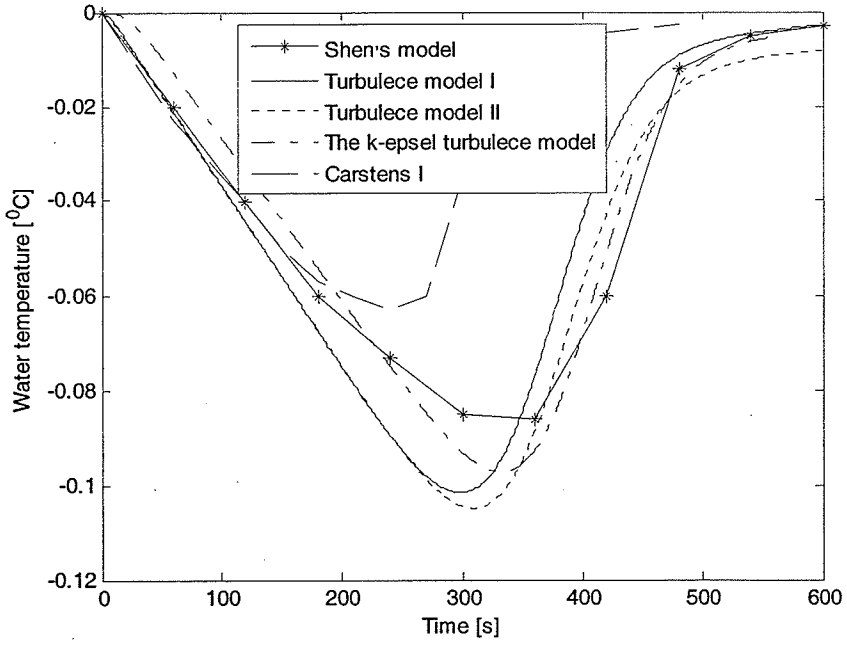

Figure 7.4 Mean water temperature variation with time.

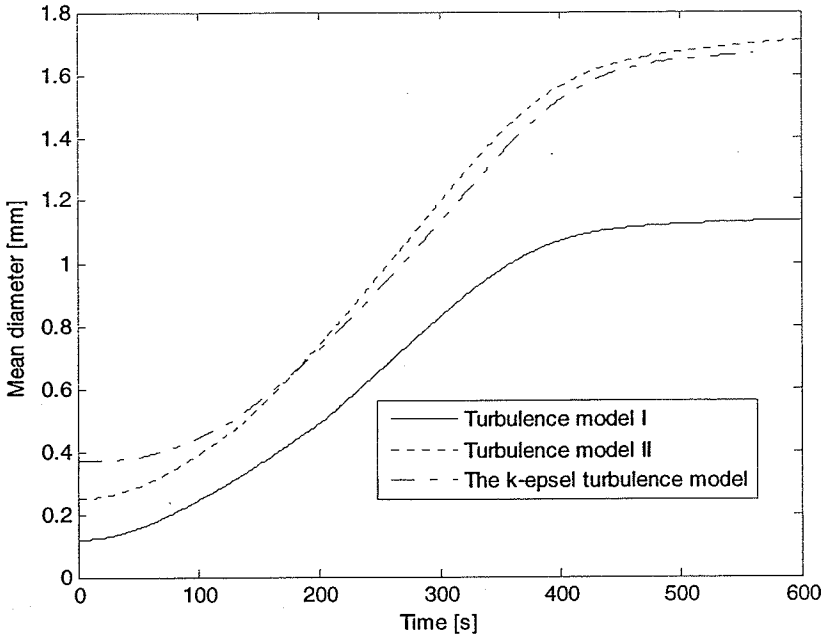

Figure 7.5 Mean size of frazil ice particle variation with time.

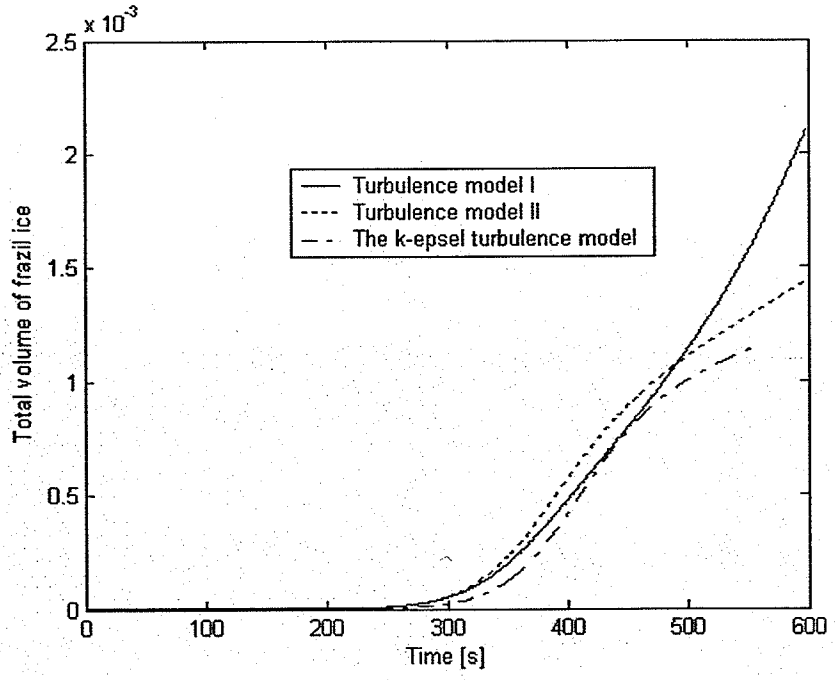

Figure 7.6 Total number of frazil ice variation with time.

CHAPTER 8 Summary and Future Works

8.1 Introduction

The formation of ice in rivers has created engineering challenges with respect to the design, operation and maintenance of hydraulic facilities. Therefore, a significant amount of research has been carried out to study ice formation. Since frazil ice is the origin of almost all the others forms of river ice (Ettema et al., 1984), research into frazil ice formation has been very important. The study of frazil ice formation has mainly focused on the supercooling process, nucleation, ice particle growth, and evolution, from both laboratory experimentation and mathematical modeling perspectives.

8.2 Summary

Zero-dimensional model

In this study a general mathematical model was formulated based on open channel flow theory. A zero-dimensional mathematical model for the formation and evolution of frazil ice

was developed based on Daly's (1984) frazil ice dynamics, and Svensson and Omstedt's (1994) model. The model considers several physical processes such as initial seeding, ice particle growth, secondary nucleation, flocculation and break up, and buoyancy removal. In this model, initial seeding was treated as a calibration factor since it has not been mathematically defined yet. Ice particle growth was modeled based on its heat transfer to the surrounding water, and an actual Nusslet number was used according to Daly's (1984) description instead of using the turbulent Nusslet number in the simulation of thermal ice growth (Hammer and Shen, 1995). Secondary nucleation was simulated based on the theory that Svensson and Omstedt (1994) suggested. The processes of flocculation/break up and buoyancy removal were modeled according to Svensson and Omstedt's (1994) formulation. The interaction of these physical processes during frazil ice evolution was modeled through the determination of different parameters. Water temperature, frazil ice concentration, and frazil ice number variation were simulated. In addition, the size distribution of frazil ice was simulated based on the method suggested by Svensson and Omstedt (1994), which was originally described by Mercier (1984). The model was calibrated with existing experimental data, namely, Carstens (1966) and Clark and Doering (2004). A good fit was developed between the simulated and the observed experimental data.

A vertical one-dimensional model

A vertical one-dimensional model for the formation and the evolution of frazil ice was also developed in this study, and was applied to simulate frazil ice formation under different

cases. First, the turbulence characteristics such as turbulent kinetic energy and turbulent dissipation rate were simulated from a simplified turbulence model, and then the water temperature and frazil ice number were modeled both in spatial and temporal space. The vertical one-dimensional model only considers the multiplication of frazil ice particles without including the other physical processes such as secondary nucleation, flocculation, or break up. The evolution of the mean size of the frazil ice was simulated and used for the computation of heat production from frazil ice growth. This vertical one-dimensional model was calibrated with existing experimental data from Carstens (1966) and Clark and Doering (2004). A good fit was observed between the simulated data and observed experimental data. Finally, this model was applied to simulate the frazil ice formation on the downstream of Limestone Generating Station with promising results.

An extended vertical one-dimensional model

A vertical one-dimensional mathematical model to simulate the formation and evolution of frazil ice was extended by considering the effects of secondary nucleation and flocculation/break up on frazil ice formation. Secondary nucleation, flocculation/break up, and the size distribution of frazil ice were modeled in the same way as in the zero-dimensional model. The simulation results of water temperature variation during the supercooling process from this model were compared with Mercier's (1984) results; an acceptable agreement was observed. Furthermore, Carstens' (1966) experimental data and Clark and Doering's data (2004) were also used to calibrate and verify the model developed.

The model was also used to simulate the frazil ice formation in the downstream of Limestone Generating Station in the Nelson River; reasonable results were obtained.

Effect of three turbulence models on frazil ice formation

Three turbulence models, including two simple turbulence models and a $k-\varepsilon$ model were used in a vertical one-dimensional model to simulate frazil ice formation and evolution, and then applied to Carstens case I. The aim was to investigate how these turbulence models affect the modeling accuracy of frazil ice formation and evolution. The results of the vertical distribution of velocity, turbulence kinetic energy, turbulent dissipation rate, mean size variation of frazil ice, and the total volume of frazil ice produced were compared among the three turbulence models. It was found that the two simple turbulence models can generate results comparable to the more complicated $k-\varepsilon$ model.

8.3 Conclusion

The following conclusions can be drawn from this study.

i). A zero-dimensional model was developed that can predict water temperature variation, frazil ice number evolution (in different size groups), ice growth, secondary nucleation, flocculation/break up, and buoyancy removal. Two calibration parameters (initial seeding and n_{max}) were used in the development of the zero-dimensional model. Specifically, the zero-dimensional model showed that:

a. the total number of frazil ice particles increases during the primary period of suprercooling then remains constant during the period of residual supercooling;

b. an increase in the initial seeding or of the parameter n_{max} shortens the supercooling process and reduces the maximum amount of supercooling;

c. the size distribution for frazil ice suggested by Svensson and Omstedt (1994) appears reasonable, although there were some differences from a measured size distribution; and

d. a zero-dimensional mathematical model can provide reasonable estimates of frazil ice formation in a well mixed water body, and can provide, therefore, preliminary information with regard to the ice formation.

ii). The stratification of a flow and its turbulence characteristics can be well modeled by a one-dimensional vertical model, and subsequently that frazil ice formation can be simulated by considering only the thermal growth of frazil ice particles, thereby neglecting other complicated physical processes. In such a simulation, only the mean size of frazil ice particles was predicted. For this case the model showed that:

a. the water gets more supercooled in the area close to the water surface than the rest of the water depth;

b. the gradient of the vertical water temperature distribution depends on the turbulent intensity; and

c. the simulation of the mean size of frazil ice fits well with experimental data, and provided a way to find the variation of the mean frazil ice particle size during the

supercooling process.

iii). Complicated physical processes such as secondary nucleation, flocculation/break up and buoyancy removal can be successfully implemented into a vertical one-dimensional model. Such a model shows that:

a. there is a notable gradient for the frazil ice number distribution over the water depth for smaller and larger frazil ice particles due to the effects of seeding on the water surface and buoyancy forces;

b. the frazil ice size distribution at different times and water depths can be modeled based on Svensson and Omstedt's (1994) formulation in the extended one-dimensional vertical model;

c. different trends in different experiments that probably depend on the intensity of flow turbulence; and

d. the total number of frazil ice particles for different size groups and water depths seems to increase during the primary supercooling period for all size groups.

iv). Two simple turbulence models can achieve results comparable to a more complicated $k-\varepsilon$ model. Therefore, two simple turbulence models can be used instead of a $k-\varepsilon$ model in the simulation of frazil ice formation in a vertical one-dimensional model. The advantage of using two simple turbulence models is the ability to avoid solving complicated equations.

8.4 Suggestions and Recommendations of Future Work

The study of the growth and evolution of frazil ice is a very difficult topic in ice engineering because it involves thermal dynamics, fluid mechanics, and mass transportation. Although this study has explored and simulated some important aspects of frazil ice growth and evolution, there are still research gaps that need attention in the future.

i). The mechanism of secondary nucleation and flocculation/break up are not fully understood, more research is required to formulate these two important physical processes.

ii). Initial seeding is a very important factor in ice formation, and it is treated as a calibration factor in most mathematical models. More studies are required to quantity the amount of initial seeding.

iii). A lognormal distribution is considered a reasonable description for the size distribution of frazil ice in the supercooling process. The mean of the distribution has been well simulated in this study, but the variation of standard deviation is still unknown. More experiments are required to generalize the variation of the standard deviation.

iv). Three mathematical models have been developed in this study, but there are some limitations for each model since the formulation of the mathematical models are based on specific assumptions. A zero-dimensional mathematical model is suitable for a well-mixed flow, whereas a vertical one-dimensional model and an extended

vertical one-dimensional model are suitable for the flow in which the vertical mean velocity can be neglected. In rivers, these two assumptions are not always true. A mathematical model to simulate frazil ice formation in open channel flow that considers the variation of air temperature is required.

v). The turbulence intensity strongly influences the frazil ice formation and evolution during the supercooling process; therefore an exact measurement of turbulence intensity distribution in a counter-rotating flume is needed for future research.

Bibliography

Andreas M., 1978. Frazil ice formation in turbulent flow. IIHR report No. 214, Iowa Institute of Hydraulic Research, The University of Iowa.

Arakawa, K., 1954. Studies on the freezing of water II, Formation of disc crystals. *Journal of the faculty of science,* Hokkaido University, series II, IV(5), 310-339.

Ashton, G. D. ed. 1986 River and Lake Ice Engineering. Water Resources Publications, Littleton, Colorado, U.S.A

Batchelor, G. K. 1980 Mass transfer from small particles suspended in turbulent fluid. Journal of Fluid Mechanics. 98(3): 609-623.

Beltaos, S. ed. 1995 River Ice Jams. Water Resources Publications, LLC.

Bukina, L.A. 1967 Size distribution of frazil ice crystals in turbulent flows. Izv. Atmospheric and Oceanic Physics, 3(1): 58-68.

Carstens, T., 1966. Experiments with supercooling and ice formation in flowing water, *Geofysiske Phblikasjoner*, 26(9): 3-18.

Celik, I and W. Rodi 1984. Simulation of free-surface effects in turbulent channel flows. Physicochemical hydrodynamics, 5:217-227.

Clark. S and Doering. J. C., 2002. Laboratory observations of frazil ice, *Proc. Of the 16th international symposium on ice,* Dunedin, New Zealand, Vol. 1: 127-133.

Clark S and Doering, J. C. 2004 A laboratory study of frazil ice size distributions, *proceeding of the 17th international symposium*, St. Petersburg, Vol. 1:291-297

Clark. S and Doering. J. C., 2006. Laboratory experiments on frazil size characteristics in a counterrotating flume, *Journal of Hydraulic Engineering,* ASCE, Vol. 132: 94-101.

Daly, S. F. 1991 Frazil ice. In K.C. Cheng and N. Seki (editors), Freezing and melting Heat Transfer and Engineering. Hemisphere Washington, D.C. Ch. 16, 523-544.

Daly, S. F. (1994) Report on Frazil ice, USA Cold Regions research and Engineering Laboratory, Special Report 94-23.

Daly, S. F. and Colbeck, S. C. 1986 Frazil ice measurements in CRREL's flume facility, IAHR Ice Symposium, Iowa City, U.S.A. 427-436

Daly, S.F., 1984. Frazil ice dynamics, *CRREL Monograph 84-1*, USA Cold Regions Research and Engineering Laboratory, Hanover, NH.

Denk, E.G., Jr. and G. D. Botsaris, 1972. Fundamental studies in secondary nucleation from solution, *Journal of. Crystal Growth*, 13/14: 493-499.

Doering, J. C. and Morris, M. P. 2003. A digital image processing system to characterize frazil ice. *Canadian Journal of Civil Engineering*. 30: 1-10

Ettema, R., Karim, M. F. and Kennedy, J. F. 1984 Frazil ice formation. US Cold Regions

Research and Engineering Laboratory (CRREL), Report 84-18.

Evans, T.W., A. F. Sarofim and G. Margolis, 1974b. Models of secondary nucleation attributable to crystal-crystallizer and crystal-crystal collisions. *American Institute of chemical engineers journal* 20(5), 959-966.

Evans, T.W., G. Margolis and A. F. Sarofim, 1974a. Mechanisms of secondary nucleation in agitated crystallizers. *American Institute of chemical engineers journal* 10(5), 950-958.

Gerard, R. 1990 Hydrology of floating ice. Northern Hydrology: Canadian perspectives, Environment Canada, Notional Hydrology Research Institute, Saskatoon, Canada.

Hammer, L., and Shen, H. T. 1995 Frazil evolution in channels. *Journal of Hydraulic Research.* 33(3), 291-306.

Hanley, T. O., and S. R. Rao, 1982, Acoustic detector for frazil. *IAHR*, Vol. 1, pp. 101-110

Horjen, I. 1994 Frazil and Glaze ice accretion on trash racks in slightly supercooled flows, *12th IAHR Symposium on Ice*, Trondheim, Norway, 571-580.

Hussain, A. K. M. F. and W. C. Reynolds. 1975 Measurements in fully developed turbulent channel flow. *Journal of Fluids Engineering*, ASCE, 97:568-580

Ishii, M. 1975. Thermo-fluid Dynamic Theory of Two-Phase Flow. Paris: Eyrolles

Jobson, H. E. and W. W. Sayre 1970. Vertical transfer in open channel flow. *Journal of Hydraulic Division*, ASCE, 96:HY-3:703-724

Lal, D.P., and R.E.A. Mason and R.F. Stickland-Constable. 1969. Collision breeding of crystal nuclei. *Journal of Crystal Growth*, 5:1-8

Launder, B. E. and D. B. Spalding 1974. The numerical computation of turbulent flow.

Computer Methods in Applied Mechanics and Engineering, 3:269-289

Lianwu Liu, Hai Li, Hung Tao Shen and Bernard Shumilak 2004. Simulation of flow and thermal conditions downstream of Limestone generating station, *Proceeding of 17th International Symposium on Ice*, St. Petersburg, Vol. 2: 323-331.

Martin, S. 1981. Frazil ice in rivers and oceans. *Annual Review of Fluid Mechanics*, 13:379-397.

Mercier, S. 1984 The reactive transport of suspended particles: Mechanics and Modeling. *Ph.D. dissertation,* Joint Program in Ocean Engineering, Massachusetts Institute of Technology, Cambridge. MA.

Nezu, I. 1977. Turbulent structure in open channel flows. *Ph.D Thesis presented to Kyoto University*, Kyoto, Japan.

Nezu, I. and H. Nakagawa 1993. Turbulence in Open-Channel flows, *Monograph, IAHR, AIRH*, Kyoto University, Japan.

Nezu, I. and W. Rodi 1986. Open-channel flow measurements with a laser Doppler anemometer. *Journal of Hydraulic Engineering*, ASCE, 112:335-355

Omstedt, A. 1985a On supercooling and ice formation in turbulent sea water. *Journal of Glaciology*, 31(109): 263-271.

Omstedt, A., and Svensson, U. 1984 Modeling supercooling and ice formation in a turbulent Ekman layer. *Journal of Geophysical Research*, Vol. 89, No. C1, p. 735-744

Osterkamp, T.E., 1978. Frazil ice formation: A review, *Journal of the hydraulics Division*, ASCE Sep.1239-1255

Osterkamp,T.E. and Gosink, J.P., 1982. Selected aspects of frazil ice formation and ice cover in turbulent streams Proceedings of the workshop on hydraulics of ice covered rivers, June, Edmonton, Alberta, 131-147. *National Research Council of Canada.*

Ottens, E.P.K., A.H. Janse and E. J. Dejong, 1972. Secondary nucleation in a stirred vessel cooling crystallizer. *Journal of Crystal Growth*, 13/14: 500-505.

Prowse, T. D. and Gridley, N. C. 1993. Environmental aspects of river ice. NHRI Science Report No. 5, National Hydrology Research Institute, Saskatoon, 155p.

Randolph, A.D. and M. A. Larson 1971. Theroy of particulate processes. New York: Academic press.

Rodi, W. 2000, Turbulence models and their application in hydraulics, A state-of-the-art review, Monograph, IAHR, AIRH.

S. Q. Ye and Doering, J. C. 2004. Simulation of the supercooling process and frazil evolution in turbulent flows, *Canadian Journal of Civil Engineering*, Vol. 31: 915-926

Scardovelli, R. and Zaleski, S. 1999 Direct numerical simulation of free-surface and interfacial flow, Annu. Rev. Mech. 31, 567-603.

Schaefer, V. J. 1950 The formation of frazil and anchor ice in cold water. *Transactions of the American Geophysical Union*, 31(6) 885-893.

Shen, H. T. 1996 River ice process-State of research, *13th IAHR Symposium on Ice*, Beijing, 1-7.

Svensson, U. & Omstedt, A. 1994 Simulation of supercooling and size distribution in frazil ice dynamics, *Cold Regions Science and Technology*. 22: 221-233.

Tryggvason, G., B. Bunner, B., Esmaeeli, A., Juric, D., Al-Rawahi, N., Tauber, W., Han, J., Nas, S. and Y.-J. Jan, 2001. A front-tracking method for the computations of multiphase flow, *Journal Computation Physics*. 169, 708-759.

Tsang, G. and Cui, W. 1994 Laboratory study of frazil distribution in a flow, *Canadian Journal of Civil Engineering,* 21, 696-709.

Tsang, G.., 1986. Preliminary report on field study at Lachine Rapid on cooling of river and formation of frazil and anchor ice. *Proceedings of the 4th workshop on Hydraulics of River Ice,* Montreal, Quebec, June Vol, II. pp. F5.1-F5.51

Ueda, H., R. Moller, S. Komori and T. Mizushina 1977. Eddy diffusivity near the free surface of open channel flow. *International Journal of Heat and Mass Transfer*, 20: 1127-1136

USACRREL, 1997 Ice engineering, U.S. Army Cold Regions research and Engineering Laboratory, Hanover, New Hampshire.

Wadia, P. H. 1974 Mass transfer from spheres and discs in turbulent agitated vessels. *Ph.D. dissertation.* Department of Chemical Engineering. Cambridge: Massachusetts Institute of Technology.

Appendix A

Discretization of Governing Equation For Zero-Dimensional Model

The number continuity equation (4.7) can be written in the following form

$$\begin{cases} \dfrac{dn_1}{dt} = \sum_{j=2}^{N} \alpha_j n_j - \beta_1 n_1 - \gamma_1 n_1 - \tau_1 n_1 \\ \dfrac{dn_2}{dt} = -\zeta\alpha_2 n_2 - \beta_2 n_2 + \delta\beta_1 n_1 - \gamma_2 n_2 - \tau_2 n_2 + \tau_1 n_1 \\ \quad \vdots \\ \dfrac{dn_N}{dt} = -\zeta\alpha_N n_N + \delta\beta_{N-1} n_{N-1} - \gamma_N n_N + \tau_{N-1} n_{N-1} \end{cases} \tag{A.1}$$

Discretizing the left hand side of equation (A.1) using an Euler forward scheme, yields

$$\frac{dn_i}{dt} = \frac{n_i(t+\Delta t) - n_i(t)}{\Delta t}. \tag{A.2}$$

Setting $n_i = (1-\theta)n_i(t) + \theta n_i(t+\Delta t)$, $0 \le \theta \le 1$ yields an implicit scheme if $\theta = 1$, and an explicit scheme if $\theta = 0$. Otherwise the scheme is semi-implicit. Then the equation becomes

$$
\begin{cases}
\dfrac{n_1(t+\Delta t)-n_1(t)}{\Delta t} = \displaystyle\sum_{j=2}^{N}\alpha_j\left(\theta n_j(t+\Delta t)+(1-\theta)n_j(t)\right)-\left(\beta_1+\gamma_1+\tau_1\right)\left(\theta n_1(t+\Delta t)+(1-\theta)n_1(t)\right) \\
\dfrac{n_2(t+\Delta t)-n_2(t)}{\Delta t} = -\zeta\alpha_2\left(\theta n_2(t+\Delta t)+(1-\theta)n_2(t)\right)-\left(\beta_2+\gamma_2+\tau_2\right)\left(\theta n_2(t+\Delta t)+(1-\theta)n_2(t)\right)+ \\
\qquad\qquad \left(\delta\beta_1+\tau_1\right)\left(\theta n_1(t+\Delta t)+(1-\theta)n_1(t)\right) \\
\quad\vdots \\
\dfrac{n_N(t+\Delta t)-n_N(t)}{\Delta t} = -\zeta\alpha_N\left(\theta n_N(t+\Delta t)+(1-\theta)n_N(t)\right)+\left(\delta\beta_{N-1}+\tau_{N-1}\right)\left(\theta n_{N-1}(t+\Delta t)+(1-\theta)n_{N-1}(t)\right) \\
\qquad\qquad -\gamma_N\left(\theta n_N(t+\Delta t)+(1-\theta)n_N(t)\right)
\end{cases}
$$

By combining the terms, the above equations become

$$
\begin{cases}
\left(1+\Delta t(\beta_1+\gamma_1+\tau_1)\theta\right)n_1(t+\Delta t)-\Delta t\displaystyle\sum_{j=2}^{N}\alpha_j\left(\theta n_j(t+\Delta t)\right) = n_1(t)-\Delta t\left(\beta_1+\gamma_1+\tau_1\right)\left((1-\theta)n_1(t)\right)+ \\
\qquad\qquad \Delta t\displaystyle\sum_{j=2}^{N}\alpha_j\left((1-\theta)n_j(t)\right) \\
-\Delta t\left(\tau_1+\delta\beta_1\right)\theta n_1(t+\Delta t)+\left(1+\Delta t(\zeta\alpha_2+\beta_2+\gamma_2+\tau_2)\theta\right)n_2(t+\Delta t) = n_2(t)-\Delta t\left(\zeta\alpha_2+\beta_2+\gamma_2+\tau_2\right)\left((1-\theta)n_2(t)\right)+ \\
\qquad\qquad \Delta t(1-\theta)\left(\tau_1+\delta\beta_1\right)n_1(t) \\
\quad\vdots \\
-\Delta t\left(\tau_{N-1}+\delta\beta_{N-1}\right)\theta n_{N-1}(t+\Delta t)+\left(1+\Delta t(\zeta\alpha_N+\gamma_N)\theta\right)n_N(t+\Delta t) = n_{N-1}(t)-\Delta t\left(\zeta\alpha_N+\gamma_N\right)\left((1-\theta)n_N(t)\right)+ \\
\qquad\qquad \Delta t(1-\theta)\left(\tau_{N-1}+\delta\beta_{N-1}\right)n_{N-1}(t)
\end{cases}
$$

If $A\begin{Bmatrix} n_1(t+\Delta t) \\ n_2(t+\Delta t) \\ \vdots \\ n_N(t+\Delta t) \end{Bmatrix} = D$ is used to replace the above form, then

$$A\begin{Bmatrix} n_1(t+\Delta t) \\ n_2(t+\Delta t) \\ \vdots \\ n_N(t+\Delta t) \end{Bmatrix} = D \tag{A.3}$$

where

$$A = \begin{bmatrix} 1+\Delta t(\beta_1+\gamma_1+\tau_1)\theta & -\Delta t\alpha_2\theta & \cdots & -\Delta t\alpha_N\theta \\ 0 & -\Delta t(\tau_1+\delta\beta_1)\theta & 1+\Delta t(\zeta\alpha_2+\beta_2+\gamma_2+\tau_2) & 0 \\ & \vdots & \vdots & \vdots \\ 0 & 0 & -\Delta t(\tau_{N-1}+\delta\beta_{N-1})\theta & 1+\Delta t(\zeta\alpha_N+\gamma_N) \end{bmatrix}$$

and

$$D = \begin{Bmatrix} n_1(t)-\Delta t(\beta_1+\gamma_1+\tau_1)((1-\theta)n_1(t))+\Delta t\sum_{j=2}^{N}\alpha_j\left((1-\theta)n_j(t)\right) \\ n_2(t)-\Delta t(\zeta\alpha_2+\beta_2+\gamma_2+\tau_2)((1-\theta)n_2(t))+\Delta t(1-\theta)(\tau_1+\delta\beta_1)n_1(t) \\ \vdots \\ n_{N-1}(t)-\Delta t(\zeta\alpha_N+\gamma_N)((1-\theta)n_N(t))+\Delta t(1-\theta)(\tau_{N-1}+\delta\beta_{N-1})n_{N-1}(t) \end{Bmatrix}.$$

Then the frazil ice number at the subsequent time step can be obtained from equation (A.3).

Appendix B

Discretization of Governing Equation for Vertical One-Dimensional Model

The kinetic eddy viscosity is related to the turbulent kinetic energy and the turbulent dissipation rate as shown in equation 2.7. Turbulent energy and turbulent dissipation rate are given in equations 2.8, and 2.9, respectively.

The derivative of ν_T with respect to z is

$$\frac{\partial \nu_T}{\partial z} = k u_* \left(1 - \frac{2z}{h}\right). \tag{B.1}$$

Noting that u_* is independent of z, then the governing equations (5.1), (5.2), and (5.3) become,

$$\frac{\partial U}{\partial t} = \frac{\partial \nu_T}{\partial z}\frac{\partial U}{\partial z} + \nu_T \frac{\partial^2 U}{\partial z^2} - \frac{1}{\rho}\frac{\partial P_w}{\partial x} = \left(k - \frac{2kz}{h}\right) u_* \frac{\partial U}{\partial z} + \nu_T \frac{\partial^2 U}{\partial z^2} - \frac{1}{\rho}\frac{\partial P_w}{\partial x} \tag{B.2}$$

$$\frac{\partial T}{\partial t} = \frac{1}{\sigma_T}\frac{\partial \nu_T}{\partial z}\frac{\partial T}{\partial z} + \frac{\nu_T}{\sigma_T}\frac{\partial^2 T}{\partial z^2} + G_T = \frac{1}{\sigma_T}\left(k - \frac{2kz}{h}\right) u_* \frac{\partial T}{\partial z} + \frac{\nu_T}{\sigma_T}\frac{\partial^2 T}{\partial z^2} + G_T \tag{B.3}$$

$$\frac{\partial n}{\partial t} = \frac{1}{\sigma_n}\frac{\partial \nu_T}{\partial z}\frac{\partial n}{\partial z} + \frac{\nu_T}{\sigma_C}\frac{\partial^2 n}{\partial z^2} + G_n = \frac{1}{\sigma_n}\left(k - \frac{2kz}{h}\right) u_* \frac{\partial n}{\partial z} + \frac{\nu_T}{\sigma_C}\frac{\partial^2 n}{\partial z^2} - W_n \frac{\partial n}{\partial z} + G_n \tag{B.4}$$

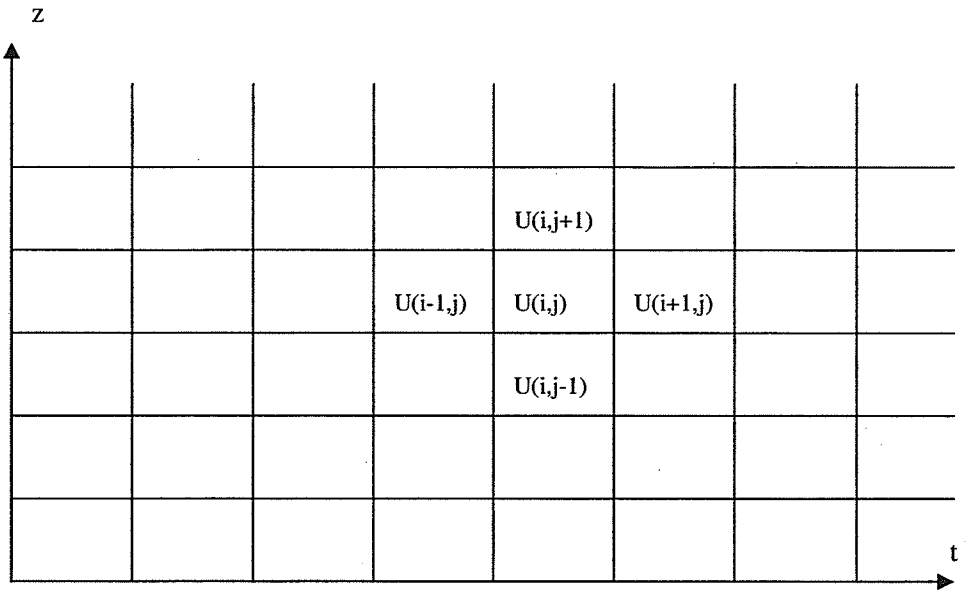

Figure B.1 Schematic of t-z plane

Discretizing equations (B.2), (B.3), and (B.4) using an explicit differential scheme for $\frac{\partial()}{\partial t}$ and an implicit scheme for $\frac{\partial()}{\partial z}$ and $\frac{\partial^2()}{\partial z^2}$, where the inside of the parenthesis can be the variables U, T or n, yields

$$\frac{\partial()}{\partial t} = \frac{()_{(i+1,j)} - ()_{(i,j)}}{\Delta t}, \quad \frac{\partial()}{\partial z} = \frac{()_{(i+1,j+1)} - ()_{(i+1,j)}}{\Delta z}, \quad \frac{\partial^2()}{\partial z^2} = \frac{()_{(i+1,j+1)} - 2()_{(i+1,j)} + ()_{(i+1,j-1)}}{(\Delta z)^2}.$$

Substituting the differential schemes into equations (B.2), (B.3), and (B.4), gives

$$\begin{aligned} &-\nu_T \Delta t U_{(i+1,j-1)} + \left((\Delta z)^2 + \Delta z \Delta t \left(k - \frac{2kz}{h} \right) u_* + 2\nu_T \Delta t \right) U_{(i+1,j)} \\ &-\left(\Delta z \Delta t \left(k - \frac{2kz}{h} \right) u_* + \nu_T \Delta t \right) U_{(i+1,j+1)} = \Delta z^2 U_{(i,j)} - \frac{1}{\rho} \frac{\partial P_w}{\partial x} \end{aligned} \tag{B.5}$$

$$-\nu_T \Delta t T_{(i+1,j-1)} + \left((\Delta z)^2 \sigma_T + \Delta z \Delta t \left(k - \frac{2kz}{h} \right) u_* + 2\nu_T \Delta t \right) T_{(i+1,j)} - \left(\Delta z \Delta t \left(k - \frac{2kz}{h} \right) u_* + \nu_T \Delta t \right) T_{(i+1,j+1)} = \Delta z^2 \sigma_T T_{(i,j)} + G_T \Delta z^2 \Delta t \sigma_T \quad \text{(B.6)}$$

$$-\nu_T \Delta t n_{(i+1,j-1)} + \left((\Delta z)^2 \sigma_T + \Delta z \Delta t \left(k - \frac{2kz}{h} \right) u_* + 2\nu_T \Delta t - \varpi_n \Delta z \Delta t \sigma_n \right) n_{(i+1,j)} - \left(\Delta z \Delta t \left(k - \frac{2kz}{h} \right) u_* + \nu_T \Delta t + \varpi_n \Delta z \Delta t \sigma_n \right) n_{(i+1,j+1)} = \Delta z^2 \sigma_T n_{(i,j)} + G_n \Delta z^2 \Delta t \sigma \quad \text{(B.7)}$$

Equations (B.5), (B.6), and (B.7) can be rewritten in the form of an upper open tri-diagonal matrix, respectively, using equation (B.7) as an example.

For simplification, assume

$$AA_{(i+1,j-1)} = -\nu_T \Delta t$$

$$AA_{(i+1,j)} = \left((\Delta z)^2 + \Delta z \Delta t \left(k - \frac{2kz}{h} \right) u_* + 2\nu_T \Delta t \right)$$

$$AA_{(i+1,j+1)} = -\left(\Delta z \Delta t \left(k - \frac{2kz}{h} \right) u_* + \nu_T \Delta t \right)$$

then,

$$AA_{(i+1,j-1)} T_{(i+1,j-1)} + AA_{(i+1,j)} T_{(i+1,j)} + AA_{(i+1,j+1)} T_{(i+1,j+1)} = \Delta z^2 T_{(i,j)} + G_T \Delta z^2 \Delta t \sigma_T \quad \text{(B.8)}$$

Equation (B.8) can be written in the form

$$\begin{cases} AA_{(2,1)}T_{(2,1)} + AA_{(2,2)}T_{(2,2)} + AA_{(2,3)}T_{(2,3)} = \Delta z^2 T_{(1,2)} + G_T \Delta z^2 \Delta t \sigma_T \;\; ; \;\; (i=1, j=2) \\ AA_{(2,2)}T_{(2,2)} + AA_{(2,3)}T_{(2,3)} + AA_{(2,4)}T_{(2,4)} = \Delta z^2 T_{(1,3)} + G_T \Delta z^2 \Delta t \sigma_T \;\; ; \;\; (i=1, j=3) \\ AA_{(2,3)}T_{(2,3)} + AA_{(2,4)}T_{(2,4)} + AA_{(2,5)}T_{(2,5)} = \Delta z^2 T_{(1,4)} + G_T \Delta z^2 \Delta t \sigma_T \;\; ; \;\; (i=1, j=4) \\ \vdots \qquad\qquad \vdots \\ AA_{(2,n-2)}T_{(2,n-2)} + AA_{(2,n-1)}T_{(2,n-1)} + AA_{(2,n)}T_{(2,n)} = \Delta z^2 T_{(1,n-1)} + G_T \Delta z^2 \Delta t \sigma_T \;\; ; \;\; (i=1, j=n-1) \end{cases}$$

The same derivation process can be applied to equation (B.5) and to equation (B.6).

Appendix C

Discretization of Governing Equation for An Extended Vertical One-Dimensional Model

The expression for ν_T and its derivative used in chapter five as described in equation (2.7), (B.1) are applied herein, therefore the equations (5.1), (6.1), and (6.2) take the following forms

$$\frac{\partial U}{\partial t}=\frac{\partial \nu_T}{\partial z}\frac{\partial U}{\partial z}+\nu_T\frac{\partial^2 U}{\partial z^2}-\frac{1}{\rho}\frac{\partial P_w}{\partial x}=\left(\kappa-\frac{2\kappa z}{h}\right)u_*\frac{\partial U}{\partial z}+\nu_T\frac{\partial^2 U}{\partial z^2}-\frac{1}{\rho}\frac{\partial P_w}{\partial x} \quad \text{(C.1)}$$

$$\frac{\partial T}{\partial t}=\frac{1}{\sigma_T}\frac{\partial \nu_T}{\partial z}\frac{\partial T}{\partial z}+\frac{\nu_T}{\sigma_T}\frac{\partial^2 T}{\partial z^2}+G_T=\frac{1}{\sigma_T}\left(\kappa-\frac{2\kappa z}{h}\right)u_*\frac{\partial T}{\partial z}+\frac{\nu_T}{\sigma_T}\frac{\partial^2 T}{\partial z^2}+G_T \quad \text{(C.2)}$$

$$\frac{\partial n_m}{\partial t}=\frac{1}{\sigma_n}\frac{\partial \nu_T}{\partial z}\frac{\partial n_m}{\partial z}+\frac{\nu_T}{\sigma_C}\frac{\partial^2 n_m}{\partial z^2}+G_n=\frac{1}{\sigma_n}\left(\kappa-\frac{2\kappa z}{h}\right)u_*\frac{\partial n_m}{\partial z}+\frac{\nu_T}{\sigma_C}\frac{\partial^2 n_m}{\partial z^2}-W_n\frac{\partial n_m}{\partial z}+G_n \quad \text{(C.3)}$$

Discretizing equations (C.1), (C.2), and (C.3) using the same differential schemes for $\frac{\partial()}{\partial t}$ and an implicit scheme for $\frac{\partial()}{\partial z}$ and $\frac{\partial^2()}{\partial z^2}$, and substituting the differential schemes into equations (C.1), (C.2), and (C.3), gives

$$-\nu_T \Delta t U_{(i+1,j-1)} + \left((\Delta z)^2 + \Delta z \Delta t \left(\kappa - \frac{2\kappa z}{h} \right) u_* + 2\nu_T \Delta t \right) U_{(i+1,j)} - \left(\Delta z \Delta t \left(\kappa - \frac{2\kappa z}{h} \right) u_* + \nu_T \Delta t \right) U_{(i+1,j+1)} = \Delta z^2 U_{(i,j)} - \frac{1}{\rho} \frac{\partial P_w}{\partial x} \tag{C.4}$$

$$-\nu_T \Delta t T_{(i+1,j-1)} + \left((\Delta z)^2 \sigma_T + \Delta z \Delta t \left(\kappa - \frac{2\kappa z}{h} \right) u_* + 2\nu_T \Delta t \right) T_{(i+1,j)} - \left(\Delta z \Delta t \left(\kappa - \frac{2\kappa z}{h} \right) u_* + \nu_T \Delta t \right) T_{(i+1,j+1)} = \Delta z^2 \sigma_T T_{(i,j)} + G_T \Delta z^2 \Delta t \sigma_T \tag{C.5}$$

$$-\nu_T \Delta t n_{\mathrm{m}(i+1,j-1)} + \left((\Delta z)^2 \sigma_T + \Delta z \Delta t \left(\kappa - \frac{2\kappa z}{h} \right) u_* + 2\nu_T \Delta t - \varpi_n \Delta z \Delta t \sigma_n \right) n_{\mathrm{m}(i+1,j)} - \left(\Delta z \Delta t \left(\kappa - \frac{2\kappa z}{h} \right) u_* + \nu_T \Delta t + \varpi_n \Delta z \Delta t \sigma_n \right) n_{\mathrm{m}(i+1,j+1)} = \Delta z^2 \sigma_T n_{m(i,j)} + G_n \Delta z^2 \Delta t \sigma_n \tag{C.6}$$

The source terms in the equations are important for the convergence of the solution, and it should be treated in the right way. The explicit scheme is used for the source terms in equation (C.4) and (C.5), while the semi-implicit scheme is used for equation (C.6), hence G_n can be written in different forms for the different frazil size groups

$$G_n = \left(\sum_{l=2}^{N} \alpha_l n_l(i,j) \right) - \beta_1 n_1(i+1,j) - \tau_1 n_1(i+1,j); \quad (m=1)$$

$$G_n = -\zeta \alpha_m n_m(i+1,j) - \beta_m n_m(i+1,j) + \delta \beta_{m-1} n_{m-1}(i,j) - \tau_m n_m(i+1,j) + \tau_{m-1} n_{m-1}(i,j) \quad (1 < m < N-1)$$

$$G_n = -\zeta \alpha_N n_N(i+1,j) + \delta \beta_{N-1} n_{N-1}(i,j) + \tau_{N-1} n_{N-1}(i,j); \quad (m=N)$$

Substituting G_n into equation (C.6), the equations become

$$-\nu_T \Delta t n_{1\,(i+1,j-1)} + \left((\Delta z)^2 \sigma_T + \Delta z \Delta t \left(\kappa - \frac{2\kappa z}{h} \right) u_* + 2\nu_T \Delta t - \varpi_n \Delta z \Delta t \sigma_n + \beta_1 + \tau_1 \right) n_{1\,(i+1,j)}$$
$$-\left(\Delta z \Delta t \left(\kappa - \frac{2\kappa z}{h} \right) u_* + \nu_T \Delta t + \varpi_n \Delta z \Delta t \sigma_n \right) n_{1(i+1,j+1)} = \Delta z^2 \sigma_T n_{1(i,j)} + \left(\sum_{l=2}^{N} \alpha_l n_l \right) (\Delta z^2 \Delta t \sigma_n)$$
$$(m=1)$$

$$-\nu_T \Delta t n_{\mathrm{m}\,(i+1,j-1)} + \left((\Delta z)^2 \sigma_T + \Delta z \Delta t \left(\kappa - \frac{2\kappa z}{h} \right) u_* + 2\nu_T \Delta t - \varpi_n \Delta z \Delta t \sigma_n + \alpha_m + \beta_m + \tau_m \right) n_{\mathrm{m}\,(i+1,j)}$$
$$-\left(\Delta z \Delta t \left(\kappa - \frac{2\kappa z}{h} \right) u_* + \nu_T \Delta t + \varpi_n \Delta z \Delta t \sigma_n \right) n_{\mathrm{m}(i+1,j+1)} = \Delta z^2 \sigma_T n_{1(i,j)} + (\delta\beta_m + \tau_m) n_m (\Delta z^2 \Delta t \sigma_n)$$
$$(1 < m < N)$$

$$-\nu_T \Delta t n_{\mathrm{N}\,(i+1,j-1)} + \left((\Delta z)^2 \sigma_T + \Delta z \Delta t \left(\kappa - \frac{2\kappa z}{h} \right) u_* + 2\nu_T \Delta t - \varpi_n \Delta z \Delta t \sigma_n + \alpha_N \right) n_{\mathrm{N}\,(i+1,j)}$$
$$-\left(\Delta z \Delta t \left(\kappa - \frac{2\kappa z}{h} \right) u_* + \nu_T \Delta t + \varpi_n \Delta z \Delta t \sigma_n \right) n_{\mathrm{N}(i+1,j+1)} = \Delta z^2 \sigma_T n_{N(i,j)} + (\delta\beta_{N-1} + \tau_{N-1}) (\Delta z^2 \Delta t \sigma_n)$$
$$(m=N)$$

For simplification,

$$AA_{(i+1,j-1)} = -\nu_T \Delta t \qquad \text{(C.7)}$$

$$\begin{cases} AA_{(i+1,j)} = \left((\Delta z)^2 \sigma_T + \Delta z \Delta t \left(\kappa - \frac{2\kappa z}{h} \right) u_* + 2\nu_T \Delta t - \varpi_n \Delta z \Delta t \sigma_n + \beta_1 + \tau_1 \right) & (for\ m=1) \\ AA_{(i+1,j)} = \left((\Delta z)^2 \sigma_T + \Delta z \Delta t \left(\kappa - \frac{2\kappa z}{h} \right) u_* + 2\nu_T \Delta t - \varpi_n \Delta z \Delta t \sigma_n + \alpha_m + \beta_m + \tau_m \right) & (for\ 1 < m < N) \\ AA_{(i+1,j)} = \left((\Delta z)^2 \sigma_T + \Delta z \Delta t \left(\kappa - \frac{2\kappa z}{h} \right) u_* + 2\nu_T \Delta t - \varpi_n \Delta z \Delta t \sigma_n + \alpha_N \right) & (for\ m=N) \end{cases} \qquad \text{(C.8)}$$

$$AA_{(i+1,j+1)} = -\left(\Delta z \Delta t \left(\kappa - \frac{2\kappa z}{h} \right) u_* + \nu_T \Delta t \right) \qquad \text{(C.9)}$$

then,

$$AA_{(i+1,j-1)}n_{m(i+1,j-1)} + AA_{(i+1,j)}n_{m(i+1,j)} + AA_{(i+1,j+1)}n_{m(i+1,j+1)} = \Delta z^2 n_{m(i,j)} + G_n^{'}\Delta z^2 \Delta t \sigma_T , \qquad (C.10)$$

where

$$G_n^{'} = \sum_{l=2}^{N} \alpha_l n_l \quad (for\ m=1)$$

$$G_n^{'} = (\delta\beta_m + \tau_m)n_m \quad (for\ 1<m<N)$$

$$G_n^{'} = (\delta\beta_{N-1} + \tau_{N-1})n_{N-1} \quad (for\ 1<m<N)\ \sigma_T\ \sigma_T\ \sigma_T\ \sigma_T\ \sigma_T\ \sigma_T\ \sigma_T .$$

The same derivation process can be applied for equation (C.4) and for equation (C.5). All of the resultant equations and their suitable boundary conditions consist of a closed soluble system. A MATLAB® based program was developed to solve the three equations simultaneously.